Unraveling the Proteome of Endothelial Cells Latently Infected with KSHV Reveals Reliance on Peroxisome Lipid Metabolism and Redox Regulation

Zoi Evelyn Sychev

A dissertation

submitted in partial fulfillment of the

requirements for the degree of

Doctor of Philosophy

University of Washington

2017

Reading Committee:

Michael Lagunoff, Chair

Alejandro Wolf-Yadlin

Adam P. Geballe

Program Authorized to Offer Degree:

Molecular and Cellular Biology

University of Washington

Abstract

Unraveling the Proteome of Endothelial Cells Latently Infected with KSHV Reveals Reliance on Peroxisome Lipid Metabolism and Redox Regulation

Zoi Evelyn Sychev

Chair of the Supervisory Committee:
Professor Michael Lagunoff
Microbiology

Viruses have evolved to modulate cell signaling transduction by reprogramming the host cell machinery to establish a long-term infection and replication. By Altering host cell signaling pathways involved in metabolism, inflammation and oxidative stress, herpesviruses can establish an environment conducive for maintenance of latent infection. In this thesis, I used systems biology technologies to identify novel cellular targets of an oncogenic virus, Kaposi's Sarcoma Associated Herpesvirus (KSHV). KSHV is the etiological agent of Kaposi's Sarcoma (KS). KS is an endothelial cell based tumor where more than 90% of the cells are latently infected with KSHV. Therefore, elucidating novel molecular targets that are critical in the latent state would lead to treatment specific for these infected cells. I performed a global proteomics as well as phosphoproteomics screen in mock and KSHV infected endothelial cells. Combining the proteomics results with the prediction of activated transcription factors obtained from high throughput mRNA sequencing of mock and KSHV infected cells allowed the prediction of many

pathways activated by KSHV. A Steiner forest analysis utilizing a database of protein-protein interactions was employed in this step. From the set of predicted activated pathways, I validated two novel pathways that are activated during KSHV latency, peroxisome biogenesis and cytoplasmic redox homeostasis. Further, I found that metabolism of very long chain fatty acids (VLCFs) in the peroxisome is required for the survival of KSHV latently infected endothelial cells and, therefore, it is critical to KSHV pathogenesis. It has been previously shown that KSHV induces oxidative stress, and I found that KSHV activation of Thioredoxin (TXN), an antioxidant protein responsible for resolving reactive oxygen species is also necessary for the survival of latently infected cells. Therefore, the systems biology approach presented here led to the identification of two pathways critical for KSHV latency. Following background (chapter 1) and methods (chapter 2), Chapter 3 shows that KSHV modulates peroxisome biogenesis and revealing a critical role for the metabolism of very long chain fatty acids (VLCFs) in the in the course of latency. In Chapter 4, I show that oxidoreductase proteins involved in regulating redox homeostasis are required during latent infection and might be responsible for regulating MAPK kinase signaling. In conclusion, this work, I demonstrate how systems biology approach was used to identify novel critical pathways required for endothelial cells latently infected with KSHV. This furthers our understanding of KSHV pathogenesis and provides potential targets for KS clinical therapies that are specific to latently infected cells.

TABLE OF CONTENTS

List of Figures

List of Tables

ACKNOWLEDGEMENTS

There have been several people that had played a major role in my career development and life. First, I would like thank Michael Lagunoff for being a great mentor, for providing me with support and flexibility to accomplish my career goals and for helping me develop as an independent scientist. Also, I would like to thank Alejandro Wolf-Yadlin for supporting me throughout my project and providing me with the tools and connections to accomplish my thesis work. I would like to thank my undergraduate advisor Alejandro Barbieri for believing in me and opening doors to opportunities without which I would not have explored. Also, I would like to thank my undergraduate biology teacher Mrs. Velazquez, which was the first female science teacher I ever had. She was a great role model and inspiration. I say thanks to my former and current lab mates (A.K.A labbies) for their unconditional support, advice, reagents, interesting discussions, their time and friendship throughout these years. To my students, Victoria Ortega and Yashmira Naidoo for being great students and allowing me to be their mentor. I am very proud of both of them. I am thankful to the Molecular and Cell Biology Program for providing me with all their support and trust. They have sponsored me annually to go to the SACNAS National conference. SACNAS organization has been a great venue for me as a career development and networking platform so I am truly thankful for their existence and mission.

I thank all my family for their endless support and love specially my mom (Evelin Santeliz), Sami, Juanita and Rosila. A special thanks to my mom and Irina Adams for taking care of my child (Andrei) allowing me to accomplish my career goals. And for my partner, I infinitely thank my husband for being the best partner and editor ever and for all his unconditional love and support and for being my source of strength and encouragement.

DEDICATION

I dedicate this thesis work to my mother Evelin Santeliz and my children Andrei and Arianna. I am very proud of my mother for being my greatest role model and for being my champion. I thank her for all her support and love. And to my children, they give me the strength that keeps me going to build the foundation for them to grow. This work is to show them that it does not matter where you are coming from as long as you follow your dreams!

Chapter 1. Introduction

1.1 Herpesviruses

The *Herpesviridae* family are viruses that cause disease in animals and humans (1). Structurally these viruses share four main features. They all contain a core with a linear double-stranded DNA (dsDNA) that ranges between 124-295 kb in length (2). Surrounding the core is an icosahedral capsid that is approximately 125 nm in diameter which comprise of 161 capsomeres. Outside of the capsid there is an amorphous material that is designated the tegument and lastly it is surrounded by a lipid envelop with viral encoded glycoproteins surrounding the layer (2).

Herpesviridae family is classified by three subfamilies *Alphaherpesvirinae*, *Betaherpesvirinae* and *Gammaherpesvirinae.* These viruses share four core major biological properties that groups them together yet present differences in host cell range, host response to infection, clinical manifestations and some other properties. First, there is an array of enzymes that are involved in nucleotide metabolism, DNA synthesis, and processing of proteins (2). Second, virus transcription, viral DNA synthesis and particle assembly occur mainly in the nucleus. Third, production of infectious virions often leads to the destruction of the host cell. Finally, the shared characteristic that will be the focus of this work is that these viruses manipulate the host mechanism to establish a long term persistent infection known as latency.

All viruses in the *Herpesviridae* family have two different life cycles following infection of a cell, lytic replication and latency. During infection, viruses first interact with a receptor or a combination of receptors for cell entry. At this stage, an interface commonly occurs between virion surface glycoprotein(s) and a cell surface heparan sulfate proteoglycan (2). Upon contact with the host cell, virions initiate entry either by membrane fusion or by receptor mediated endocytosis

leading to cytoskeleton penetration. After entry, mechanisms of virion disassembly vary across the *Herpesviridae* yet virions dock to the nuclear pore and immediately release their DNA content which is then taken up through the pores in an active process powered by ATP (2). Viral DNA is partially chromatinized and cellular and viral factors will determine if the virus enters the lytic cycle or establishes latent infection. During lytic replication, there is regulated temporally determined gene expression, genomic replication, virion assembly, egress, transmission to new cells and counteraction to immune responses to complete the cycle. During the latent state, there is no virion production. The viral genomes remain as circular episomes in the nucleus and few viral genes are expressed for the maintenance of latency. Mechanisms of reactivation from latent to lytic cycles vary among the herpesviruses and depend on the cell type the virus is latent in (3).

There are eight herpesviruses (HHV1-8) that have been identified to infect primarily humans. (2). The human alphaherpesviruses include Herpes Simplex Virus 1 (HSV-1 or HHV-1), which causes oral cold sores, Herpes Simplex Virus 2 (HSV-2 or HHV-2), which typically causes genital sores and Varicella-Zoster Virus (VZV or HHV-3) which causes chicken pox and, if reactivated to lytic replication later in life, can cause shingles. The *Betaherpesvirinae* subfamily infects humans and has a restricted host. The life cycle is very long (more than 7 days), and its distinct characteristic is that the infected cells become enlarged (2). There are four human betaherpesviruses. Human cytomegalovirus (HCMV or HHV-5) causes severe damage to immunocompromised patients and can also cross the placental barrier potentially leading to birth defects. It can also lead to liver failure, inflammation in the retina, gastrointestinal tract, and lungs. HHV-6A and HHV-6B cause roseola in infants and may be associated with other diseases (2). HHV-7 can also cause roseola in infants but most frequently the infection is asymptomatic. The *Gammaherpesvirinae* subfamily includes Epstein-Barr Virus (EBV or HHV-4), which is the agent

of mononucleosis as well as an oncogenic virus that is associated with different cancers such as Hodgkin's Lymphoma, Burkitt's lymphoma, gastric cancer, nasopharyngeal carcinoma and disorders of immunodeficiency and Kaposi's Sarcoma Herpesvirus (KSHV or HHV-8),which is the etiological agent of Kaposi's Sarcoma (KS), an endothelial cell based tumor and other two lymphoproliferative disorder, Primary Effusion Lymphoma (PEL) and Multicentric Castleman Disease (MCD) (4-6).

1.2 KSHV and KS

Kaposi's Sarcomas (KS) was first described as multiple pigmentation of the skin by a Hungarian dermatologist, Moritz Kaposi who was practicing in the University of Vienna in 1872 (4). He made this observation mainly in older men, and it was considered an indolent disease. KS has four clinical variants that have similar histologic features but have different manifestation, target populations and disease progression. These include: Classic, Endemic, Iatrogenic and Epidemic KS. Classic KS generally occurs in elderly men and is more common in the Mediterranean region including southern Italy. KS became an endemic problem in parts of Africa in the latter part of the 20^{th} century where it is currently one of the most common tumors in parts of sub-Saharan Africa. KS spread to many areas including the United States with the AIDS epidemic where KS became the most common tumor of AIDS patients occurring in nearly a third of the cases (7). Common histologic characteristics are spindle-shaped tumor cells with extravasiated vascular slits and erythrocytes (8). Endemic KS was observed in Zambia in 1983 with an increase in incidence. It is more aggressive and is particularly more common in African children (2). Iatrogenic KS, presents in organ-transplant patients receiving immunosuppressive

therapy (9). This type of KS tends to be aggressive in half of the affected population involving lymph nodes, mucosa, and visceral organs without any skin lesions (10, 11). AIDS-related KS affects patients infected with HIV, especially homosexual or bisexual men and is the most common AIDS-associated cancer in the United States (7).

Kaposi's Sarcoma-Associated Herpevirus (KSHV) or human herpevirus 8 (HHV-8) is the etiologic agent of KS. In 1994 KSHV was discovered by Chang et. al using representational difference analysis to isolate unique sequences from patients with acquired immunodeficiency syndrome (AIDS) (4). Based on sequence analysis KSHV is classified as a gammaherpesvirus and further subclassified as *a rhadinovirus* separating it from the other human gammaherpesvirus EBV which is a *lymphocryptoviruse* (2). KSHV genome is a double-stranded linear DNA (dsDNA) that is approximately 165 kb long. It has a central unique region of approximately 145 kb that encodes more than 100 viral genes and is flanked by G-C rich direct terminal repeats (TRs). These TRs contain variable numbers of repeats. Although repeats might vary between isolates, the average length of the repeats is similar (12).

Open reading frames of the KSHV genome sequence are divided in groups based on sequence uniqueness to KSHV or shared homology with other herpesviruses. KSHV genomes contains blocks of highly conserved genes that are present in all herpesviruses. These genes are typically involved in viral replication or components of the virion structure. KSHV unique genes are named K1-K15 numbered from left to right. Many of these genes are homologous to the human genes such as vCyclin and vFLIP which have antagonistic activities compared to the host genes. KSHV genes also code for non-coding RNAs, including microRNA (miRNAs) and polyadenylated nuclear RNA (PAN) (7, 13).

KSHV infects several cell lines and encodes multiple envelope glycoproteins: gB, gH, gL that are involved in membrane fusion. Upon attachment to cells, several cell surfaces receptors are involved in entry including heparan sulfate, integrins, DC-SIGN and xCT. Receptor clathrin-mediated endocytosis is the predominant mode of entry into the cells (2). These events trigger numerous signaling pathways including those mediated by FAK activation, PI3K, and Rho GTPases, which lead to cytoskeleton rearrangements that allow the transport of the viral capsid into the nucleus. Once the viral DNA enters into the nucleus, the KSHV viral genome circularizes and chromatinizes becoming ready for host RNA pol II transcription.

As all herpesviruses, KSHV presents with both latent and lytic programs that allows the virus to hijack the host machinery. The dynamics between lytic and latent phases depends on the host environment. It has been described that in fibroblast and in primary endothelial cells the kinetics between the two states depends of the levels of expression of either classical latent or lytic genes (13). For example, early upon infection there are high levels of lytic gene expression while low levels of latent viral genes being expressed (13). After 24 hours post infection (hpi), there is a switch of lytic to latent genes expression that then dominate leading to establishment of latency.

Latency is the default pathway where very few viral genes are expressed and less than 5% of cells express a lytic protein marker- ORF 59. During latency, no virion production occurs. KS tumors cells are more than 90% latently infected suggesting that latency is the dominant state. During this dormant state, the latency associated region is expressed and it comprises of Latency Associated Nuclear Antigen (LANA), viral Cyclin (vCYC), FADD-like interleukin-1-β–converting enzyme inhibitory protein (vFLICE), the Kaposin family members A, B and C, as well as a number of viral microRNAs (miRNAs) which are expressed from 12 loci. This section of the genome is denominated the KSHV latency associated region (KLAR) (7–10).

LANA is a major KSHV- encoded protein that is involved in genome maintenance and segregation. Although there is controversy about genome maintenance during cell division, the viral genome replicates with the host genome and is evenly divided between daughter cells (2, 14). It is a multifunctional protein that is primarily found in the nucleus of infected cells (15). LANA C-terminal domain binds to the TR of the KSHV genome and binds to the host genome by the N-terminal domain (15). LANA is commonly a marker of latency, and it is identified as a nuclear punctate staining when visualized by immunofluorescence microscopy (16). It has been determined to bind several host proteins, including p53 (17), pRB (18) and several transcription factors such STAT1, ATF4, Myc and other proteins involved in cell signaling such as negative regulating glycogen-synthase kinase-3 (GSK-3), causing a cell-cycle-dependent nuclear accumulation (15, 19-21), influencing host cellular machinery and controlling KSHV pathogenesis (15).

KSHV ORF72 encodes for vCyclin/vCyc which is a human homologue of cellular cyclin D. Similar to the human cyclin homologue, it constitutively activates CDK6 regulating cell cycle and proliferation. vCyclin has been shown to interact cdk9, leading to increased phosphorylation of p53 at serine 33, which results in cell cycle arrest (2). Interestingly, it has been shown that overexpression of vCyclin induces apoptosis mediated by the inactivation of BCL2 (22). Furthermore, in human dermal microvascular endothelial cells over expression of vCyclin induces cellular stress and leading to senesce (23). Therefore, establishing a cell line over expressing vCyc is very challenging.

KSHV ORF71 encodes vFLIP also referred to as K13, that mirrors the human homologue FLIP. There are two cellular FLIPs: the long ($FLIP_L$) and the short form ($FLIP_S$). vFLIP is more similar to the short form (2). vFLIP lacks the caspase-like domain similar to $FLIP_S$. vFLIP blocks

the death-inducing signaling complex (DISC) by competitively binding with the cellular FLIP proteins and evading apoptosis. Mechanistically vFLIP has been shown to upregulate NF-KB known to have an anti-apoptotic activity (24). In addition to modulating NF-KB activity, vFLIP protects infected cells from autophagy by binding with Atg3 (25). In endothelial cells, it has been shown to be required for formation of the cell spindling morphology. Therefore, vFLIP plays a major role in evading cell death and maintaining a stable latency.

Kaposin A, B and C are upstream of ORF71 (vFLIP). The encoded proteins come from a single mRNA and starts at different translation initiation sites (2, 7). Kaposin A is highly hydrophobic and is found in the plasma and intracellular membranes (2). It is involved in regulating GTPases interactions that are important for transformation activity (26). Kaposin B, a small soluble nuclear protein, which acts like a scaffold or adaptor protein and activates the p38/MAPK signaling pathway (27) and enhances the stability of PROX1 mRNA transcripts. Kaposin C is less well understood. Another key player from the KLAR region is the miRNAs. The cluster of miRNAs includes 12 pre-miRs 3K1-K12 (28), which are highly expressed during latency. Since their discovery, there have been numerous works characterizing their role during KSHV pathogenesis linking their activity to carbon metabolism (29), tumorigenesis and angiogenesis (30).

Latently infected cells can be induced to enter the lytic viral phase either by using HDAC inhibitors or phorbol ester treatments that mimic the action of diacyl-glycerol (DAG), an activator of protein kinase C, which leads to different signal transduction pathways affecting chromatin regulation (2). Upon activation, all the lytic genes are expressed in a temporal cascade of events to support virion production. Early during this process, Immediately-Early (IE) genes are activated., Reactivation is predominantly controlled by ORF50 that encodes RTA, the key lytic

switch from latency that is both sufficient and necessary for reactivation (31). RTA has been shown to bind to at least 19 sites in the KSHV viral genome (32). Subsequently, after IE gene expression, Early-genes are activated and involve DNA polymerase, thymidine kinase and ribonucleotide reductase which play a major role in viral DNA replication as well as immune evasion, host shut off and modulation of signal transduction (2). Viral DNA replication allows activation of the next group of lytic late genes, which mainly codes for structural proteins ready for virion assembly and egress.

1.3 KSHV Latent Experimental Cell Culture Systems

To study KSHV pathogenesis there have been several attempts to establish an animal model with very little success since KSHV infections are host restricted and only affect humans. Cultures from PEL patients with advanced disease have provided the closest insights where cell cultures were readily established. PEL cells predominantly are latently infected with KSHV and can be reactivated using phorbol ester and HDAC inhibitors resulting in 15-30% of cell reactivation (7). Primary endothelial cells are the most relevant cell type to study KS pathogenesis but using primary cells presents significant obstacles: the typically limited number of available cells and their passages, restricts such studies to short term experiments. Another established model relies on use of immortalized endothelial cells created with human papillomavirus E6 and E7 (33) and tert-immortalization of microvascular endothelial cells (TIME). Both of these models are well suited for studying pathogenesis since these cell lines can go for more than 100 passages. However, most of experiments should be conducted in early passages after immortalization.

1.4 Mass Spectrometry Based Proteomics and Herpesviruses

Protein identification and sequencing posed a substantial challenge as recently as 14 years ago. It required large amounts of protein and long times for sample processing. In the recent past, the majority of protein sequencing was done using gel-electrophoresis based methods, predominantly relying on 1D-PAGE. This method is used to separate denatured proteins according to their molecular weight in a polyacrylamide gel. The 2-D PAGE is an enhanced electrophoretic technique which separates proteins based on their isoelectric point along a pH gradient in the first dimension and subsequently by the molecular mass along the second dimension. The latter approach allows identification of more than > 10,000 different proteins however this resolution is technically complex (34). Currently, technological advancements including High Pressure Liquid Chromatography (HPLC), mass spectrometer instruments, Electro-spray Ionization (ESI) and stable isotope labeling have significantly facilitated discoveries and understanding of proteome profiles, and allowed analysis and quantification based on shotgun proteomics.

To evaluate cell signal transduction, propagation and amplification of post-translational modifications (PTMs) can be examined. In a complex cell mixture, often PTMs are in low abundance and, therefore, are more challenging to detect against the background of highly abundant proteins, such as cytoskeletal proteins. Therefore, affinity-based purification in tandem with sequencing and quantification is recommended to obtain better detection and identification. Despite these advancements, it is critical to highlight that the detection rate of modern proteomics techniques is on the order of 10% of true protein diversity, which is a major technical challenge in the field (35). Therefore, targeted proteomics that relies on enriching for a specific organelle and/or PTM is the best recommended route.

A better understanding of oncogenic gamma-herpesviruses has been uncovered through the proteomics lens. Several studies on virion tegument content in EBV and KSHV show that these viruses bring in viral proteins that help them evade immunity as well as to turn on gene transcription such as RTA in KSHV and HSp90 and Hsc70 in EBV (34). Furthermore, specific viral factors and interactions have been evaluated focusing on individual KSHV and host proteins. For example, using 2-D gel method on overexpressed KSHV vFLIP cells were analyzed. From this, 16 proteins were identified to be upregulated and out of these, superoxide dismutase (MnSOD) is significantly altered. MnSOD is involved in mediating resistance of endothelial cells to superoxide-induced cell death (36). In addition, another study showed the dynamic changes of NCP cell lines in response to EBV LMP1 oncoprotein using isobaric Tag for Relative and Absolute Quantification (iTRAQ) labeling methods. This group identified several proteins that were differentially expressed. Similar to our work presented in this thesis, a 1.33-fold change of was considered significant (37). Furthermore, metabolic labeling has been used as well, such as SILAC in KSHV overexpressing K5 viral protein. In this study, K5 was identified to be involved in immunomodulating MHC I for lysosomal degradation (38). Additionally, study of purified cellular compartments such ER and Golgi apparatus led to successful identification of novel peptides (38).

Interestingly another comprehensive proteomic study was conducted in the Glaunsinger lab where they mapped host-protein interactions of 89 KSHV viral proteins and human cells by using affinity tags and Mass Spectrometry. Several host proteins that directly bind to KSHV viral proteins were identified (39). They identified over 500 interactions and then they followed –up and validated their approach by elucidating a mechanism by which ORF24 binds to RNA polymerase II, an interaction predicted by their screen (39). ORF24 mimics and replaces TATA-

box-binding protein (TBP) and connects this transcription complex to viral late gene promoters. Prior to this work this mechanism was very poorly understood (39).

Transcriptomics offers an additional insight into proteomic changes by evaluating transcriptional activity. There is increasing evidence, however, that protein levels and activity do not correlate with mRNA levels as well as with transcription factor activity. This adds an extra layer of complexity to the central dogma of protein expression and function suggesting additional regulatory mechanisms involved. To unravel this complexity recently it has become more common to employ a combinations of multiple high throughput techniques. Thus, several high-throughput analyses are integrated within an experimental approach to increase detection and facilitate interpretations of relevant agents, pathways, and events within a global view of cellular biological processes. This integrated approach is able to provide interesting discoveries that any one technology alone is not able to accomplish with confidence. The increasing trend of using large-scale systems biology approaches has led to development of numerous automated tools and databases that allow in depth data analysis by systematic correlation between data outputs generated by multiple parallel high-through techniques. As the power of search databases and computational algorithms improves, we will be able to make better predictions and increase our understanding of cellular processes by combining experimental data with computational models to answer biological questions.

1.5 Altered Redox Homeostasis and Viral Induced Oncogenesis

1.5.1 Peroxisomes and Redox Homeostasis

While we have previously shown that FA synthesis is required for the survival of

endothelial cells latently infected with KSHV, how these downstream FAs are utilized and why they are necessary have not been determined (40). Peroxisomes have been identified as a nexus of lipid metabolism and signaling (41, 42). Peroxisomes have been studied in the context of infection with RNA viruses including influenza (43-48). Interestingly, infection with influenza virus led to an increased reliance on peroxisomes while infection with flaviviruses led to a significant decrease in peroxisome metabolism. One major function of peroxisomes is to metabolize very long chain fatty acids (VLCFAs). Peroxisomal defects have been associated with several clinical disorders, including Zellweger syndrome, a disease characterized by abnormal peroxisome lipid metabolism, deficiency of ACOX1 function, deficient D-bifunctional protein (D-BP) and X-linked adrenoleukodystrophy (X-ALD), a diseased characterized by a mutation in ABCD1 or ABCD3 transporters (49). ACOX1 is a peroxisomal enzyme that synthesizes DHA by partial β-oxidation of 24:6n3, a precursor that is transported into the peroxisome by the peroxisomal lipid transporter ABCD3 (42, 50, 51). Lipidomics analysis of fibroblasts from patients with ACOX1 deficiency demonstrate abnormal lipid profiles, specifically high levels of VLCFAs and low levels of DHA indicating abnormal function of VLCFAs breakdown and DHA synthesis (52). DHA is an important metabolite that possess anti-inflammatory properties. Peroxisome alterations have also been observed in prostate cancer cells. Valenda, I. et. Al. identified that in several prostate cancer cell lines there is increased levels of beta-oxidation attributing to malignant transformation (53). Therefore, peroxisomes are a vital organelle that is involved in viral infections as well as cancer cells to target for therapeutic treatments.

Redox Homeostasis became an important subject of biological investigation after the formulation of the free radical theory of oxygen toxicity in 1954 (54) that postulates that the toxicity of oxygen comes from partially reduced forms (54). Later, Denham Harman proposed the

role of free radicals in ageing which stimulated vigorous studies leading to the discovery of superoxide dismutase thereby providing evidence of free radical regulation in living systems (55). In 1977, another important discovery was that hydroxyl radicals triggered formation of the secondary messenger cyclase guanosine monophosphate (cGMP) (56). All these findings indicated that living systems developed mechanisms to counteract free radical toxicity via redox regulatory molecules.

Free radicals encompass oxygen and nitrogen based molecules. Oxygen free radical are also known as reactive oxygen species (ROS). ROS arises from sequential reduction of oxygen to superoxide, hydrogen peroxide, and hydroxyl radicals, and constitute a product of normal cellular metabolism (57). ROS levels have dual physiologic effects. At low/moderate levels they are beneficial and involved in regulating cell signal transduction, gene expression through transcription factor regulation, cell proliferation and differentiation (57). On the other hand, accumulation of these molecules can be detrimental leading to damage of cellular components. A common mechanism of damage is DNA lesions that involve the formation of 8-OH-G, leading to a permanent modification of gene expression resulting in mutagenesis, carcinogenesis and ageing (57, 58). Other important cellular components that fall victim to ROS are proteins and lipids, the latter occurring via peroxidation. Peroxyl radicals can react with lipids producing malondialdehyde (MDA) as well as 4-hydroxy-2-nonenal (HNE) both of which are major toxins to lipid membranes (57). Proteins are also very susceptible to oxidation in particular amino acid residues such as cysteine. This residue is highly reactive and its oxidation can lead to changes in protein function including constitutive protein activation and loss of regulation.

Cells have evolved to develop several defense mechanisms to counteract extracellular insults and deregulated cellular metabolism. To prevent ROS damage to cellular components,

enzymatic antioxidant systems employ superoxide dismutase (SOD), glutathione and thioredoxin peroxidases (GPX, TXN), and catalase (CAT) (57). These major enzymes maintain normal intracellular balance of ROS, essential for cell survival. The intracellular redox capacity is primarily regulated by glutathione (GSH) and thioredoxin (TXN). Redox stress arises as a temporary imbalance in the steady state homeostasis maintained through these antioxidant systems.

Redox signaling is defined as signaling that is processed and transduced through redox reactions. Several biological processes are affected by redox activity involving signaling mechanism that are prone to changes in thiol/disulphide states. Examples of such signaling include: transcription factors regulation such as AP-1 NF-KB (59), p53 (60), NFAT (61), HIF-1 (62), etc.; protein tyrosine phosphatases, Src family kinases, JNK and p38 MAPK signaling pathways, insulin and EGFR signaling as well as others (63-65). Redox signaling has also being implicated in several human diseases such as in cancer, angiogenesis, cardiovascular disease, diabetes, rheumatoid arthritis, Alzheimer disease and ageing.

Altered metabolism is one of the major sources of ROS production. During proliferation, cells metabolize higher levels of bioenergetics, leading to higher metabolite consumption and upregulation of anabolic and catabolic processes. Accordingly, there is an increase in rates of oxygen consumption for ATP production. Cancer cells reprogram metabolism such that there is an increased flux through the pentose phosphate pathway (PPP), high glutamine consumption, reduction/oxidation (redox) imbalance (favoring either oxidative or reducing environment depending on cancer type), and elevated rates of lipid biosynthesis including fatty acid synthesis (66, 67). During active metabolic cellular states, the major sources of ROS come from

mitochondria (oxidative phosphorylation) and peroxisome (β-oxidation) (68), which involves breakdown of fatty acids providing intermediates for the synthesis of glycerolipids as well as ATP production (42). On the other hand, increased flux into the PPP allows increased production of NADPH, which is the major reducing power in cells (67). Therefore, increase metabolism to produce bioenergetics goes hand in hand with production of NADPH to support reducing potential needed to sustain altered metabolic states in tumorigenic cells. In summary, redox homeostasis is a fundamental principle that affects global biological processes.

1.5.2 Oncogenic Viruses and Redox Homeostasis

Human oncogenic viruses have evolved mechanisms to adapt to host defenses, for example, evading immunity to maintain a persistent infection. Following the Hanahan and Weinberg (69) hallmarks of cancer paradigm, these viruses reprogram host cellular processes to sustain a tumor microenvironment favorable to cancer. Alteration of host machinery has been well studied in infection by the following oncogenic viruses: hepatitis B virus (HBV), hepatitis C virus (HCV), Epstein-Barr virus (EBV), human papillomaviruses (HPVs), human T cell lymphotropic virus-1 (HTLV-1), and KSHV.

Currently with the advent of newer technologies such as next generation sequencing, mass spectrometry based proteomics and metabolomics paired with comprehensive search databases, systems biology studies have provided a better and more detailed understanding of the underlying cellular mechanisms occurring in the course of infection as well as a perspective into how these mechanisms are synchronized and orchestrated on a global scale. For example, metabolomic flux and lipidomic analyses of HCMV and KSHV infected cells that traced the final products of two

major carbon sources (glucose and glutamine) have revealed that while, and despite of the fact that, there are no changes in protein expression or mRNA levels, metabolite production is highly upregulated (40, 70-75). These findings imply activation of post-translational regulation mechanisms.

Redox Homeostasis is an important biological process. Viral infections control redox homeostasis by modulating antioxidant systems. For example, mTORC1 signaling is a vital pathway for HCMV infections (76). Serine 792 of mTORC1 kinase is sensitive to oxidation which leads to deactivation of the enzyme. However, in the course of HCMV infection activity of mTORC1 is preserved despite increased production of ROS, suggesting that a regulatory mechanism is activated (76). HCMV upregulates the glutaredoxin systems to counteract oxidative stress thereby protectingmTORC1 from inhibition by ROS (76). It has also been demonstrated that HCMV upregulates NRF2 a transcription factor that controls antioxidant gene expression and protects HCMV infected cells from oxidative stress and viral reactivation (77). In EBV infections, similarly there is an increase in gene expression of antioxidants proteins, superoxide dismutase and catalase, suggesting that maintenance of redox homeostasis is important for sustained infection and to prevent reactivation of EBV to lytic phase (78). Redox regulation plays a vital role during herpesvirus infection, accordingly, specific viral mechanisms have evolved to prevent oxidative stress.

1.5.3 KSHV and Host Redox Homeostasis

KSHV infections presents with oxidative stress, a hallmark that it shares with various cancer types (79). In 2008 it was shown that cells overexpressing vFLIP/K13 display upregulated

superoxide dismutase via action by NF-kB thereby preventing superoxide induced cell death. This finding has sparked an interest in studying oxidative stress in the context of KSHV infection. Subsequently, Xudong Li et. al., identified that in PEL, oxidative stress induced reactivation of KSHV from latency and cell death. This group showed that inhibition of NF-kB upregulates ROS and depletion of GSH induces KSHV reactivation indicating that ROS is regulated during latency or otherwise can lead to changes on infection rates (80). Furthermore, in primary endothelial cells exogenous treatments of hydrogen peroxide lead to reactivation of lytic gene expression which is dependent on mitogen-activated protein kinase ERK1/2, JNK, and p38 pathways (81). This work shows that KSHV infected endothelial cells are sensitive to oxidative stress, which can trigger reactivation.

On the other hand, two studies revealed that upon initial KSHV infection, hydrogen peroxide is advantageous for viral entry and increases vascular permeability. Guilluy et. al. identified that knocking down Rac1 and inhibition of ROS using a free radical scavenger NAC, resulted in decreased permeability by reducing phosphorylation of VE-cadherin in umbilical endothelial cells (82). In human dermal microvascular endothelial cells (hDMVECs), there is a reduced KSHV LANA gene and protein expression during antioxidant NAC treatment. Furthermore, the antioxidant NAC treatment did not block KSHV binding but blocked the entry of KSHV into hDMVECs by reducing translocation of $\alpha V\beta 3$ and EphA2 activation (83). This data indicates that elevated ROS levels during primary infection are advantageous for successful viral entry.

A previous metabolomics screen performed in the Lagunoff lab measured nearly 200 metabolites and almost one third of these were altered by KSHV infection during latency (40).

Interestingly, several metabolites that were altered are synthesized in the peroxisome either by lipogenesis or lipolysis (DHA-P and DHA, respectively), indicating that these organelles are metabolically active and play an important role during infection. To this day, little is known about the dominant source of ROS during latent KSHV infection. Identification of this source and assessment of effects of its attenuation may provide valuable insights into KSHV biology. Hydrogen peroxide is a byproduct of lipid breakdown by β-oxidation. This suggests that peroxisomes may serve as an important source of ROS.

1.6 Hypothesis

KSHV alters host cell signal transduction to reprogram biological processes to maintain a quiescent infection and avoid reactivation that could elicit an immune response. During latency despite altered metabolism and oxidative stress, KSHV latent viral genes manipulate endothelial cells such that the redox homeostatic levels are altered favoring the tumor microenvironment. Several lines of evidence indicate that cell signal transduction is sensitive to redox switches triggered in the course of the latent infection leading to induction of classical KSHV phenotypes such as spindle cells formation, viral entry**,** reactivation, migration and permeability in PEL and endothelial cells. ROS are known to be generated in the course of the altered metabolism induced by KSHV infection where utilization of the two major carbon sources, glucose and glutamine, is upregulated. These ROS may serve as a mediator influencing redox-sensitive cellular signaling thereby favoring formation of the latent infection microenvironment.

Therefore, I hypothesize that KSHV orchestrates the induction of peroxisome biogenesis to meet the demand for lipid metabolites (DHA) that are upregulated in the course of infection. In

the meantime, KSHV infected cells meet the challenge of increased intracellular levels of ROS created as a by-product of peroxisomal metabolism by upregulating antioxidant systems to counteract the increase. Therefore, identifying targets that are connected with redox homeostasis may provide efficient avenues for drug development and treatment of KSHV tumors.

Chapter 2. Material and Methods

2.1 Cell Culture Systems

Tert-Immortalized Microvascular Endothelial (TIME) cells (84) and primary human dermal microvascular endothelial cells (1° hDMVECs) (Lonza, MD) were maintained as monolayer cultures in EBM-2 media (Lonza or Cellgro) or EndoGrow media (Millipore) supplemented with a bullet kit containing vascular endothelial growth factor, basic fibroblast growth factor, insulin-like growth factor 3, epidermal growth, hydrocortisone, and 5% FBS. iSLK cells (a kind gift from Jae Jung), stably maintaining a selectable GFP-expressing WT KSHV genome (KSHV.219), were maintained in Dulbecco's Modified Eagle Medium (DMEM) media containing 5% FBS, 1% Pen-strep, and 1% L-glutamine selected with puromycin (10 mg/mL), G418 (95 mg/mL) and Hygromycin B (50 mg/mL), as previously described (24,65). Stable LANA expressing TIME cells were previously describe (85).

2.2 Viruses

KSHV inoculum from induced BCBL-1 cells was titered and used to infect TIME cells or 1° hDMVECs as previously described (86). KSHV Bacterial Chromosome virus (KBAC) was obtained from induced doxycycline and sodium butyrate treatments to iSLK cells (a kind gift from

Jae Jung), stably maintaining a selectable GFP-expressing WT KSHV genome (KSHV.219), were maintained in Dulbecco's Modified Eagle Medium (DMEM) media containing 5% FBS, 1% Pen-strep, and 1% L-glutamine selected with puromycin (10 mg/mL), G418 (95 mg/mL) and Hygromycin B (50 mg/mL), as previously described (87, 88). To express the KSHV latent genes in the absence of other viral gene expression, the 12.6 kbp KSHV latency associated region (KLAR) containing the native LANA promoter, LANA, vCyc, vFLIP, all 12 miRNA loci and the kaposins through the native polyadenylation signal downstream of the kaposins, was obtained from the Renne lab. The helper dependent Adenovirus contains the adenovirus packaging signal but no adenovirus genes and was purchased from MicroBix. To create Adenovirus KLAR (AdKLAR) and Adenovirus GFP (AdGFP), the KSHV KLAR region or GFP was cloned into a shuttle vector (pBShuttle) flanked by adenoviral sequences. The KLAR/adenovirus expression cassette was then excised from this plasmid and electroporated into BJ5183 cells (Stratagene) along with pC4Hsu helper adenovirus vector (Microbix Biosystems) to allow for homologous recombination. The resulting plasmid (AdKLAR or AdGFP) was transfected into 293Cre cells, which stably express a Cre recombinase enzyme, selectable with puromycin. Cells were passaged in the presence of helper adenovirus (HD14; Microbix), which contains the adenovirus coding regions and allows to produce AdKLAR adenovirus. The Helper Adenovirus contains a modified packaging sequence flanked by loxP sites; therefore, the helper adenovirus is not packaged due to an excision of the packaging sequences. After expansion of the adenovirus, cells were collected, pelleted, and freeze-thawed three times using liquid nitrogen and 37 C water bath. Cell debris was spun out at 2000rpm and the cell-free supernatant was collected. The cleared lysate was layered onto a continuous 15% to 40% CsCl gradient and centrifuged for 2-3 hours at 35,000g using a SW41Ti rotor (Beckman Coulter, Inc., Fullerton, CA). The mature virus band was collected and purified in a second CsCl

density gradient. The virus band was collected, dialyzed against three changes of A195 buffer. Infections were performed in serum-free EBM-2 medium supplemented with 1µg/mL poly-L-lysine for 1 hour, after which the medium was replaced with complete EGM-2 media. Infection rates were assessed for each experiment by immunofluorescence for LANA, a latent marker, and GFP for AdGFP expression.

2.3 Latent KSHV Infections

KSHV latent infections were performed in serum-free EBM-2 media for 4 hours plus polybrene. Subsequently, media was replaced with complete EBM-2 media, containing serum and supplements. Infection rates were assessed for each experiment by immunofluorescence using LANA, a latent marker, and ORF59, a lytic marker, antibodies. Experiments where greater than 89 % of the cells expressed LANA and less than 5% of the cells expressed ORF59 were used. In a subset of the siRNA transfection experiments, where larger quantities of siRNA were used, there was a slight increase in the cells expressing ORF59, but this always occurred in both the control and gene specific siRNA transfections and did not alter the results of the experiments.

2.4 Reagents

QVD-OPH (SMBiochemicals) was dissolved in DMSO and used at a final concentration of 20 µM. YOYO-1 and SytoGreen24 were diluted in DMSO and used at a final concentration of 100 nM and 50 nM respectively (Life Technologies). 8-plex iTRAQ reagents (AB Sciex) used as included in the product protocol. PMX464 (Tocris) was dissolved in DMSO and used at a final concentration of 500 nM.

2.5 Flow Cytometry Cell Analysis

Mock-, KSHV-infected cells were washed with PBS and removed by trypsinization, fixed, with 4% paraformaldehyde for 30 min on ice and processed for flow cytometry. Cells were permeabilized and blocked with .1% triton and 1% NGS. The ABCD3 transporter was detected with the PMP70 (ABCD3) antibody from thermoscientific, MLYCD from Proteintech Group, PEX3 from Novus a Biotechne brand, PEX19 from Abcam, TXN from Santa Cruz Biotechnology and PRDX1 from Cell signaling Technology. After staining with the primary antibody for 1 hour, the cells were reacted with a secondary Alexa Fluor 594 or Alexa Fluor 488 both anti-rabbit antibodies. Samples were subject to LSR II cytometer for cell analysis and data was analyzed by FLOWJO, a flow cytometry analysis software.

2.6 Confocal Microscopy

TIME cells were seeded on a 4-well glass chamber and were processed for confocal microscopy by fixing in paraformaldehyde (4% in 1XPBS) at 37 °C. Samples were permeabilized with Triton X-100 (0.5% in 1XPBS). Incubations with primary antibodies diluted (1:1,000) in blocking buffer (3% bovine serum albumin [BSA] and 1XPBS) were carried out at room temperature (RT) for 30 minutes. Samples were then incubated with secondary antibodies (Alexa Fluor 594 or 488 anti-rabbit) in blocking buffer for 25 min at RT. Prior to mounting; samples were incubated with DAPI for 5 min at RT coverslips were mounted on microscope slides. Confocal images were acquired using Zeiss LSM 510 Meta confocal microscope Olympus.

2.7 Quantification of Peroxisome Numbers

2-5um Z-stacks were acquired using a Zeiss 510 META confocal microscope equipped with a 63X / 1.4 NA Oil DIC objective. The exported images were then processed using Imaris 7.2.3 software (Bitplane) for peroxisome quantification and ImageJ was use for figure images. Cytoplasmic peroxisomes were quantified based on voxels graphics. The data were then analyzed using student's t-tests.

2.8 Immunoblot Analysis

Cells were harvested and resuspended in RIPA lysis buffer (50 mM Tris-HCl, pH 7.6, 150 mM NaCl, 1 mM EDTA, 1% NP-40, 0.5% deoxycholate, 0.1% sodium dodecyl sulfate, 1 mM sodium orthovanadate, 1 mM sodium fluoride, 40 mM b-glycerophosphate, and Complete Mini protease inhibitor tablet [Roche]), and cell debris was removed after a 30-min incubation by centrifugation. Protein concentrations were determined by the bicinchoninic acid assay (Pierce), and 15 g protein was fractionated on a 4 to 20% sodium dodecyl sulfate-polyacrylamide gradient gel, transferred to Immobilon FL polyvinylidene difluoride membranes (Millipore), blotted with the appropriate antibody (dilutions were 1: 1,000 for anti-TXN, anti-PRDX1, and 1: 10,000 for anti-b-actin), and subsequently probed with secondary antibody IRD680 goat anti rabit IgG (H+L) product # 926-6807 and blots were processed in an auto-processor or scanned and quantified with the Odyssey CLx Infrared Imaging System (LI-COR) for fluorescent blots.

2.9 RNA Isolation and Quantitative RT-PCR Analysis

Cells were washed with PBS twice, followed by centrifugation. RNA was purified using the Macherey-Nagel Nucleospin RNA kit. iScript Reverse Transcription Supermix and SsoAdvanced SYBR Green Supermix (BioRad) were used according to manufacturer's protocols. The primers used were: TXN-F 5' CTT GGACGCTGCAGGTGATA3', TXN-R 5'-TCTGAAGCAACATCCTGACAGT-3', PRDX1-F 5'-GGAAGATGTCTTCAGGAAATGC-3', PRDX1-R 5'-GAATCCACAGAAGCACCAATC-3', ACOX1-F 5'-GGCGCATACATGAAGGAGACCT-3', ACOX1-R 5-AGGTGAAAGCCTTCAGTCCAGC-3', ABCD3-F 5'-GTTCCTTTAGCAACGCCAAATGG-3', ABCD3-R 5'-CTCTTTCCGCAGCCATTTGGAC-3', or GAPDH-F: '5-GGACTCATGACCACAGTCCA-3', GAPDH-R '5-CCAGTAGAGGCAGGGATGAT-3'. Relative levels of SLC1A5 mRNA were normalized by the delta threshold cycle method to the abundance of GAPDH mRNA.

2.10 Measurements of Reactive Oxygen Species

24 hours post transfection TIME cells were seeded in a 6-well plate and 2 hours post seeding cells were infected with KSHV. Upon completion of the infection, cells were loaded with 1uM CELLROX (Invitrogen) for 30 minutes at 37°C under 5% CO_2. After loading, the medium was removed and cells were washed 3 times with 1X PBS, harvested and fixed with 4% paraformaldehyde for 30 min on ice and processed for flow cytometry. Samples were subject to LSRII cytometer and analyzed using FLOWJO, flow cytometry analysis software.

2.11 siRNA Transfection and Cell Death Assay

siRNAs specifically targeting ACOX1 (pre-validated) were purchased from Santa Cruz Biotechnology, negative-control siRNA (siSCRB), TXN and PRDX1 (pre-validated) were purchased from Ambion (Invitrogen Corporate/ Life Technologies). TIME cells were transfected with 3 ug of siRNA using the Amaxa Nucleofector Kit by Lonza per the manufacturer's protocol. At 24-hour post transfection, cells were Mock- or KSHV-infected. At 48 or 96 hpi cells were harvested for subsequent analysis. For cell death, trypan blue assay was used for Chapter 3 and 4 experiments and for chapter 3 upon completion of the infection, cells were washed and treated with complete media containing YOYO-1. Relative fluorescence was measured at 48 hours post treatment using an Incucyte Bioessence.

2.12 Phosphoproteome and Proteome Analysis

2.12.1 Sample Preparation

Approximately 5 million cells were lysed in 2 mL of 8M Urea. Protein concentration was determined by the BCA assay (Pierce). Samples were reduced with 5 mM dithiothreitol at 56 C for 1 hour, and then alkylated with 15 mM iodoacetamide for 1 hour at RT in the dark. Samples were diluted 4-fold with 100 mM Ammonium Acetate, pH 8.9, and digested with Sequencing Grade Modified Trypsin (Promega) at a ratio of 1:100 (trypsin to total protein), overnight at RT. Following digestion, peptides were desalted and concentrated using Sep-Pak Plus C18 cartridges (Waters, cat. no. WAT020515) per the manufacturer's recommendations. Samples were then dried by vacuum centrifugation, lyophilized, and stored at -80 C until further processing.

2.12.2 Isobaric Labeling of Peptide Samples

Phosphorylation samples were labeled with 8-plex iTRAQ reagents (AB Sciex). Lyophilized peptides derived from approximately 1 million cells were resuspended in 30 uL of dissolution buffer (0.5 M $N(Et)_3HCO_3$ pH 8.5-9). iTRAQ labels were resuspended in 70 uL of isopropanol and added to the peptide mixture. Samples were incubated at RT for 2 hours, combined, and dried overnight by vacuum centrifugation. The following day, samples were desalted and concentrated using Sep-Pak Vac 1cc (50mg) cartridges (Waters, cat. no. WAT054955) according to the manufacturer's recommendations. Samples were then dried by vacuum centrifugation, lyophilized, and stored at -80 C until further processing.

2.12.3 IMAC and Phosphotyrosine Enrichment

Approximately 100 uL of packed Ni beads (Ni-NTA Superflow beads, Qiagen) were washed three times in water and stripped with 100 mM EDTA pH ~8.9 for 30 min. Beads were then washed three times with water and once with 80% ACN in 0.1% trifluoroacetic acid. Lyophilized iTRAQ samples were resuspended in 1.5 mL of ACN in 0.2% TFA and incubated with prepared beads for 1 hour at RT. Beads were then washed three times with 80% ACN in 0.1% TFA, and phosphopeptides were eluted from beads with 2 incubations in 75 uL of 1.4% Ammonia. Samples were then vacuum centrifuged down to ~20 uL. 2 uL of 200 mM ammonium formate pH 10 was added and samples were directly analyzed by mass spectrometry.

2.12.4 Mass Spectrometry Analysis

Peptide samples were loaded onto a first-dimension trap column (Waters Xbridge, C18, 10

uM particle size, 100 Å pore size, 4 cm packing length 150 uM column inner diameter). Online peptide separation coupled to MS/MS was performed with a 2D-nanoLC system (nanoAcquity UPLC system, Waters) and a Velos-Pro/Orbitrap-Elite hybrid mass spectrometer (ThermoFisher Scientific). Six discrete elutions were performed at 1.5 uL/min with 5mM ammonium formate pH 10 using increasing concentrations of ACN (1%, 3%, 6%, 15%, 25% and 44%) and diluted with 6 uL/min 0.1% formic acid (FA) prior to loading onto a second dimension trap column (Dr. Maisch ReproSil-Pur, C18, 5 uM particle size, 120 Å pore size, 4 cm packing length 150 uM column inner diameter) connected to an analytical column (Orochem Reliasil, C18, 3 uM particle size, 90 Å pore size, 20-25 cm packing length 50 uM column inner diameter) with an incorporated electrospray emitter. Peptide separation was achieved using a gradient from 3 to 80% (V/V) of ACN in 0.1% FA over 115 minutes at a flow rate of 200 nL/min. The mass spectrometer was operated in data-dependent mode using a Top 10 method. Full MS scans (m/z 300-2000) were acquired in the Orbitrap analyzer (resolution = 120,000), followed by high energy collision induced dissociation (HCD) MS/MS (fm/z 100-2000, resolution = 15,000) at a normalized collision energy of 35%.

2.12.5 Mass Spectrometry Data Processing

MS data files were searched using the COMET (89, 90) algorithm and the output was imported into the Trans-Proteomic Pipeline (91) with the following parameters: variable oxidation of methionine, variable phosphorylation of Serine, Threonine, or Tyrosine, up to 4 variable modifications per peptide, fixed oxidation of Cysteine, and fixed iTRAQ labeling of Lysines and the N-terminus, maximum charge of 7. Peptide false discovery rate (FDR) was set to 5% for

phosphorylation analysis. Peptide quantification based on the iTRAQ labels was determined using the LIBRA software embedded in the Trans-Proteomic Pipeline. Phosphopeptides were normalized to an internal control peptide (VNQIGpTLSESIK) from the enolase digest containing phosphorylated peptides. For each biological replicate, 2 technical replicates were run. A total of 12 fractions for the phosphoproteome, 12 fractions for the proteome and 2 fractions for phosphotyrosine- enriched runs were analyzed. 3,579 peptide spectra profiles were analyzed for the proteome, 4982 for the phosphoproteome including the phosphotyrosine residues. From the phosphotyrosine enrichment 1053 total spectra were analyzed. There was approximately 70% overlap of proteins identified from both technical runs and approximately 50% overlap in the phosphoproteome (S2A Fig).

Each peptide included in the analysis was identified in a minimum of 2 spectra, and each protein included in the analysis was identified by a minimum of two unique peptides. To deconvolve complex overlapping spectra profiles, we used the Hardklör algorithm (92, 93) in conjunction with the MassSpecUtil tool to merge spectra for iTRAQ analysis quantification. This was done to separate any possible overlapping isotopic envelope and providing better peptide identification. Comet search algorithm was used to identify the peptide spectra with a 5% FDR.

To assess significantly changing protein phosphorylation and abundance, peptide-spectrum matches that did not have an intensity of at least 10 in all channels were removed. All channels were median normalized, and the intensities were summed over all peptides of the same protein for each condition. The KSHV-specific effects were assessed by computing the log2(K/M) fold change for the means of the KSHV- (K) and mock (M)-infected biological replicates. A paired t-test was used to calculate the significance of the changes. Each technical replicate was analyzed independently.

2.13 RNA-sequencing

TIME cells were Mock- or KSHV-infected with virus isolated from BCBL-1 cells, as described above, and incubated for 48 hours. Total mRNA was isolated from TIME cells using the NucleoSpin RNA kit (Machery-Nagle, Bethlehem, PA). mRNA was further concentrated and purified using the RNA Clean and Concentrator kit (Zymo Research, Irvine, CA). Purified mRNA samples were processed at the Benaroya Research Institute Genomics core facility and sequenced using an Illumina HiSeq 2500. Image analysis and base calling were performed using RTA v1.17 software (Illumina). Reads were aligned to the Ensembl's GRCh37 release 70 reference genome using TopHat v2.08b and Bowtie 1.0.0 (94, 95). Counts for each gene were generated using htseq-count v0.5.3p9. The data have been deposited in NCBI's Gene Expression Omnibus (96) and are accessible through GEO Series accession number GSE84237.

2.14 Motif Scanning for Transcription Factor Prediction

DNA sequences 1000bp upstream of annotated transcription start sites were downloaded from the Genome Reference Consortium at http://hgdownload.cse.ucsc.edu/goldenpath/hg19/bigZips/upstream1000.fa.gz on May 29, 2015. Position-frequency matrices of 426 motifs were taken from a database of consensus motifs compiled from a variety of experimental techniques downloaded from http://meme-suite.org/meme-software/Databases/motifs/motif_databases.12.11.tgz. For each motif, FIMO software was used to find the top 1000 instances by p-value of each motif in the sequences. A motif was considered to flank a gene if an instance of the motif exists within 1000bp upstream of the gene's transcription start site.

2.15 Wilcoxon Rank-sum Tests for Putative Binding Site Enrichment

For each TF with at least 50 reads in all three mock-infected replicates or all three KSHV-infected replicates, a two-tailed Wilcoxon rank-sum test compared the change in expression post-infection of the genes flanked by of its motif locations to the change in expression of genes that are not. For the test, the genes were ranked by the significance and direction of their change in expression as analyzed by DESeq, where the highest-ranking genes were associated with low DESeq p-values and increased expression post-infection, the lowest-ranking genes were associated with low DESeq p-values and decreased expression, and the intermediate genes had high p-values. The Wilcoxon rank-sum tests compared the sum of the ranks of binding-site- flanked genes to a null normal model.

2.16 Steiner Forest Network Analysis

We conducted network analysis with the Prize-Collecting Steiner Forest (PCSF) algorithm from the Omics Integrator package, which uses msgsteiner for optimization (97). PCSF identifies a sparse sub-network that connects the proteins highlighted by mass spectrometry with the TFs identified by the motif-based analysis. It assigns positive scores (prizes) to the proteins and TFs that reflect how relevant they are to KSHV infection and edge costs to protein-protein interactions that represent how trustworthy they are, with reliable edges receiving lower costs. The sub-network maximizes the cumulative prizes of the included proteins while minimizing the edges costs. It can include Steiner nodes, which are proteins that were not assigned prizes but form critical links

between other proteins. We created an endothelial-specific weighted interaction network by integrating our RNA-seq data with the iRefIndex PPI network (98).

The PCSF algorithm requires protein prizes that quantify how relevant they are to the biological process of interest and PPI edge costs that describe how reliable they are. To calculate protein prizes, we scaled the p-values from the proteomic and phosphoproteomic technical replicates into the range [0,1] by computing $-\log_{10}$(p-value), subtracting the minimum value across all proteins, and dividing by the maximum value across all proteins. Each proteomic and phosphoproteomic replicate was scaled independently. For the TF prizes, we transformed the Wilcoxon rank-sum q-values as $-\log_{10}$(q-value) but did not rescale them. Visualizing the histograms of the proteomic and TF scores revealed that the proteomic scores would dominate the TF scores if the TF scores were rescaled. For each protein, we then selected the maximum score from the two proteomic technical replicates, two phosphoproteomic technical replicates, and TF motif scores, which produced prizes for 3080 unique proteins.

We used the iRefIndex (version 13.0) PPI network (98). The iRefIndex database aggregates PPI from multiple primary interaction databases such as BioGRID (99), DIP (100), HPRD (101), and IntAct (102). All edges represent direct, experimentally-detected physical interactions between two proteins as opposed to predicted PPI or other types of functional relationships. We calculated edge costs between 0 and 1 based on the interaction metadata such as the interaction type, experimental assay, and number of supporting publications as in Ceol *et al.* (103). PPIs identified using reliable, low-throughput experiments (for example, co- crystallization) are assigned much lower costs than interactions detected in large-scale screens. Interactions reported in multiple publications similarly receive lower costs. Low cost edges are more likely to be selected

by PCSF so the PCSF subnetwork preferentially includes trustworthy protein-protein relationships. We created an endothelial-specific network by removing all unexpressed genes from the iRefIndex PPI network, which initially contains interactions from many types of human cells and tissues. Originally, the network contained 175854 interactions among 15404 proteins. After filtering genes that were not expressed at 50 counts or greater in all six of the RNA-seq replicates, the endothelial-specific network contained 121059 interactions among 9489 genes. To select PCSF parameters, we performed a grid search testing all combinations of β from 0.25 to 5.0 with a step size of 0.25, μ from 0 to 1.0 with a step size of 0.005, and ω from 0.5 to 3.0 with a step size of 0.5. Under some parameter combinations, the hub node ubiquitin C (UBC) was directly connected to a large portion of genes in the network so we discarded all networks containing UBC. The parameters β=4.75, μ=0.02, and ω=2.5 produced the largest network without UBC, and we used these parameters for further analysis. We ran PCSF 1000 times with these parameters and additionally set r=0.01 to add random noise to the edge costs. The multiple executions of PCSF with random noise were used to identify parallel paths between proteins in the different runs. Our final network was the union of the 532 of these 1000 PCSF networks that did not contain UBC. The union network contained 1253 interactions among 734 proteins, of which 44 were Steiner nodes. For visualization, we calculated edge frequency as the fraction of the 532 PCSF networks that contain a particular edge. The edge thickness in the network figures reflects edge frequency in the collection of PCSF networks, not the original interaction confidence score in the PPI network.

To assess whether the PCSF subnetworks are specific to KSHV infection, we ran PCSF 1000 times with the same parameters and randomized protein prizes. Each random run reassigned the observed KSHV protein prizes to random proteins in the PPI network. We removed the random

PCSF outputs that contained the hub node UBC and computed node and edge frequencies with the 131 remaining forests.

We supplemented the PCSF union network with KSHV-human protein-protein interactions obtained from VirHostNet 2.0 (39, 104) (downloaded January 7, 2016). We considered only latency-related KSHV genes as defined by Davis *et al*.: K1 (K1_HHV8P), K2 (VIL6_HHV8P), K12A (K12_HHV8P), K12B, K12C, ORF71 (VFLIP_HHV8P), ORF72 (VCYCL_HHV8P), and ORF73 (ORF73_HHV8P). We queried VirHostNet and the Davis *et al*. interactions for all host-virus PPI between these latency-related KSHV genes and any human protein in our PCSF network. We then added all the relevant KSHV-human interactions to our network figures and did not use the PCSF algorithm to filter these edges.

We used WebGestalt (105) to identify KEGG pathways (106) that are enriched for proteins in our PCSF network. Because the predicted network can only contain proteins from the initial iRefIndex interaction network, we used all proteins in the protein-protein interaction network as the reference set. We required a minimum overlap of 5 proteins and used the Benjamini and Hochberg multiple hypothesis test correction (FDR < 10%). To visualize the network regions that are relevant to the enriched KEGG pathways we used Cytoscape (107) to select all proteins in the enriched pathway and their directly connected neighbors in the PCSF network. We then included all KSHV- human PPI that involve the KEGG pathway members and their PCSF neighbors.

Chapter 3. Integrated Systems Biology Analysis of KSHV Latent Infection Reveals Viral Induction and Reliance on Peroxisome Mediated Lipid Metabolism

Adapted from an article originally published in the scientific journal PloS Pathogens

Zoi E. Sychev[1,2], Alex Hu[3], Terri A. DiMaio[2], Anthony Gitter[4], Nathan D. Camp[3], William S. Noble[3], Alejandro Wolf-Yadlin[3] #, Michael Lagunoff[2] #

[1] Molecular and Cellular Biology Program, University of Washington, Seattle, Washington, USA,
[2] Department of Microbiology, University of Washington, Seattle, Washington, USA,
[3] Department of Genome Science, University of Washington, Seattle, Washington, USA,
[4] Department of Biostatistics and Medical Informatics, University of Wisconsin-Madison and Morgridge Institute for Research, Madison, Wisconsin, USA.

3.1 Abstract:

Kaposi's Sarcoma associated Herpesvirus (KSHV), an oncogenic, human gamma-herpesvirus, is the etiological agent of Kaposi's Sarcoma the most common tumor of AIDS patients world-wide. KSHV is predominantly latent in the main KS tumor cell, the spindle cell, a cell of endothelial origin. KSHV modulates numerous host cell-signaling pathways to activate endothelial cells including major metabolic pathways involved in lipid metabolism. To identify the underlying cellular mechanisms of KSHV alteration of host signaling and endothelial cell activation, we identified changes in the host proteome, phosphoproteome and transcriptome landscape following KSHV infection of endothelial cells. A Steiner forest algorithm was used to integrate the global data sets and, together with transcriptome based predicted transcription factor activity, cellular networks altered by latent KSHV were predicted. Several interesting pathways were identified, including peroxisome biogenesis. To validate the predictions, we showed that KSHV latent infection increases the number of peroxisomes per cell. Additionally, proteins involved in

peroxisomal lipid metabolism of very long chain fatty acids, including ABCD3 and ACOX1, are required for the survival of latently infected cells. In summary, novel cellular pathways altered during herpesvirus latency that could not be predicted by a single systems biology platform, were identified by integrated proteomics and transcriptomics data analysis and when correlated with our metabolomics data revealed that peroxisome lipid metabolism is essential for KSHV latent infection of endothelial cells.

3.2 Summary:

Kaposi's Sarcoma herpesvirus (KSHV) is the etiologic agent of Kaposi's Sarcoma, the most common tumor of AIDS patients. KSHV modulates host cell signaling and metabolism to maintain a life-long latent infection. To unravel the underlying cellular mechanisms modulated by KSHV, we used multiple global systems biology platforms to identify and integrate changes in both cellular protein expression and transcription following KSHV infection of endothelial cells, the relevant cell type for KS tumors. The analysis identified several interesting pathways including peroxisome biogenesis. Peroxisomes are small cytoplasmic organelles involved in redox reactions and lipid metabolism. KSHV latent infection increases the number of peroxisomes per cell and proteins involved in peroxisomal lipid metabolism are required for the survival of latently infected cells. In summary, through integration of multiple global systems biology analyses we were able to identify novel pathways that could not be predicted by one platform alone and found that lipid metabolism in a small cytoplasmic organelle is necessary for the survival of latent infection with a herpesvirus.

3.3 Introduction

Viruses have evolved functions to reprogram the proteomic landscape of their host and modulate cellular signaling pathways to adjust the regulation of cellular machinery. These cellular alterations support the survival of infected cells to allow replication and spread of the virus. Many viruses rewire host cell signaling pathways to activate the host cell and to enable lytic replication, and in the case of the herpesviruses, to support long-term latent infection (108, 109). During latency, herpesviruses are known to modulate host cell signaling pathways that lead to inhibition of apoptosis, subversion of the host immune response, and alteration in host carbon and lipid metabolism among many other pathways. Importantly, alteration of these pathways by some oncogenic gamma-herpesviruses may influence tumor formation given the optimal cellular milieu (79, 110).

Kaposi's Sarcoma Associated Herpesvirus (KSHV), a human gamma-herpesvirus, is the etiological agent of Kaposi Sarcoma and two B-cell lymphoproliferative diseases, Primary Effusion Lymphoma (PEL) and Multicentric Castleman Disease (MCD) (4-6). KS is the most common AIDS-associated malignancy worldwide and among the most common tumors overall in Sub-Saharan Africa (111). KSHV is found in the main KS tumor cells, the spindle cells, which are cells of endothelial origin (112, 113). In the KS spindle cells, KSHV is predominantly in the latent state (>90%) where only a handful of the more than 90 annotated viral genes are expressed as well as a number of viral microRNAs (13, 114). A limited number of spindle cells (< 5%) express markers of lytic replication as well (115). While there are limited animal models for the disease, there are well-established mammalian cell culture systems that recapitulate the latent and lytic infection rates seen in KS tumors (33, 116-118). We and others have successfully used these cell culture models to demonstrate that KSHV promotes angiogenesis, modulates carbon utilization

and alters lipid profiles in KSHV latently infected endothelial cells (16, 40, 119, 120). Our previous work showed that latent KSHV infection leads to profound changes in central carbon metabolism and fatty acid (FA) synthesis and that both are required for the survival of latently infected cells indicating the importance of altered metabolism and lipid homeostasis to latent infection (40, 70). Many of these cellular changes induced by KSHV are similar to phenotypes that commonly occur in cancer cells (110).

Several of the signaling pathways modulated by KSHV infection have been studied through traditional approaches of identifying individual host proteins or pathways predicted to play a role in the phenotype investigated. Here we are applying a more comprehensive approach where the global response of cell host in response to KSHV infection during latency at the protein and transcript levels are evaluated. Systems biology approaches can be utilized to identify important cellular networks on a cell-wide scale. In particular, advancement of recent mass spectrometry-based techniques using affinity-based phosphopeptides enrichment coupled with chemical labeling and high-resolution chromatography have been adapted to query changes in protein phosphorylation (89, 121, 122). In addition, the assembly of large-scale, high-quality, protein-protein interaction databases provide an extensive and detailed context for interpreting proteome changes (98). To evaluate gene expression profiles, next generation sequencing technology provides comprehensive analysis of the presence and quantity of the transcriptome. The use of transcriptomics data to predict transcription factor (TF) activity as a function of changes in mRNA provides an effective tool to link proteomics to transcriptomics data (123). The integration of these two different data types has been successfully demonstrated in several biological systems, including glioblastoma (124), breast cancer (125), epithelial-mesenchymal transition (126), yeast salt stress response (127) and influenza virus infection (128). These studies

have provided insights and a comprehensive view of cellular networks from stimuli to gene expression/suppression.

We performed a systems-level data integration approach to identify global changes in cellular networks that are important for KSHV latent infection. To dissect cellular changes and examine the signal transduction from upstream signaling to downstream targets induced by KSHV infection, we first conducted a mass spectrometry-based proteomics and phosphoproteomics analysis, including both tyrosine and serine/threonine phosphoproteomics. We also evaluated gene expression profiles following KSHV infection using high throughput sequencing to generate global cellular transcriptomics data. Virally induced changes in both the proteome and the transcriptome were integrated using an inference algorithm to predict TF activation. A comprehensive protein-protein interaction network was used to identify predicted cellular pathways subverted by KSHV. This integrated systems biology approach identified multiple pathways altered by KSHV infection including peroxisome metabolism.

Peroxisomes have been identified as a nexus of lipid metabolism and signaling (41, 42). While we have previously shown that FA synthesis is required for the survival of endothelial cells latently infected with KSHV, how these downstream FAs are utilized and why they are necessary have not been determined (40). Peroxisomes have been studied in the context of infection with RNA viruses including influenza (43-48). Interestingly, infection with influenza virus led to an increase in peroxisomes while infection with flaviviruses led to a significant decrease in peroxisomes metabolism. Our results show that KSHV latent infection of endothelial cells leads to increased numbers of peroxisomes. One major function of peroxisomes is to metabolize very long chain fatty acids (VLCFAs). Peroxisomal defects have been associated with several clinical disorders, including Zellweger syndrome, a disease characterized by abnormal peroxisome lipid

metabolism presenting with deficiency of ACOX1 function, D-bifunctional protein (D-BP) and X-linked adrenoleukodystrophy (X-ALD) (49). Lipidomics analysis in fibroblasts cells from these patients present with abnormal lipid profiles specifically high levels of VLCFs and low levels of DHA indicating abnormal function of VLCFs breakdown and DHA synthesis (52). ABCD3 is a peroxisomal lipid transporter of VLCFAs involved in transporting 24:6n3, the precursor of DHA (42). After 24:6n3 is transported into the peroxisome; it gets further metabolized by ACOX1, a peroxisomal enzyme. ACOX1 synthesizes DHA by partial β-oxidation of 24:6n3 (50, 51). In the current studies, transient knockdown of ACOX1 and ABCD3 led to cell death in the KSHV latently infected endothelial cells but not the mock-infected control. Overall, these findings validate our integrated global approach and strongly suggest that KSHV modulates peroxisomal lipid metabolism for the increased maintenance of latently infected cells.

3.4 Results

3.4.1 KSHV alters the proteome and phosphoproteome of endothelial cells during latency

To quantify global signaling events modulated by KSHV, we used quantitative phosphoproteomics and proteomics to compare mock and KSHV infected endothelial cells (Figure 3.1A). Tert-immortalized microvascular endothelial cells (TIME) (117) were mock or KSHV infected and harvested at 48 hours- post-infection (hpi), when latency has been established. Three biological replicates were performed with separate infections performed on different days (Figure 3.1A). Latent infection, in greater than 90% of the cells was confirmed by immunofluorescence (IFA) assays. This approach identifies the presence of a latent protein (ORF73) and the absence of

ORF59, a protein marker of lytic infection. ORF59 stained positive in less than 2% of the infected cells in all experiments. To quantify differential peptide expression levels between mock and KSHV infected cells, each sample was chemically labeled with isobaric tags for relative and absolute quantification (iTRAQ) (129) (Figure 3.1A). Peptide quantification was normalized prior to labeling using quantitative fluorometric peptide assay to ensure that similar amounts of peptides were labeled across all samples. Labeled peptides from each biological sample were pooled (Figure 3.1A). Peptides were, then separated, sequenced and analyzed using one or two-dimensional (1D or 2-D) HPLC tandem high-resolution mass spectrometry (LC- MS/MS) for phosphotyrosine enrichment and total phosphroteome and proteome, respectively (Figure 3.1A).

LC-MS/MS analyses were conducted in three stages. First, low-abundance phosphotyrosine (pT) containing peptides were identified and quantified after enrichment by immunoprecipitation (IP) (Figure 3.1A). The IP flow-through was then used to enrich and quantify peptides containing phosphorylated serine (pS), threonine (pT) and the remaining tyrosine residues using immobilized metal affinity chromatography (IMAC). Finally, the IMAC flow-through was used to quantify total protein levels (Figure 3.1A). Upon data acquisition and analysis, we confirmed there was not a statistically significant difference between the mean relative abundance of peptides across the samples, indicating that the sample labeling was equally effective in each case (S_Figure 3.8A-D). A total of 2304 unique proteins from the proteome and 1038 unique phospho-proteins from the phosphoproteome runs were analyzed that includes phospho-tyrosine/threonine and serine. Activation of a phosphorylated residue within the same protein can vary; therefore, we analyzed individual peptides. From the phosphoproteome, we analyzed 1644 unique phospho-peptides, including 175 unique phosphotyrosine peptides that comprised 75 unique phosphotyrosine proteins (Figure 3.1B). The protein and peptide population distribution

for the proteome and phosphoproteome, respectively, were plotted based on the sum of relative peptide intensities from the iTRAQ reporter ions from mock and KSHV infected samples versus log10 of the ratios/fold change of KSHV over mock (Figure 3.1D-E and Table 3-5). Of the 1644 unique phospho-peptides identified, 192 were differentially phosphorylated, of which half were upregulated and half were down regulated (paired t-test $p < .05$). Phosphorylated signal transducer and activator of transcription 3 (STAT3) is the top hit of the tyrosine-phosphorylated residue from the phosphoproteome analysis (Figure 3.1D). Our lab has previously shown that KSHV induces persistent activation of phospho-STAT3 during latency validating the our phosphoproteome results (86). From the upregulated hits including both phosphoproteome and proteome, there are several proteins involved in metabolism, immunity, insulin resistance, endocytosis, NFk-B signaling and others, providing potentially interesting targets for future studies. From the proteome analysis, we measured 2304 unique proteins among which 289 were altered by KSHV latent infection; 164 were upregulated and 125 downregulated. This corresponds to viral induced changes in 13% of the proteins detected and 12% of the phosphorylated residues, including unique phosphotyrosine (Figure 3.1B). Kyoto Encyclopedia of Genes and Genomes (KEGG) pathway analysis of the phosphoproteins and proteins measured and altered during KSHV infection identified several pathways consisting of more than 4 proteins annotated (106) (Figure 3.1C). These pathways include metabolic processes involved in carbon and lipid metabolism as well as hypoxia inducible factor (HIF) signaling, both of which had been previously associated with KSHV latent infection, providing internal positive controls for our proteomic data (16, 70, 130). Gene Ontology analysis also provided similar results (S_Figure 3.9 2B).

3.4.2 KSHV alters the cellular transcriptome of endothelial cells during latency

To identify changes at the transcriptional level, high throughput cDNA sequencing from mRNA was performed to identify genes expression differences between mock and KSHV infected endothelial cells at 48 hpi. Three separate mock and KSHV infections of TIME cells performed on different days were analyzed by high throughput sequencing of cDNA. Expression of 12,375 cellular genes in all replicates were identified. Of the genes measured, 985 cellular genes were significantly upregulated following KSHV infection of endothelial cells and 1,134 were significantly downregulated at a 1% FDR using a method based on the negative binomial distribution (Figure 3.2A and S_Figure 3.9 A).

3.4.3 Putative transcriptional regulators inferred in KSHV latently infected endothelial cells

The transcriptomic data was used to predict the activities of transcription factors based on binding motifs in the promoter regions of transcripts that are activated or repressed following latent KSHV infection. The enrichment of a motif in the promoters of genes whose expression is significantly altered implicates the motif's associated TF as a possible regulator (Figure 3.2B). The software FIMO identified putative binding sites by motif presence (131), and two-sided Wilcoxon rank-sum tests (132) quantified and assigned p-values to the enrichment of those binding sites in promoters of genes significantly changed in expression after KSHV infection (Figure 3.2B).

FIMO was used to scan for the locations of 426 TF binding motifs, from a curated database of position-weight matrices compiled and derived from multiple experimental types, in 1000bp regions upstream of annotated transcription start sites (123). The enrichment scores of the 261

motifs whose corresponding TF's mRNAs were reliably detected in the RNA-seq data and the mRNA's fold-change in expression after KSHV infection (Figure 3.2C). A positive enrichment z-score indicates that the motif's putative target genes increase in expression on average, and a negative enrichment score indicates that the motif's putative target genes decrease in expression on average. Wilcoxon rank-sum tests assigned statistical significance to the motif enrichments and found that five motifs were significantly enriched at a 5% FDR (p-value < 0.001) and twenty-four more were enriched at a less stringent cutoff of p-value < 0.05 (Figure 3.2C).

The motif of four of these TFs, interferon regulatory factors 1, 2, 7 (IRF1, IRF2, IRF7) and STAT2, are enriched only in upregulated promoters. However, because the motifs for these factors are similar (S_Figure 3.10C), it is not clear which of the TFs or TF complexes are actually relevant from just the motifs. The mRNA of IRF1 exhibits a 3.3-fold increase in gene expression (p-value < 0.001) as measured by our transcriptomics data, which may imply that IRF1 is a more relevant player. A motif associated with the transcriptional repressor zinc finger protein 148 (ZNF148), was significantly enriched in downregulated promoters (S_Figure 3.10C), suggesting that ZNF148's repressor activity increased post-infection. The repressor E2F5's motif was also significantly enriched in downregulated promoters (p-value = 0.0038). It has been shown that E2F5 is inhibited by retinoblastoma protein 1, which is directly inhibited by the KSHV protein, LANA (133). These data support that motif enrichment scores can successfully denote prediction of transcription factor activity for use in the analyses below.

3.4.4 Integration of proteomic and transcriptomic data of endothelial cells latently infected with KSHV into a single network model

To build a comprehensive network model that describes the host response to viral infection, we used the Prize-Collecting Steiner forest algorithm to integrate the proteomic and TF motif analyses (134). This algorithm parsimoniously identifies the protein-protein interaction most likely to be relevant for connecting the relevant factors identified in the two types of analyses. In addition, it identifies Steiner nodes, which are proteins that were not implicated in the proteomic or TF analyses but form crucial connections between other important proteins identified as altered by KSHV in the global data sets generated. The proteomic data was integrated with the TF enrichment scores rather than the differentially expressed genes from the RNAseq data because TF transcript levels do not necessarily reflect regulatory activity (135). When combining gene expression data with other types of protein scores for pathway reconstruction, it is therefore preferable to use inferred TF activities (124, 125, 128, 136). The complete predicted Steiner forest network is large, connecting hundreds of proteins that respond to KSHV infection and the TFs inferred to regulate the transcriptional changes (S_Figure 3.11). Randomization analysis shows that the selected proteins and interactions are specific to KSHV infection and do not reflect biases in the protein-protein interaction network or Steiner forest algorithm (S_Figure 3.14 A-B).

To focus on specific biological functions, we assessed the overlap between the proteins in our Steiner forest network and KEGG pathways. We required a minimum overlap of 5 proteins and used the Benjamini and Hochberg multiple hypothesis test correction (FDR < 10%). The significantly enriched pathways included pathways involved in phagocytosis, immune response and several metabolic processes among others (Figure 3.3A and Table 1 for complete list). Our lab has shown that metabolism is altered during latent KSHV infection, including carbon and lipid

metabolism, which supports our integrated network analysis (40, 70, 130). There are several interesting pathways that are predicted to be altered during KSHV latent infection (Table 1). From this analysis, we decided to follow up on proteins that clustered together, particularly those involving peroxisome metabolic lipid signaling. We have previously identified that lipid metabolism is required during latency (40) , but how these metabolites are further utilized during KSHV latent infection still unknown. Therefore, we chose to further analyze activation of peroxisomes by KSHV. Peroxisome related proteins identified in the subnetwork including SCP2, PRDX5, ACSL3, MLYCD, AGPS, EHHADH, PEX19 were upregulated following KSHV infection and two Steiner nodes PEX12 and PEX5 were predicted by the algorithm to be activated by KSHV (Fig 3C). The proteins in this cluster are involved in lipid metabolism (SCP2, ACSL3, MLYCD, AGPS, EHHADH) and peroxisome organelle biogenesis and transport (PEX19, PEX12 and PEX5). Therefore, this sub- network predicts that KSHV induces peroxisome pathways involved in lipid metabolism and biogenesis. In addition, IRF3 is an interferon inducible gene activator that was predicted in the TF analysis to have increased transcriptional activity. It is not annotated as a peroxisome pathway protein, but the Steiner forest algorithm includes IRF3 in our peroxisome subnetwork due to its predicted relationship with PEX19 and previous evidence of a direct IRF3-PEX19 interaction (137) cataloged in the iRefIndex database. This observation suggests that peroxisomes might also play a role in immune signaling during latency, which might be an important regulatory control point of KSHV infection.

In addition, we incorporated a protein-protein interaction database from a study that mapped global interactions between KSHV genes and host proteins using viral gene pulldowns (39). Since our study is mainly focused on latency, we included only the KSHV latent viral proteins and host proteins hits with our predictive Steiner forest network. From the database, we found that

two viral genes have been shown to interact with proteins associated with peroxisome biogenesis. The latent KSHV proteins that are predicted to be associated with peroxisome biogenesis are shown as purple diamonds in figure 3.3C. The KSHV protein-protein interaction database used total protein pull downs and therefore does not demonstrate direct interactions, rather it shows associations with the identified protein. All the proteins from the KSHV major latent locus were included in the Steiner forest analysis shown in figure S_Figure 3.11. The utilization of KSHV protein-protein interaction dataset with the other protein-protein interaction databases advances our predictions of pathways that could be important to KSHV pathogenesis.

3.4.5 KSHV upregulates peroxisome formation during latent infection

To validate the prediction that peroxisome pathways involved in lipid metabolism and likely peroxisome biogenesis are increased during latent infection, we examined the protein levels of ABCD3, an ATP Binding Cassette Subfamily D Member 3, a lipid transporter specific to peroxisomes and a common marker to study peroxisomes, using flow cytometry at 48 and 96 hpi (Figure 3.4A-H). Staining with an antibody to ABCD3 showed a significant increase in fluorescent staining in the KSHV infected cells compared to mock infected cells in three different infections at 48 and 96 hpi in TIME cells and 96 hpi in primary human dermal microvascular endothelial cells (hDMVECs) and lymphatic endothelial cells (LECs) (Figure 3.4E-H), indicating that during latent infection KSHV significantly upregulates ABCD3 protein expression. In addition, we evaluated MLYCD and PEX19 and a non-clustered peroxisome protein PEX3 levels, in TIMECs, hDMVECs and LECs. PEX3 is a PEX19 docking factor required for PEX19 to deliver proteins into the peroxisome matrix (138). Staining with MLYCD and PEX3 antibody showed a significant

increase of the protein levels in KSHV infected TIME cells, primary hDMVECs and primary LECs compared to mock infected at 96 hpi (S_Figure 3.13 A-F) while PEX19 was significantly upregulated in TIME cells (S_Figure 3.13).

We next evaluated the peroxisome organelle number using confocal imaging analysis of mock and KSHV infected TIME cells stained with antibody to ABCD3. Peroxisome size ranges approximately between .4-1 uM. We evaluated 3D particles using z-stacks imaging and then quantified the particle number as a proxy of peroxisome organelle per cell with a minimum threshold of .5 uM. There is an approximately 50% increase in the number of peroxisomes per cell in the KSHV infected endothelial cells as compared to mock infected cells (Figure 3.4I-J). Representative pictures of the mock and KSHV infected cells stained with an antibody to ABCD3 are shown in figure 3.4I. Combined, these observations support the prediction from the Steiner forest analysis that KSHV promotes peroxisome biogenesis.

3.4.6 KSHV latent locus is sufficient to induce peroxisome lipid transporter

To determine that the increase of peroxisome numbers per cell was not a cellular response to infection but rather induced by virally encoded genes, cells infected with UV irradiated KSHV were stained with ABCD3 antibody and measured by flow cytometry. UV irradiated virus can bind and enter cells but does not express viral genes. Flow cytometry analysis showed no increase in the expression of ABCD3 following infection with UV irradiated virus (Figure 3.5A and B). Therefore, the increase of ABCD3 in latently infected cells requires KSHV gene expression and it is not a cellular response to virus entry into the cell.

The KSHV latent locus is comprised of LANA, vCyclin, vFlip, Kaposins and 12 microRNA loci. To assess the role of the KSHV latent locus in increasing the number of peroxisomes, we evaluated whether the KSHV latency associated region (KLAR) is sufficient to induce the increase of ABCD3 protein expression levels. The KLAR locus (a kind gift from Dr. Rolf Renne) was cloned into a helper-dependent gutted adenovirus vector that does not express any adenovirus genes. Cells were infected with a control gutted adenovirus (Ad) only expressing GFP (AdGFP) and the gutted adenovirus expressing KLAR (AdKLAR) and stained with ABCD3 antibody. Infection rates for AdGFP and AdKLAR were 59% and 97% respectively as determined by expression of GFP or LANA. To adjust for the differences in the infection rates, we gated on the GFP positive cells from the AdGFP infected cells and then compared to the AdKLAR cells. Cells infected with the AdKLAR expressing gutted adenovirus exhibited increased ABCD3 protein expression compared to mock infected cells and AdGFP (Figure 3.5C and D). Therefore, the latency genes are sufficient to induce ABCD3 protein expression levels.

3.4.7 KSHV requires peroxisome proteins involved in lipid metabolism during latent infection

Peroxisomes are involved in lipid signaling and metabolism. Our previous metabolomics screen indicated that several lipid metabolites are altered by KSHV during latent infection of endothelial cells, including two metabolites generated in the peroxisome, dihydroxyacetone phosphate (DHA-P) and docosahexaenoate (DHA; 22:6n3) (40) and metabolites upstream of DHA are also upregulated as indicated in red numbers (Figure 3.6A). DHA is synthesized from 24:6n3 by Acyl-CoA Oxidase 1 (ACOX1) an enzyme mainly expressed in the peroxisome and it is

involved in the first step of peroxisomal β-oxidation (50) (Figure 3.6A). To determine if ACOX1 is necessary during KSHV latent infection, small interfering RNA (siRNA) was used to knockdown its gene expression (Figure 3.6B). Loss of ACOX1 did not alter the cellular proliferation of uninfected cells or the KSHV infection rates but resulted in a significant increase in cell death of the KSHV infected cells compared to controls at 96 hpi (Figure 3.6C-E). As ACOX1 is the main enzyme involved in metabolizing DHA, these observations suggest that DHA might be required during infection.

The precursor of DHA, 24:6n3 is transported into the peroxisome by the lipid transporter ABCD3 (42, 139). Therefore, we evaluated if ABCD3 is required during latency by transiently silencing its gene expression. Similarly, to ACOX1, loss of ABCD3 did not alter cellular proliferation of uninfected cells or KSHV infection rates but resulted in a significant increase in cell death of the KSHV infected cells compared to controls at 96 hpi (Figure 3.6C-E). Therefore, both ACOX1 and the ABCD3 transporter are required for the survival of endothelial cells latently infected with KSHV. In parallel, we treated cells with a pan-caspase inhibitor, QVD, to test whether apoptosis was the main cell death mechanism. KSHV-siABCD3 and KSHV-siACOX1 cells treated with QVD showed a 3-fold decrease in cell death, indicating that apoptosis was the main cell death mechanism (Figure 3.6D). Therefore, this data strongly indicates that peroxisomal proteins involved in lipid metabolism are required for the survival of endothelial cells latently infected with KSHV.

3.5 Discussion

We integrated transcriptomics, proteomics and metabolomics analyses, to provide a comprehensive view of cell signaling in an oncogenic virus infection in human endothelial cells, the cell type likely to be most relevant to KS tumor cells (Figure 3.7). From quantitative measurements of the phosphoproteome and proteome analysis of endothelial cells latently infected with KSHV, we found that latent infection alters the levels of at least 289 proteins, approximately 13% of the proteome quantified, as well as 192 altered phosphorylation sites, approximately 12% of the phosphosites quantified in this study. Previous studies using mass spectrometry based proteomics and KSHV, was done with targeted proteomics to identify protein-protein interactions specific to single viral proteins, LANA and K5 for example, using immunoprecipitation and 2D-gel mass spectrometry (38, 140-149). Our dataset is the first that we are aware of, that analyzes the global response to latent KSHV infection with both phosphoprotein and proteomic studies in endothelial cells. The list of phosphosites altered by KSHV infection may provide deeper insights into cell signaling activation following KSHV infection of endothelial cells and should serve as a useful dataset for future studies. From transcriptomics analysis, we found that KSHV infection leads to alterations in approximately 17% of the host cellular transcriptome. This dataset was generated using next generation sequencing providing more comprehensive gene expression profiles in endothelial cells latently infected with KSHV than previously published. Transcriptomic analysis of KSHV infection has been done in KS tumors and in PEL cells, but only older microarray technology for endothelial cells has been previously done (150-158). The activity of several TFs was predicted to be activated or repressed by latent infection as identified from transcription factor motifs found in the promoters of host genes that were up or down regulated following KSHV infection of endothelial cells. These TFs serve as a link to map protein-protein

interactions, connecting upstream signaling to downstream gene-expression targets. The goal of this integrated systems biology approach was to identify novel pathways that could not be predicted by one platform alone. Various functional networks, including phagosomes, endocytosis and multiple metabolic pathways including peroxisome biogenesis were identified by the Steiner forest analysis providing a rich data set for future studies. We chose to further analyze peroxisome biogenesis as peroxisomes are involved in several pathways likely to be important for KSHV pathogenesis including redox control and the breakdown of very long chain fatty acids. A sub-network cluster of peroxisomal proteins predicted to be activated by the Steiner forest analysis is shown in figure 3.3C. The presence of this sub- network implies increased peroxisome activity in KSHV latently infected endothelial cells. The integrated analysis is further substantiated by a significant increase in the number of peroxisomes per cell during KSHV latency, induced specifically by KSHV latent gene expression as opposed to a cellular response to a viral infection. Upregulation of peroxisomes was further validated by identifying the upregulation of several peroxisomal proteins in TIME cells, primary dermal microvascular endothelial cells as well as in primary lymphatic dermal microvascular endothelial cells, the cell type that most closely resembles KS spindle cells (158).

We previously found that KSHV latent infection dramatically alters the lipid profile of endothelial cells (40). In the KSHV infected cells, there was a significant increase in most of the LCFAs measured. We also found that FAs synthesis was necessary for the survival of endothelial cells latently infected with KSHV (40). In our metabolomic screen we also noted that DHA and its precursors, as well as DHA-P, were increased following KSHV infection during latency (40) (Figure 3.6A). DHA is an important metabolite involved in anti-inflammatory responses and

cellular development and is mainly produced in the peroxisome by partial β-oxidation (50, 51, 159). Knockdown of ACOX1, the enzyme that produces DHA, results in a significant increase in the death rate of latently infected endothelial cells but not their mock infected counterparts. Furthermore, the peroxisome-specific lipid transporter ABCD3, which transports VLCFAs including a precursor of DHA, is also essential for KSHV-infected endothelial cell survival. Therefore, lipid metabolism in the peroxisome is essential for the survival of endothelial cells latently infected with KSHV.

Peroxisomes appear to play a role in the response to lytic viral infection for several viruses. This organelle serves as a signaling platform for antiviral response against unrelated non-enveloped and lipid-enveloped RNA and DNA viruses including Reovirus, Sendai virus, Dengue virus and Influenza virus in infected mouse embryonic fibroblast cells (44-47). Interestingly, one study established that Influenza virus modulates and requires peroxisomal ether lipid metabolism for efficient virion replication in A549 epithelial cells (45). These observations underscore complex and sometimes paradoxical cellular changes that involve peroxisomes during viral infection; while Influenza requires peroxisome metabolism for virion production, peroxisomes also play an important role in the immune response triggered by infection. The interplay between peroxisome responses and viral infection may depend on the cellular environment and virus type. Our study elucidates a novel mechanism by which a latent herpesvirus infection manipulates peroxisomal lipid signaling required for survival in a long-term infection.

KSHV is known to activate COX-2/PGE2/EP vector during *de novo* infection mediating an underlying pro-inflammatory state conducive to long-term latency (120). COX-2 converts Arachidonic Acid (20:4n6, or AA) to PGE2, which then regulates autocrine and paracrine

signaling. Our previously published metabolomics screen demonstrates that KSHV latent infection upregulates precursors of the COX-2/PGE2/EP signaling, such as AA indicating that signaling upstream of the COX-2/PGE2/EP pathway is active during latency. Furthermore, upregulation of DHA-P and DHA as shown by our metabolomics screen indicates, that the peroxisomes are enzymatically active and producing these metabolites (41). Therefore, the peroxisome represents a crossroads of lipid signaling and bridges the gap between upstream essential fatty acids (AA, EPA and DPA) and how they are metabolized downstream (DHAP, DHA) during latent KSHV infection (Figure 3.6A).

AA is a pro-inflammatory metabolite and DHA has been associated with anti-inflammatory responses (160); however, both are upregulated during latency. The KS tumor environment is characterized by a chronic inflammatory state (13). Therefore, we hypothesize that KSHV commandeers control of cellular metabolic pathways to fine-tune a higher level of chronic inflammation by altering homeostatic mechanisms and maintaining a shifted equilibrium in this new inflammatory state required for the maintenance of latency. Further work is required to elucidate whether the primary role of peroxisomes is to regulate lipid signaling and inflammation, if peroxisomal ether lipid metabolism is required or if peroxisomes are also involved in regulating H_2O_2, which often occurs in parallel. It has been shown that in primary endothelial cells during exogenous stress, inflammatory cytokine expression is downregulated by using DHA as anti-inflammatory treatment (161). It would be interesting to determine if altering DHA synthesis influences inflammatory signaling proteins in endothelial cells latently infected with KSHV.

Currently, pharmacological approaches that target herpesvirus infection focus on lytic replication and there are no treatments specific for latent infections. Since KS tumors primarily

exhibit latent infection, this study elucidates critical control point mechanisms in the latent phase offering an understanding of KSHV viral pathogenesis and provides potential novel and combinatorial molecular therapeutic targets through large scale identification of pathways activated by KSHV latent infection of endothelial cells.

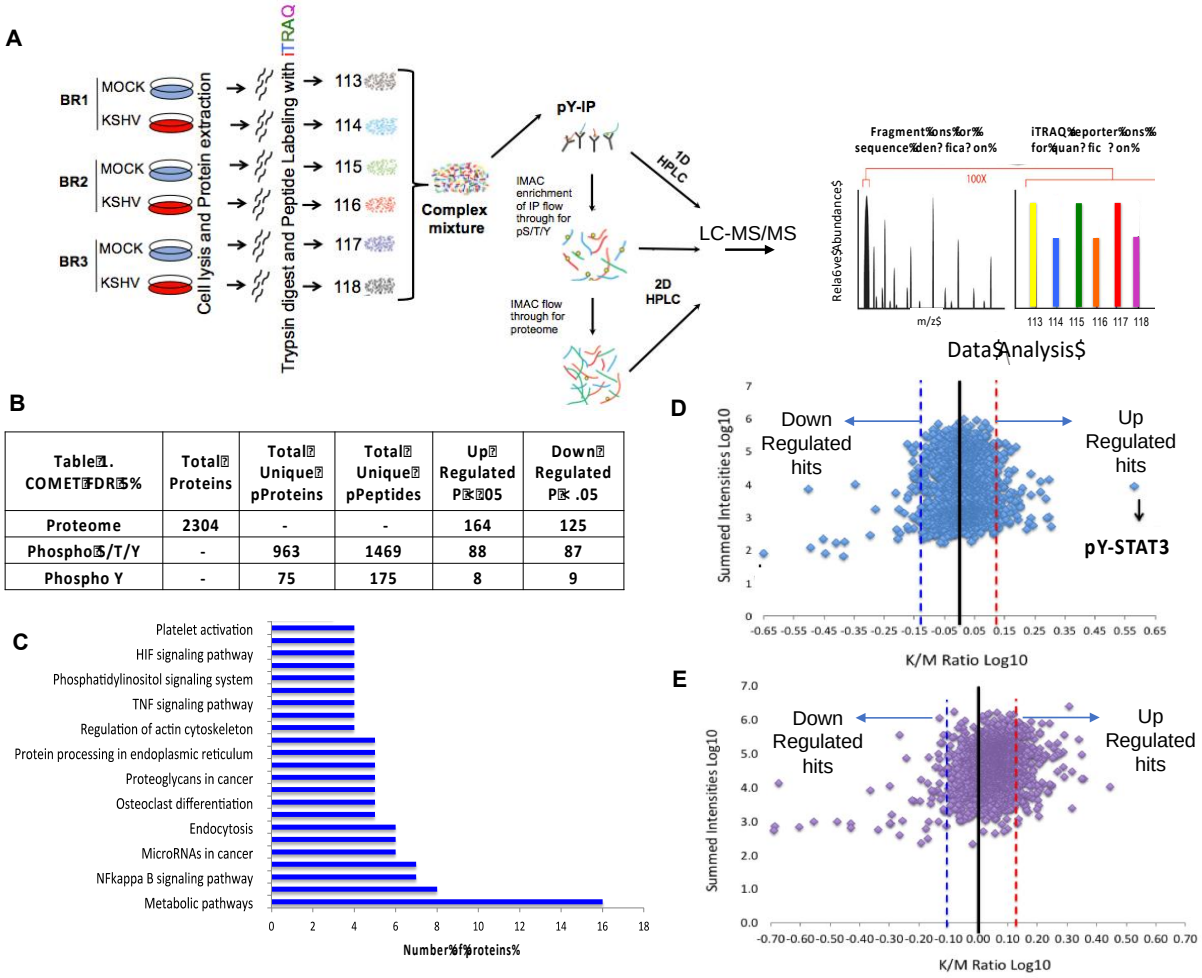

Table 1. COMET FDR 5%	Total Proteins	Total Unique pProteins	Total Unique pPeptides	Up Regulated P< .05	Down Regulated P< .05
Proteome	2304	-	-	164	125
Phospho S/T/Y	-	963	1469	88	87
Phospho Y	-	75	175	8	9

Figure 3.1 Phosphoproteome and Proteome Profiling of endothelial cells infected with KSHV. A.) Overview of the workflow of proteomics and phosphoproteomics sample preparation and data collection. TIME cells were infected with KSHV derived from BCBL-1 cells and harvested 48 hpi, labeled with iTRAQ and used for tyrosine phospho-proteomic analysis, global phosphoproteomic analysis, including serine and threonine phosphopeptides, and global proteomic analysis using LC-MS/MS. Biological Replicate (BR), Immunoprecipitation (IP), phosphotyrosine, phosphoserine, phosphothreonine (pY/pS/pT), 1-dimesional or 2- dimensional High Pressure Liquid Chromatography (1D HPLC, 2D HPLC) Liquid Chromatography Mass Spectrometry (LC-MS/MS). **(B.)** Table showing the number of proteins detected and the upregulated and downregulated proteins in the proteome as well as the specific phosphopeptides detected from the phosphoproteome following KSHV using Comet peptide search algorithm 5% FDR and $p < .05$. **(C.)** KEGG pathway analysis of the upregulated hits of the phospho and proteome analysis. **(D and E.)** Scatter plots demonstrating changes in relative abundance for the peptides detected in the phosphoproteome **(D)** and total proteome **(E)** following KSHV 48 hpi. The dotted lines represent the significance cut off where the points to the right of the red dotted line are up significantly upregulated hits and points to the left of the blue dotted line are significantly downregulated hits.

A.

Negative binomial distribution, FDR 1%	Total Transcripts	Up Regulated	Down Regulated
Transcriptomics	12375	985	1134

B.

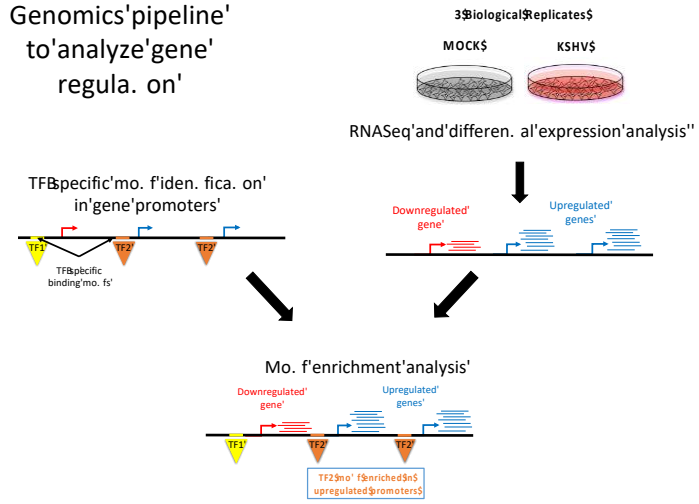

C.

TF	Enrichment z-score	p-value	False Discovery Rate (q-value)	Expression Fold Change post-infection
IRF1	5.58	2.37E-08	9.98E-06	3.30
IRF2	5.04	4.67E-07	9.82E-05	1.30
STAT2	4.39	1.14E-05	0.001594	1.27
ZN148	-3.57	0.000356	0.025458	0.99
IRF7	3.57	0.000363	0.025458	1.31
IRF3	3.25	0.001163	0.061221	1.24
E2F5	-2.89	0.003805	0.160207	1.28
RXRA	2.86	0.004294	0.164357	0.80
RFX2	2.75	0.006045	0.184256	1.47
ATF1	2.68	0.007339	0.187541	0.84
ERR1	2.65	0.008018	0.187541	0.96
PO6F1	2.54	0.010989	0.24349	0.94
USF2	-2.51	0.012125	0.255224	1.07
TFAP4	2.38	0.017255	0.318914	1.53
STAT1	2.35	0.018786	0.318914	1.59
ATF2	2.33	0.019695	0.318914	0.96
ATF4	2.33	0.019695	0.318914	0.81
CREB1	2.33	0.019695	0.318914	0.96
FOXJ2	-2.29	0.021861	0.335291	0.92
PRDM1	2.29	0.0223	0.335291	1.17
GCR	2.17	0.030239	0.409133	0.85
SNAI1	-2.15	0.03162	0.409133	2.26
KLF3	2.13	0.032863	0.409133	0.96
SP4	-2.13	0.033042	0.409133	0.87
NR2C2	2.09	0.036184	0.415682	0.91
E4F1	2.09	0.036533	0.415682	1.09
COT2	2.07	0.038186	0.423055	1.15
TFCP2	-2.05	0.040599	0.438257	1.02
PEBB	2.00	0.045393	0.477758	1.23

Figure 3.2 Transcription factor (TF) enrichment analysis. (A) Total mRNAs identified in the endothelial cells and the numbers upregulated and downregulated following infection with KSHV using a negative binomial distribution with an FDR% of 1 **(B.)** Schematic of RNAseq and TF enrichment analysis. Three biological replicates of KSHV infected endothelial cells harvested at 48 hpi for RNAseq of mRNA were analyzed. TF-specific binding motifs identified upstream of transcription start sites and differential expression p-values between mock and KSHV-infected cells from RNASeq data were used for the motif enrichment hypothesis tests. Colored arrows represent transcription start sites. Red and blue lines represent downregulated and upregulated transcripts, respectively. Triangles represent transcription factors binding upstream of transcription start site. **(C.)** List of significant TFs that are predicted to be altered by KSHV during latency with a $p < .05$ that were used for the Steiner forest analysis.

A.

Pathway name	# Genes	Adjusted p-value
Phagosome	17	0.0104
Endocytosis	20	0.0152
Citrate cycle (TCA cycle)	6	0.0234
Propanoate metabolism	6	0.0243
Leukocyte transendothelial migration	13	0.0243
Regulation of actin cytoskeleton	19	0.0389
Oxidative phosphorylation	12	0.0389
Adherens junction	9	0.0389
Fc gamma R-mediated phagocytosis	10	0.0578
Lysine degradation	6	0.0578
Peroxisome	9	0.0578
Cell cycle	12	0.0628

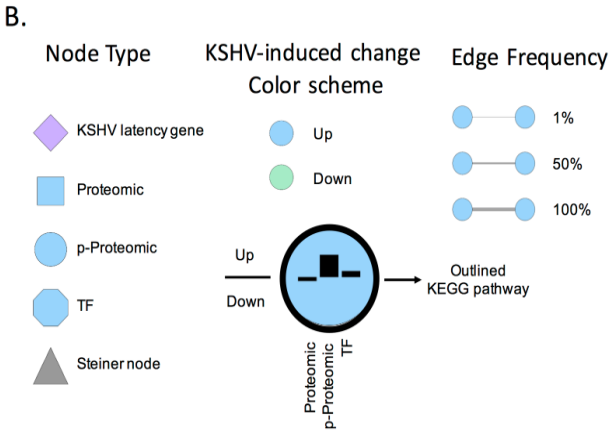

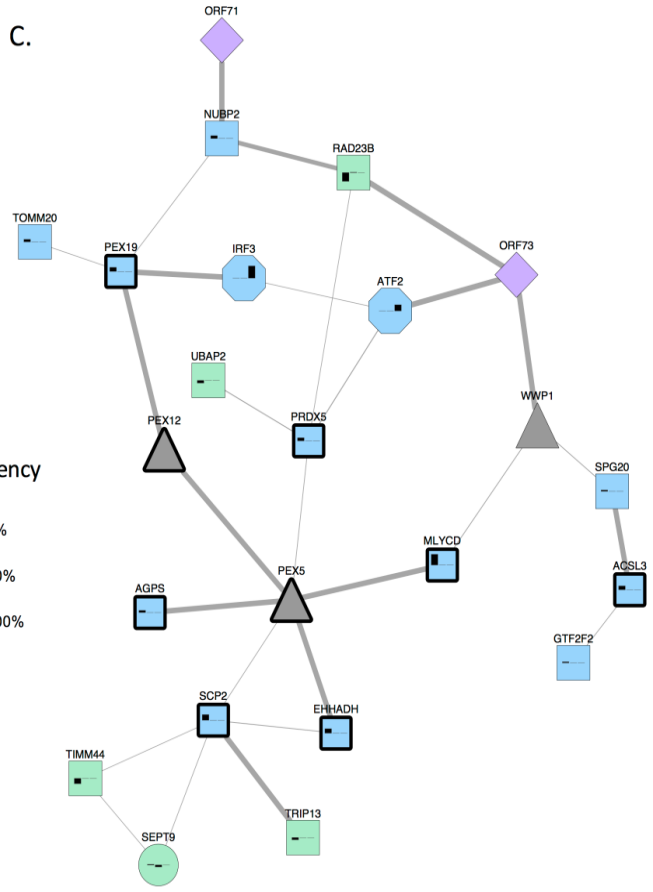

Figure 3.3 Steiner forest prediction of pathways activated by KSHV infection. (A.) List of the top KEGG pathways predicted to be altered by KSHV infection of endothelial cells from Steiner forest network and KEGG pathways database analysis (complete list in S1 Table). **(B.)** The bar graph on each node displays a signed version of the prizes used as input for the Steiner forest analysis. Each bar from left to right indicates the proteomic, phosphoproteomic (p-Proteomic), and TF scores. Positive scores (above the horizontal line) indicate the protein had higher intensity or the TF's target genes were more highly expressed in KSHV infection than mock infection. Negative scores indicate that KSHV infection decreases intensity or lowers activity. Node color indicates whether the protein primarily upregulated (blue) or downregulated in response to viral infection (green). Node shape indicates the largest score for that protein: proteomic (square), phosphoproteomic (circle), TF (octagon), or Steiner node with no score (triangle). Latency-related KSHV genes are shown as purple diamonds. Steiner nodes are shown in gray. Edge thickness indicates the fraction of Steiner forest networks that contain the edge when the algorithm is run multiple times. **(C.)** Proteins with bold borders are peroxisome pathway members: SCP2, PRDX5, ACSL3, MLYCD, AGPS, EHHADH, PEX19 and two predicted Steiner nodes, PEX12 and PEX5. Their direct neighbors in our KSHV network are displayed as well to show their relationships. A Full Steiner forest is shown in figure S_Figure 3.11.

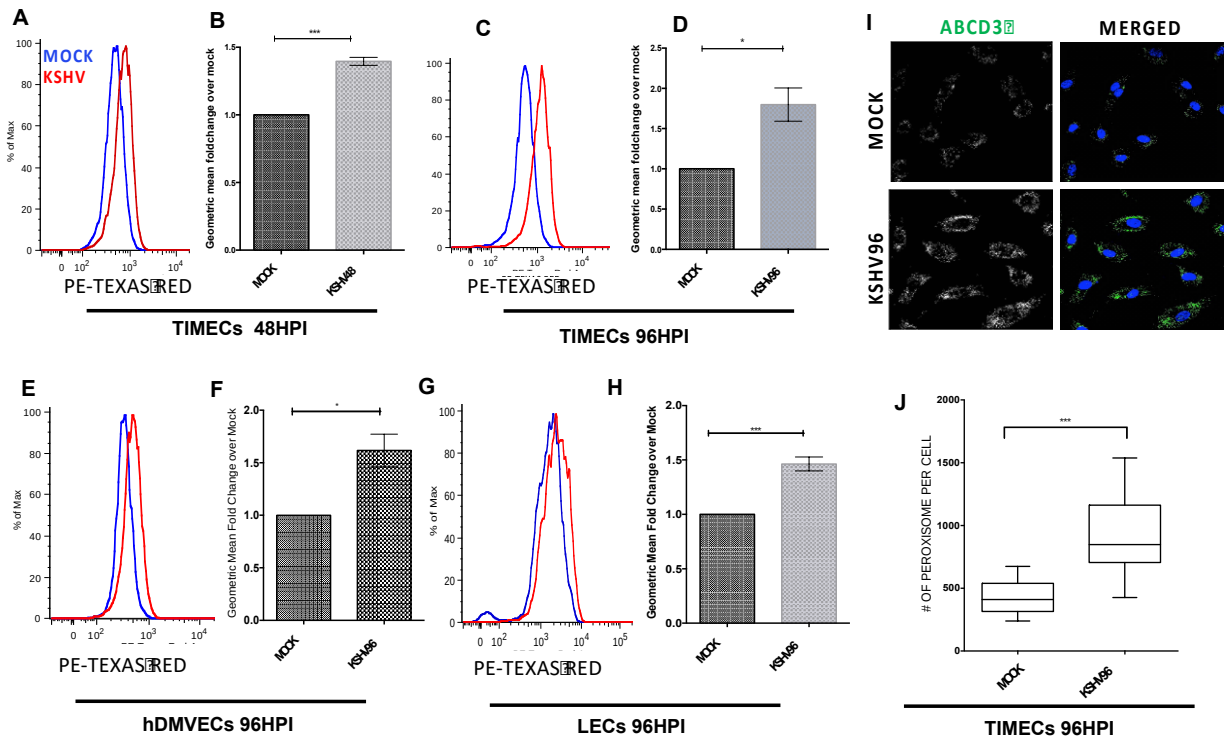

Figure 3.4 KSHV latently infected endothelial cells induces peroxisome formation. (A.) Flow cytometry of mock- and KSHV- infected TIME cells (TIMECs) harvested at 48 hpi, fixed and stained with antibody to ABCD3, a peroxisome marker. **(B.)** Geometric mean fold change of KSHV over mock at 48hpi for 3 experiments as in panel A, $p < 0.05$ student's t-test. **(C.) Flow cytometry of** mock- and KSHV- infected TIMECs, harvested at 96 hpi, fixed and stained as in panel A. **(D.)** Geometric mean Fold change of KSHV over mock at 96 hpi for 3 experiments as in panel C, $p < .05$ student's t-test. **(E.)** Flow cytometry of mock- and KSHV- infected primary human dermal microvascular endothelial cells (hDMVECs) harvested at 96 hpi, fixed and stained as in A. **(F.)** Geometric mean fold change of KSHV over mock at 96 hpi for 3 experiments as in E, $p < .05$ student's t-test. **(G.)** Flow cytometry of mock- and KSHV- infected lymphatic endothelial cells (LECs) harvested at 96 hpi, fixed and stained as in A. **(H.)** Geometric mean fold change of KSHV over mock at 96 hpi for 3 experiments as in panel B, $p < .05$ student's t-test. All the data are represented as mean +/- SEM and were analyzed using FlowJo software. **(I)** Representative confocal images of Mock and KSHV infected TIME cells at 96 hpi stained with antibody to ABCD3 and DAPI to identify the nuclei**. (J)** Quantification of number of peroxisomes per cell in three biological replicates of Mock and KSHV-infected cells stained as in panel I, analyzed using student's t-test $p < 0.0001$.

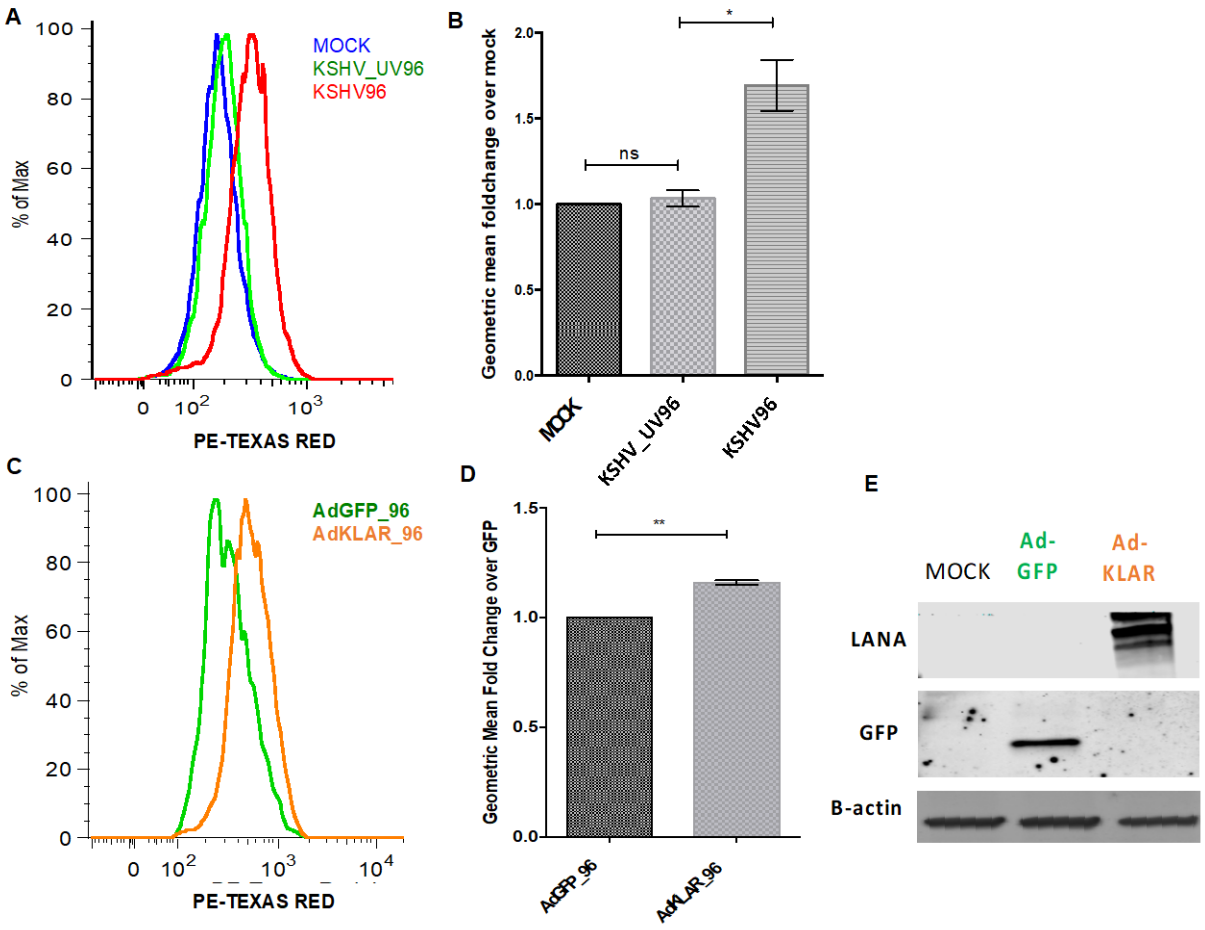

Figure 3.5 KSHV latency locus is sufficient to induce a peroxisome marker in endothelial cells. (A.) Flow cytometry of mock-, KSHV-UV irradiated and KSHV- infected TIME cells harvested at 96 hpi, fixed and stained with antibody to ABCD3. **(B.)** Geometric mean fold change of KSHV, KSHV-UV-irradiated over mock at 96 hpi for 3 experiments as in A, $p < .05$ student's t -test. **(C.)** Flow cytometry of AdGFP or AdKLAR (KSHV latency-associated region in a gutted adenovirus) infected TIME cells harvested at 96 hpi, fixed and stained with antibody to ABCD3. **(D.)** Geometric mean fold change of AdGFP over AdKLAR at 96 hpi $p < .05$ student's t-test. All the data are represented as mean +/- SEM and were analyzed using FlowJo software. **(E.)** Western blot analysis of TIME cells mock infected or infected with AdGFP-, or AdKLAR stained with antibodies to GFP or LANA.

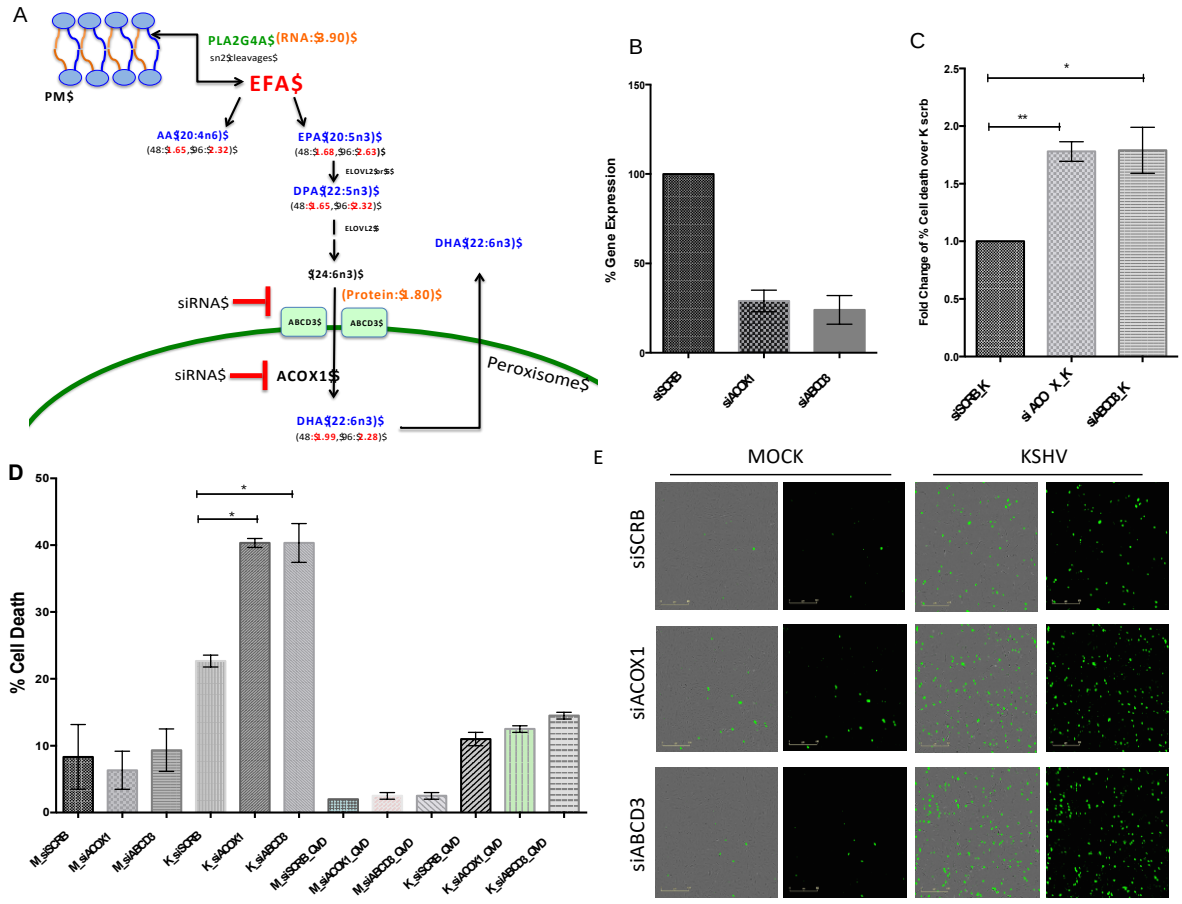

FIG 3.6 KSHV latently infected endothelial cells require peroxisome proteins. (A) Overview of Essential Fatty Acids (EFA) and peroxisome lipid metabolism. Numbers indicate genes altered by KSHV (48 or 96 hpi in black and fold change in red) as identified by a previously published metabolomics screen (49) in blue and flow cytometry validation of ABCD3 and RNA-seq (*PLA2G4A*) in orange; siRNA treatments of ABCD3 and ACOX1 for panel B are indicated in blocked red sign. **(B.)** TIME cells were transfected with a control siRNA (siSCRB) or siRNA to ABCD3 or ACOX1. siABCD3 and siACOX1 treatments lead to greater than 70% reduction in ABCD3 and ACOX1 expression as determined by qRT-PCR normalized to the housekeeping genes GAPDH. **(C.)** TIME cells were transfected with siRNAs as in panel B and 24 later were Mock- or KSHV-infected. 96 hpi (120 hours post transfection) cells were harvested and % cell death was measured using Trypan blue stain. In parallel, cells were treated with 20 μM QVD, a pan-caspase inhibitor. Data shown is from three independent experiments. Student's t-test (**D**.) Data shows the average fold change in % dead cells over control siRNA transfected cells from three independent experiments from panel C. **(E.)** IncuCyte microscopy images identifying dead cell nuclei (YOYO-1) for Mock- and KSHV-infected cells transfected with siSCRB, siABCD3 or siACOX1 at 96 hpi. Essen software was used to identify cell nuclei by size and fluorescent intensity, with background subtracted. YOYO-1 positive nuclei are in fluorescent green. All the data are represented as mean +/- SEM.

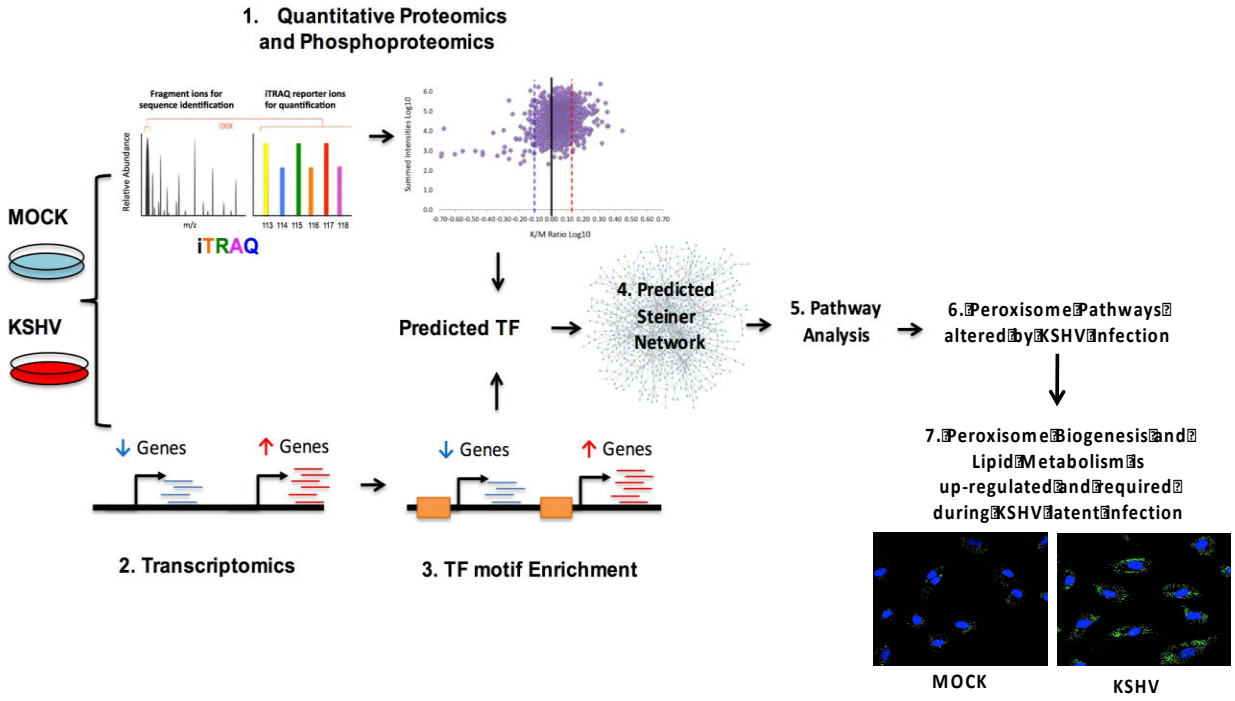

Figure 3.7 Workflow of the systems biology data integration analysis and Schematic of the metabolism of VLCFs in the peroxisome. Experimental conditions of mock and KSHV infected TIME cells were processed using proteomics techniques and in parallel transcriptomics analysis. The RNA-seq data was used for TF prediction and then TFs were used as the link to generate the predicted protein-protein interaction Steiner forest network. Analysis of the Steiner forest network was done using KEGG pathway analysis and followed by experimental validation of peroxisome biogenesis and mediated lipid metabolism.

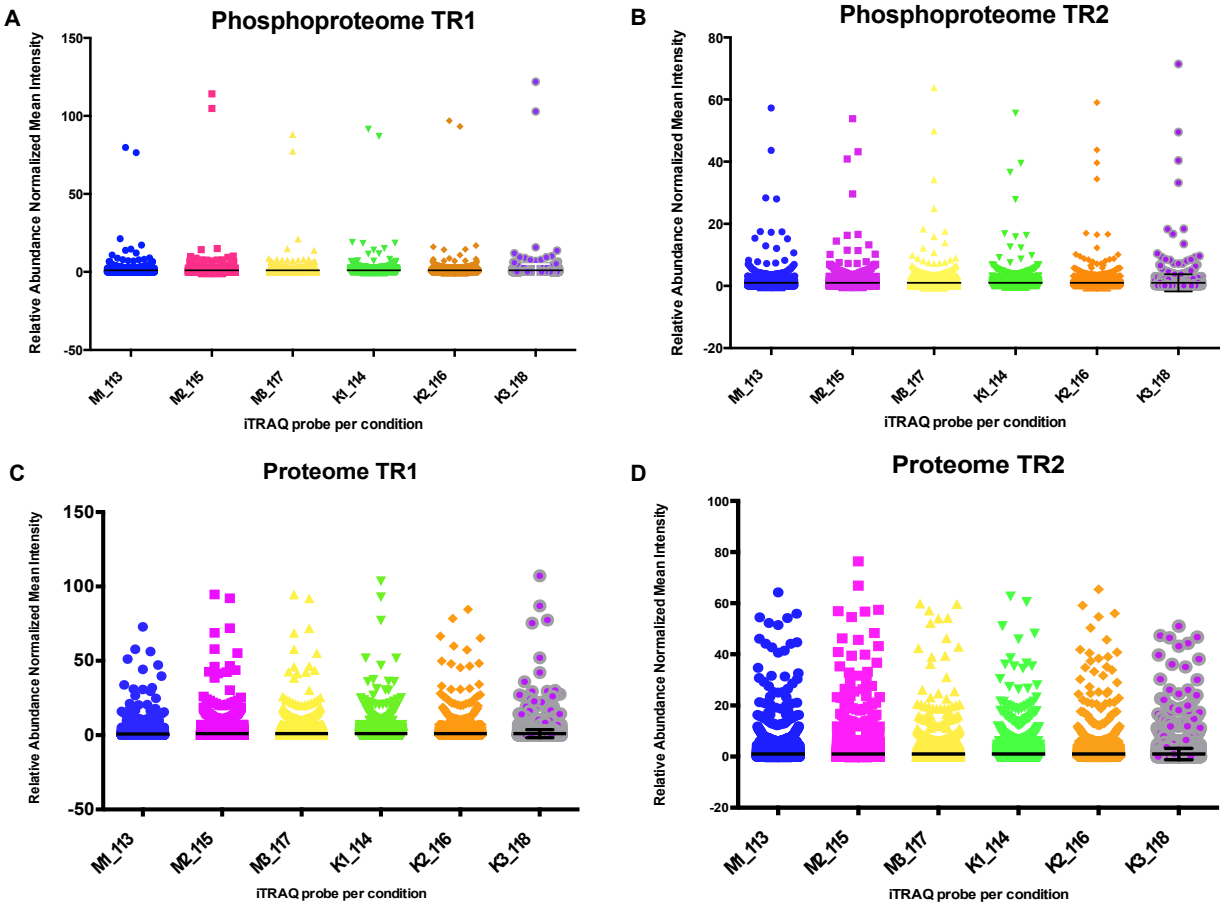

S_Figure 3.8 Relative abundance plot of normalized mean intensities of iTRAQ labeling in the proteome and phosphoproteome. (A.) Phosphoproteome technical replicate (TR) 1. **(B.)** Phosphoproteome technical replicate (TR) 2. **(C.)** Proteome technical replicate (TR) 1. **(D.)** Proteome technical replicate (TR) 2.

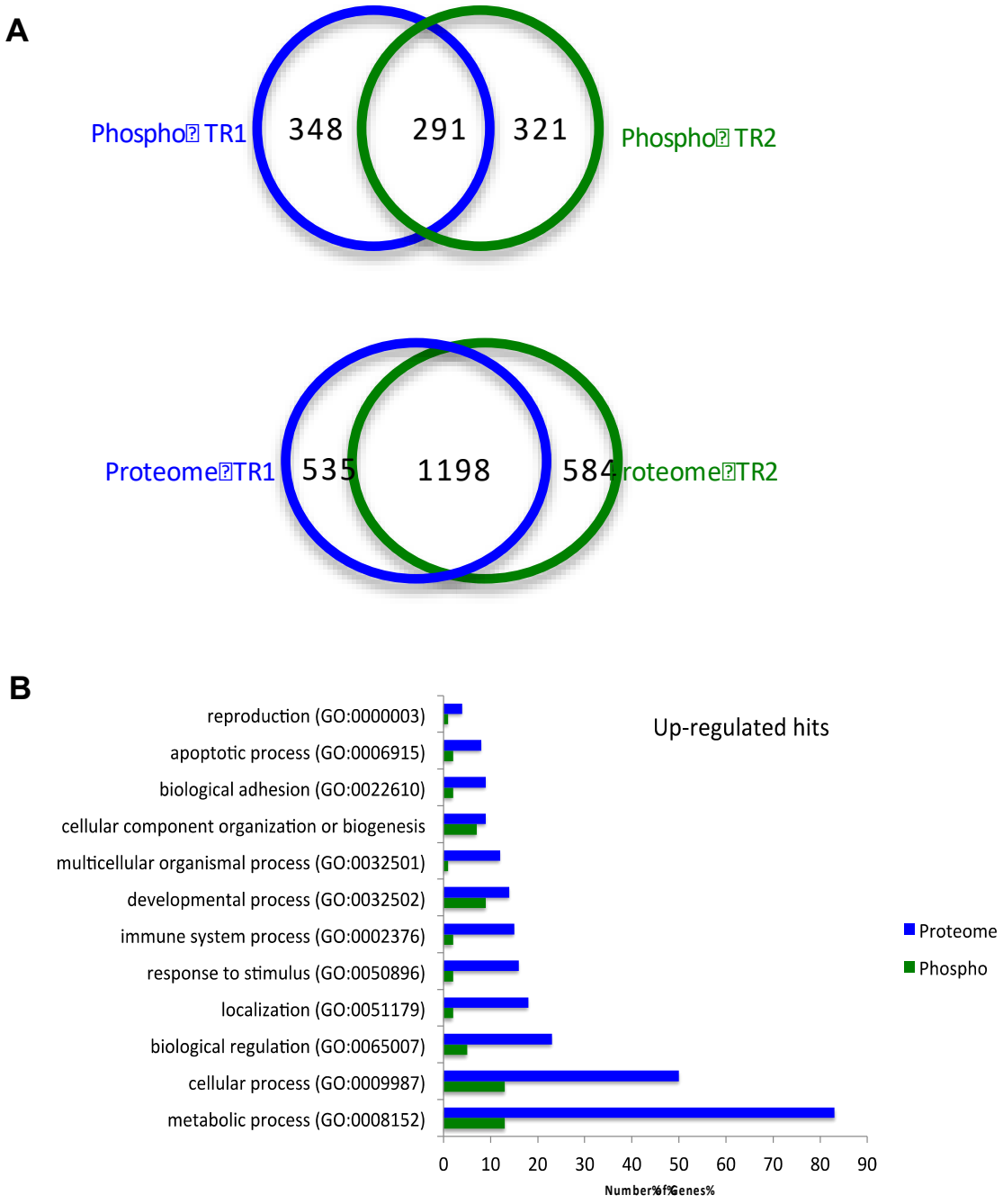

S_Figure 3.9 Proteome and phosphoproteome profiling. (A.) Venn diagrams of both technical replicate runs from phosphoproteome and proteome. **(B.)** GO biological process analysis of the upregulated hits from the phosphoproteome and proteome measured proteins.

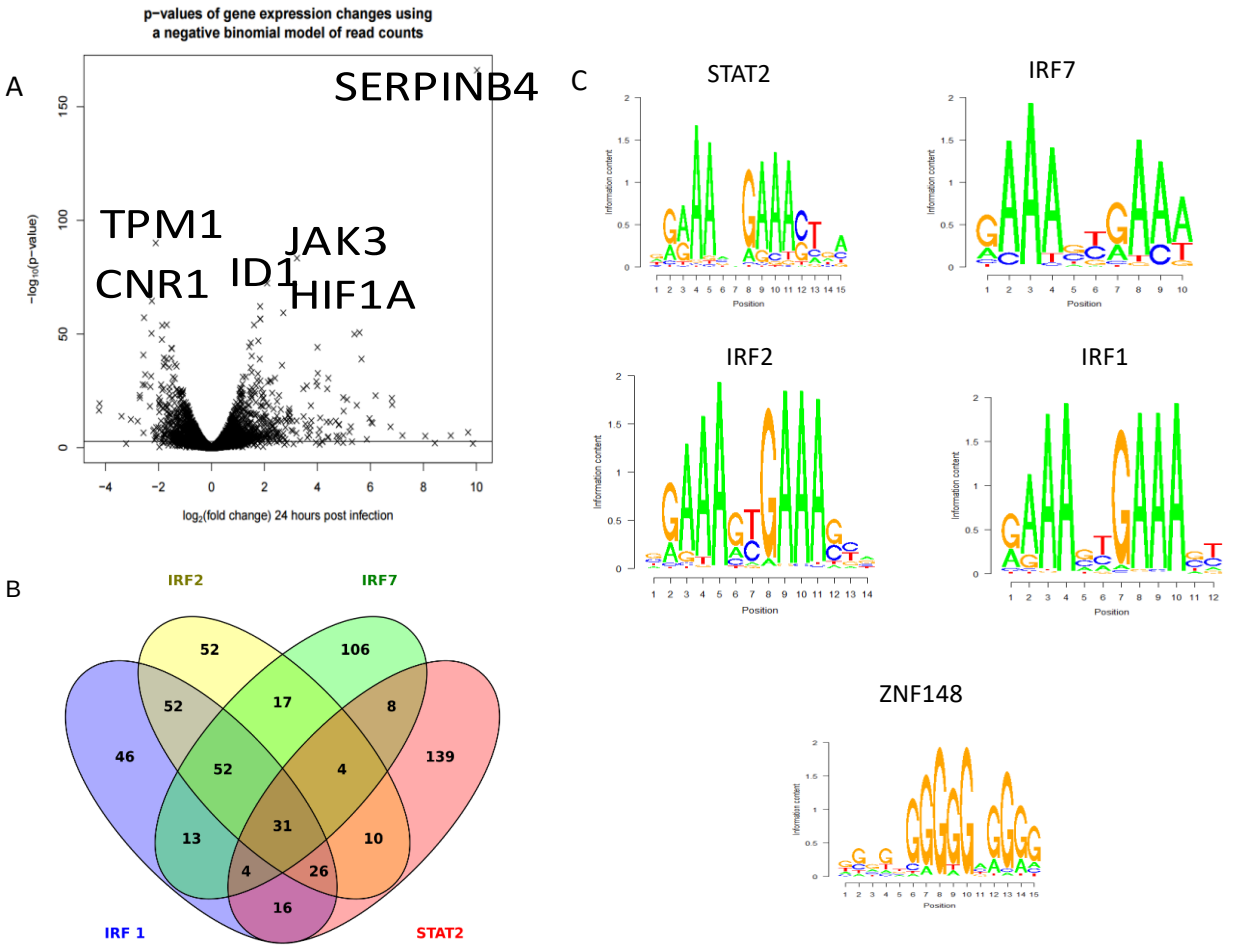

S_Figure 3.10 Transcriptomics profiling and motif enrichment comparisons (A.) RNA-seq volcano plot. Highlighting the most highly upregulated and downregulated genes. **(B.)** Venn diagram of the genes inferred to have motif instances of IRF1, IRF2, STAT2, and IRF7 1000bp upstream of their transcription start site. The numbers show the numbers of genes that have the combination of motif instances associated with the regions of the diagram. **(C.)** Position weight matrices of the five TF motifs enriched at a less than 5% false discovery rate in the 1000bp regions upstream of significantly changed genes post- infection, taken from the HOCOMOCO database.

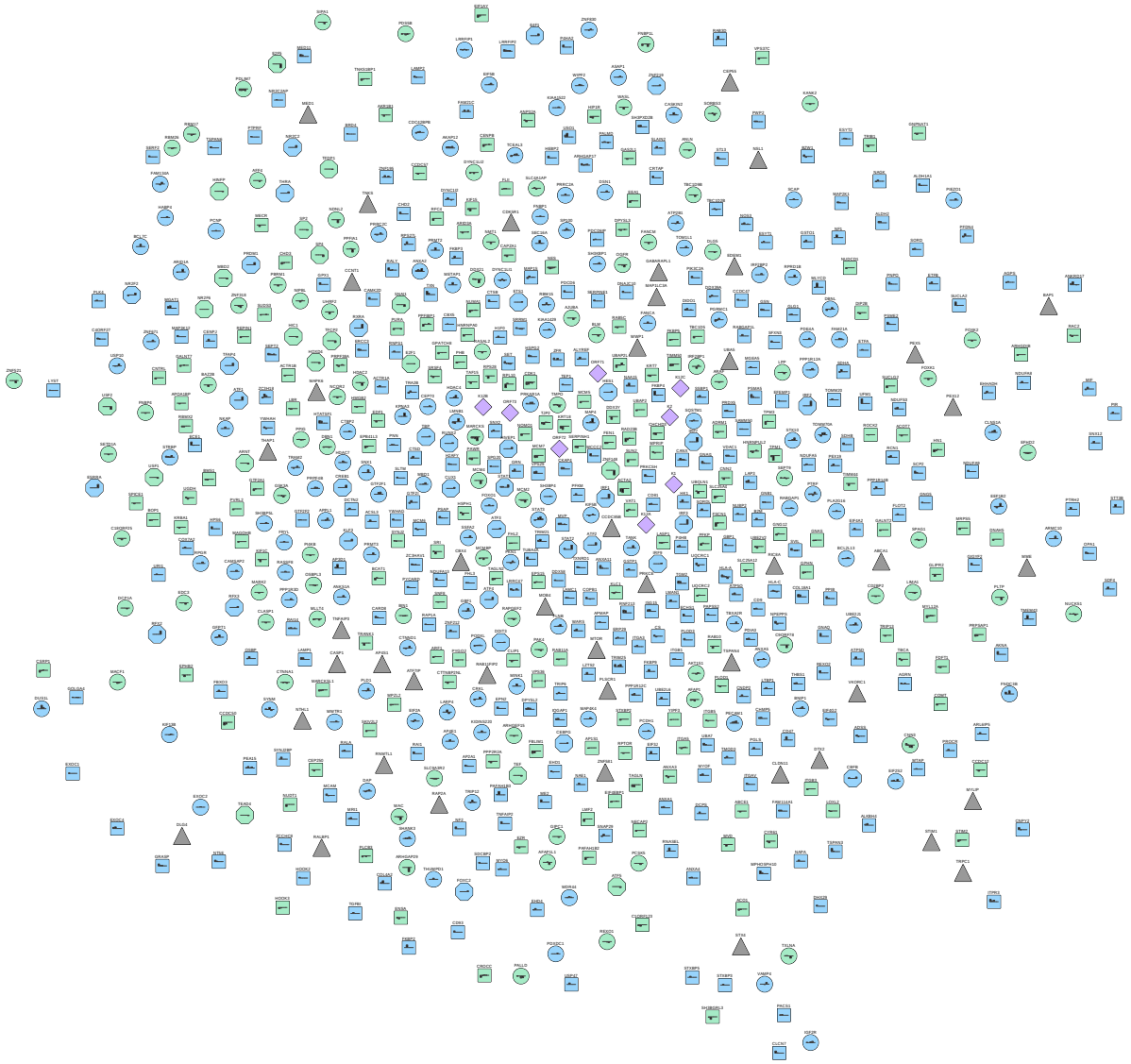

S_Figure 3.11 Complete Steiner forest network of endothelial cells latently infected with KSHV at 48 hpi. Please refer to legend from Figure 3B for network interpretation.

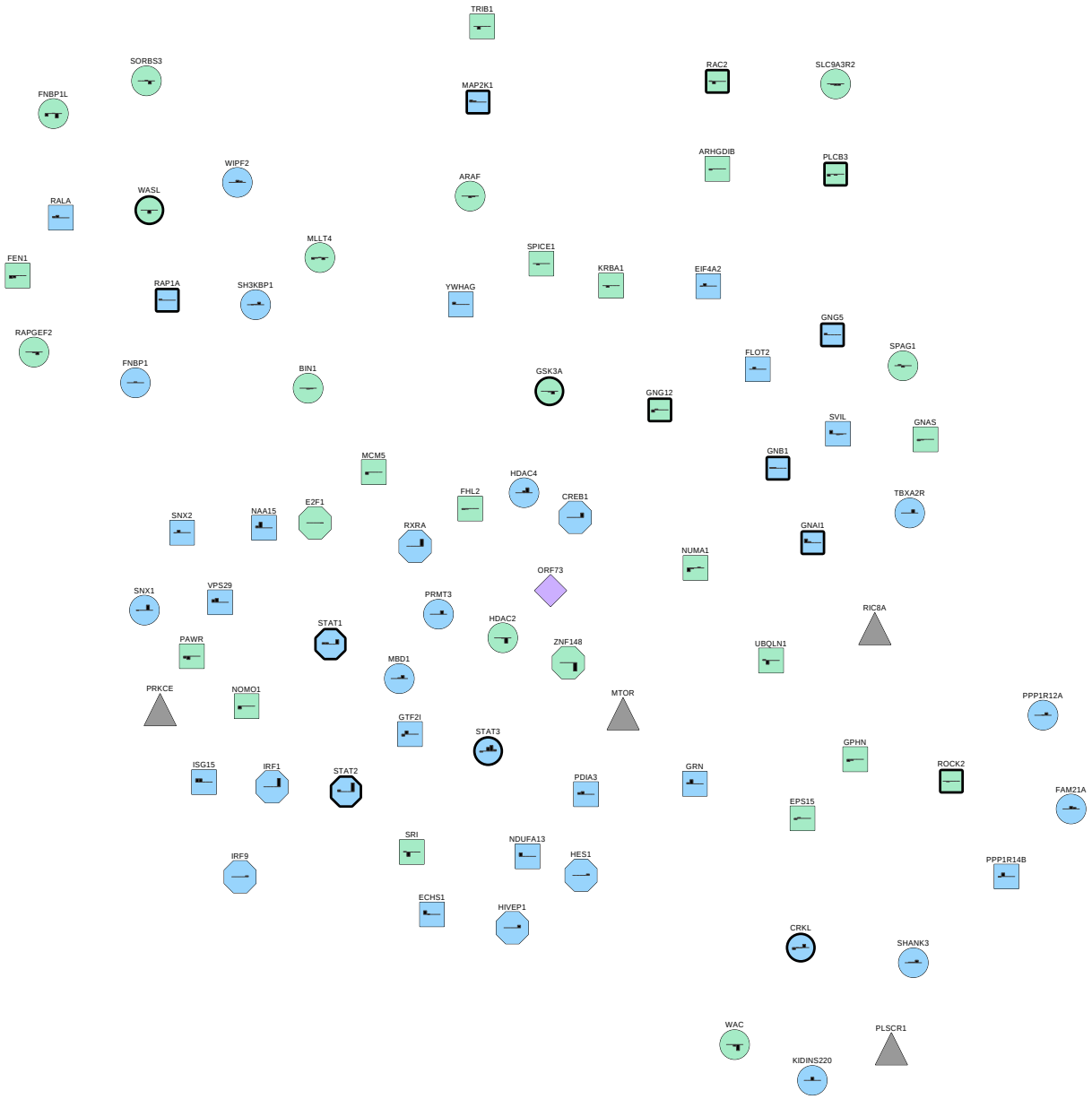

S_Figure 3.12 Steiner forest subnetwork from Metabolism KEGG pathways. Please refer to legend from Figure 3B for network interpretation.

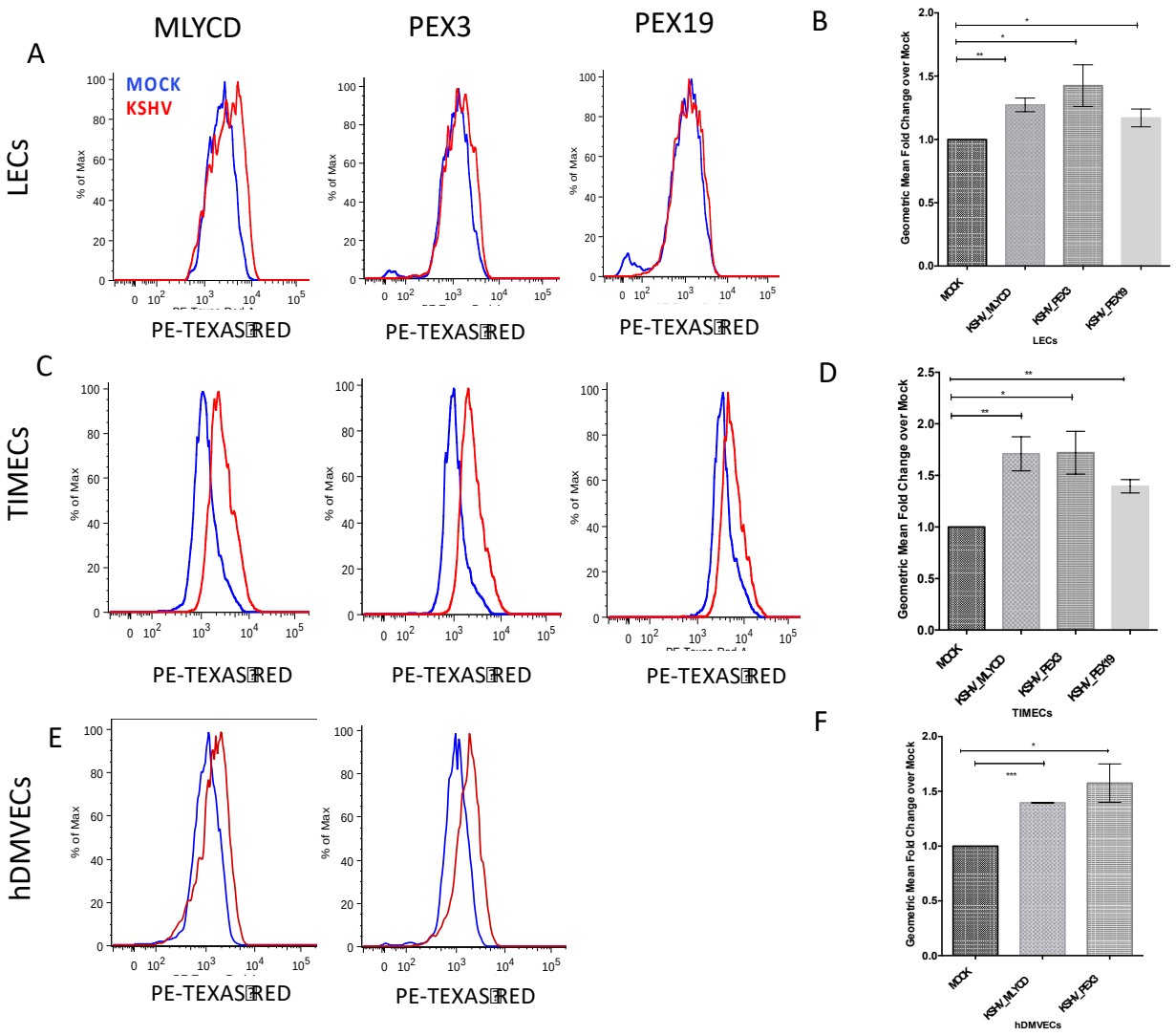

S_Figure 3.13 KSHV latently infected endothelial cells induces peroxisome proteins. (A.) Flow cytometry of Mock- and KSHV- infected LECs cells harvested at 96 hpi, fixed and stained with PEX3 and MLYCD **(B.)** Geometric mean fold change of KSHV over mock at 96 hpi $p < 0.05$ student's t-test. **(C.)** Flow cytometry of Mock- and KSHV- infected TIMECs cells harvested at 96 hpi, fixed and stained with PEX3, PEX19 and MLYCD **(D.)** Geometric mean fold change of KSHV over mock at 96 hpi $p < 0.05$ student's t-test. **(E.)** Flow cytometry of Mock- and KSHV-infected hDMVECs cells were harvested at 96 hpi, fixed and stained with PEX3 and MLYCD **(F.)** Geometric mean fold change of KSHV over mock at 96 hpi $p < 0.05$ student's t-test.

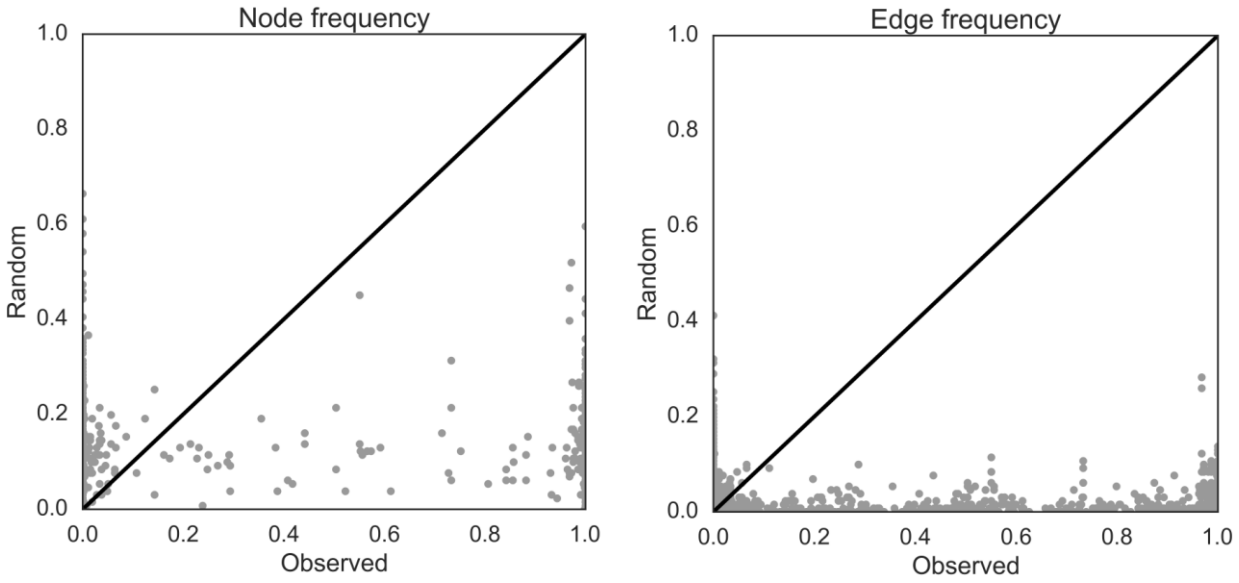

S_Figure 3.14 Distribution of node and edge frequencies in observed and random Steiner forests. We run the Steiner forest algorithm multiple times with the real KSHV protein scores (Observed) and equivalent scores randomly assigned to proteins in the PPI network (Random). Node frequency is the fraction of Observed or Random Steiner forest subnetworks that contain a node, likewise for edges. In general, the nodes and edges that appear in nearly all the Observed subnetworks have a low probability of being included in a Random subnetwork. Very few nodes and no edges lie near the diagonal lines that denote equal frequencies in the Observed and Random subnetworks. The Random subnetworks also contain thousands of nodes and edges that are not relevant to KSHV infection and do not appear in any Observed subnetworks.

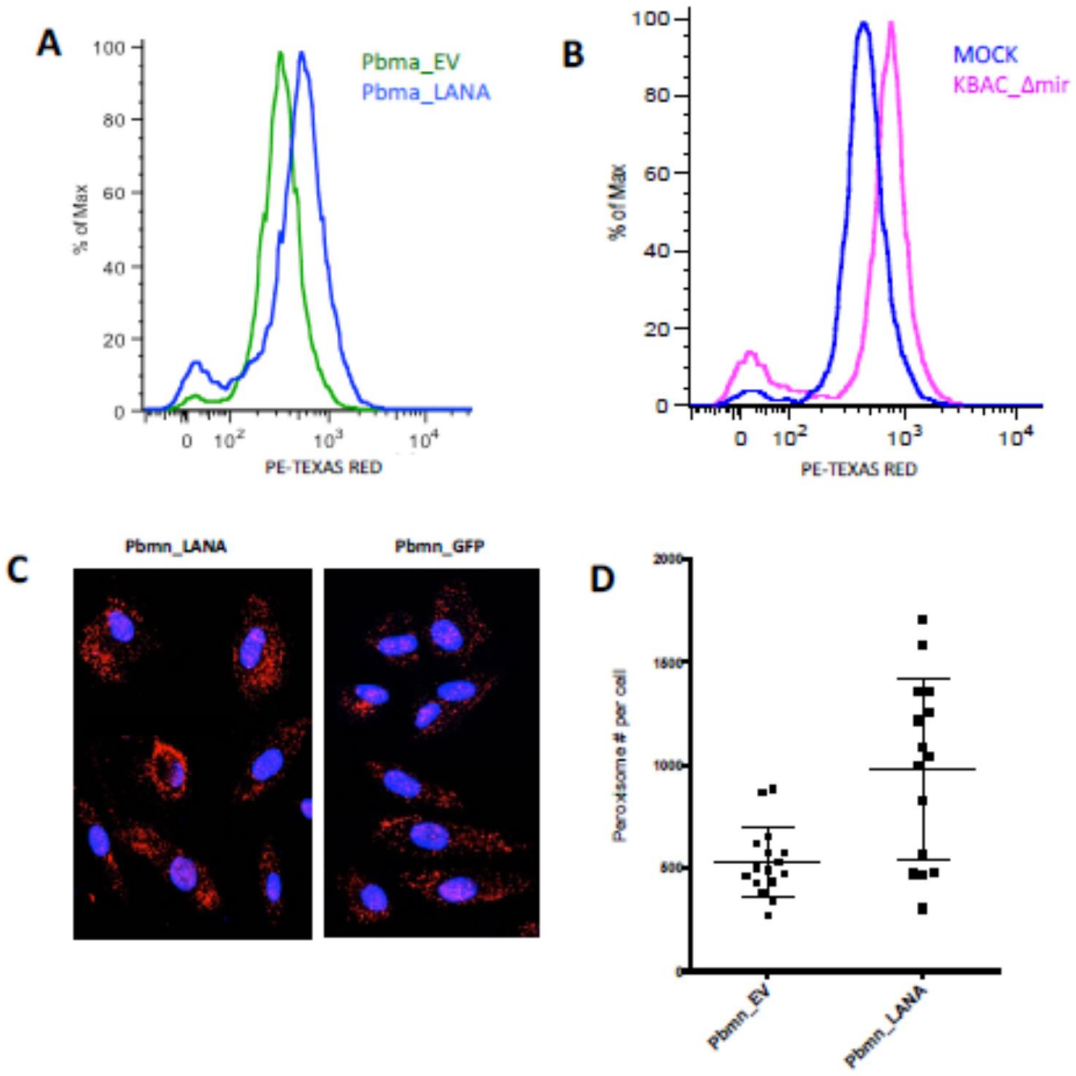

S_Figure 3.15 LANA is sufficient to upregulate ABCD3 protein and peroxisome number per cell. (A.) Flow cytometry analysis pbmnGFP and pbmnLANA expressing TIME cells harvested at 96 hpi, fixed and stained with antibody to ABCD3. **(B.)** Flow cytometry analysis mock and KBAC- dmir infected TIME cells and harvested at 96 hpi, fixed and stained with antibody to ABCD3. **(C.)** Confocal images of pbmnGFP and pbmnLANA expressing TIME cells at 96 hpi stained with antibody to ABCD3 and DAPI to identify the nuclei**. (D)** Quantification of number of peroxisomes per cell from panel C, one biological replicate.

Table 1. Complete list of the top KEGG Pathways that overlapped significantly with the predicted Steiner Forest Network.

Pathway name	# Genes	Adjusted p-value
Huntington's disease	24	0.0002
Parkinson's disease	17	0.001
Vasopressin-regulated water reabsorption	10	0.0012
DNA replication	8	0.0061
Alzheimer's disease	18	0.0081
ECM-receptor interaction	12	0.0095
Phagosome	17	0.0104
Endocytosis	20	0.0152
Citrate cycle (TCA cycle)	6	0.0234
Propanoate metabolism	6	0.0243
Leukocyte transendothelial migration	13	0.0243
Hepatitis C	14	0.0243
Protein processing in endoplasmic reticulum	16	0.0336
Long-term potentiation	9	0.0353
Pathways in cancer	26	0.0389
Pancreatic cancer	9	0.0389
Focal adhesion	18	0.0389
Regulation of actin cytoskeleton	19	0.0389
Oxidative phosphorylation	12	0.0389
Adherens junction	9	0.0389
Fc gamma R-mediated phagocytosis	10	0.0578
Lysine degradation	6	0.0578
Peroxisome	9	0.0578
Cell cycle	12	0.0628
RNA transport	13	0.0732
Basal transcription factors	5	0.0732
Dilated cardiomyopathy	9	0.0732
Antigen processing and presentation	8	0.0732
Pancreatic secretion	9	0.0751
Fructose and mannose metabolism	5	0.0751
Vascular smooth muscle contraction	10	0.081
Insulin signaling pathway	12	0.0851
Hypertrophic cardiomyopathy (HCM)	8	0.0858
Long-term depression	7	0.0858
RIG-I-like receptor signaling pathway	7	0.0879
Chemokine signaling pathway	15	0.0963

Table 2. Technical replicate 1 of the phosphoproteome analysis in KSHV infected cells compared to mock infected cells at 48 hpi.

Protein Name	Peptide with Modified Amino Acid Residue	Fold Change	Platform	HPLC
TTC7B	VIEQDET[181.01]R	8.4259	LC/MS-MS	1-Dimensional
STAT3	KYCRPESQEHPEADPGSAAPY[243.03]LK.T	3.7035	LC/MS-MS	1-Dimensional
STAT3	KYCRPESQEHPEADPGAAPY[243.03]LK.T	3.2824	LC/MS-MS	1-Dimensional
SYNM	GLQT[181.01]PVKDAGGGTGR	1.8645	LC/MS-MS	1-Dimensional
NCOA3	KES[167.00]SVSVTSPSGVSSSTSGGVSSTSNMHGSLLQEK.H	1.7540	LC/MS-MS	1-Dimensional
AP4E1	KLLMNDS[167.00]VS[167.00]S[167.00]ETK.A	1.7237	LC/MS-MS	1-Dimensional
none	MPS[167.00]QSVEVCGISY[243.03]LGEFQFEDGFEMKMSGGCGARWGG	1.7037	LC/MS-MS	1-Dimensional
AKAP2	SPGALET[181.01]PSAAGSQGNTASQGK	1.6085	LC/MS-MS	2-Dimensional
DHX30	SLRS[167.00]ELAALPPS[167.00]VQEEHGQLLALLAELLR	1.5705	LC/MS-MS	2-Dimensional
BCL7C	GTEPSPGGTPQPSRPVS[167.00]PAGPPEGVPEEAQPPR	1.5683	LC/MS-MS	2-Dimensional
AKAP2	DALGDSLQVPVS[167.00]PSSTTSSR	1.5509	LC/MS-MS	2-Dimensional
IFI16	EVDATS[167.00]PAPSTSSTVKTEGAEATPGAQKR	1.5266	LC/MS-MS	2-Dimensional
EIF4G1	EAALPPVS[167.00]PLKAALSEEELEKK	1.5119	LC/MS-MS	2-Dimensional
RASSF8	KS[167.00]LT[181.01]FTGGAKGLMDIFGK	1.5085	LC/MS-MS	2-Dimensional
MAP2	SGTSTPTTPGSTAITPGT[181.01]PPSYSSR	1.4842	LC/MS-MS	2-Dimensional
SYNPO	GALPPS[167.00]PALPRPSR	1.4799	LC/MS-MS	2-Dimensional
AGRN	AGPCEQAECGSGGSGS[167.00]GEDGDCEQELCR	1.4670	LC/MS-MS	2-Dimensional
MAP4K5	LAS[167.00]ELSFDFR	1.4668	LC/MS-MS	2-Dimensional
PECAM1	KDTETVY[243.03]SEVRK.A	1.4651	LC/MS-MS	2-Dimensional
DNM1L	SKPIPIMPAS[167.00]PQKGHAVNLLDVPVPVAR	1.4638	LC/MS-MS	2-Dimensional
MAP7D1	SSQPS[167.00]PTAVPASDSPPTK	1.4562	LC/MS-MS	2-Dimensional
AKAP2	S[167.00]PGALETPSAAGSQGNTASQGK	1.4511	LC/MS-MS	2-Dimensional

AKAP12	SAESPTS[167.00]PVTSETGSTFKK	1.4432	LC/MS-MS	2-Dimensional
PECAM1	KDTETVYS[167.00]EVRK.A	1.4165	LC/MS-MS	2-Dimensional
PECAM1	KDTETVY[243.03]SEVR.K	1.4018	LC/MS-MS	2-Dimensional
VIM	ETNLDS[167.00]LPLVDTHSK	1.3995	LC/MS-MS	2-Dimensional
SSB	FAS[167.00]DDEHDEHDENGATGPVKR	1.3770	LC/MS-MS	2-Dimensional
TRIM25	ASAPS[167.00]PNAQVACDHCLK	1.3741	LC/MS-MS	2-Dimensional
VIM	ETNLDS[167.00]LPLVDTHSKR	1.3714	LC/MS-MS	2-Dimensional
MINK1	GTPKPPGPPAQPPGPPNAS[167.00]SNPDLRR	1.3656	LC/MS-MS	2-Dimensional
PLEC	AQLEPVAS[167.00]PAKKPK	1.3653	LC/MS-MS	2-Dimensional
MYCT1	RVGLSTPPPPAY[243.03]ESIIK.A	1.3643	LC/MS-MS	2-Dimensional
NEDD9	RQAGRPDLRPEGVY[243.03]DIPPTCTKPAGK.D	1.3628	LC/MS-MS	2-Dimensional
ZNF280A	NDS[167.00]WEDHT[181.01]T[181.01]CQHCHR	1.3591	LC/MS-MS	2-Dimensional
LRRFIP1	GSGDTS[167.00]ISIDTEASIR	1.3478	LC/MS-MS	2-Dimensional
SSRP1	EGMNPSYDEY[243.03]ADSDEDQHDAYLER	1.3477	LC/MS-MS	2-Dimensional
DAP	EEKDKDDQEWESPS[167.00]PPKPTVFISGVIAR	1.3429	LC/MS-MS	2-Dimensional
AHNAK	GGVTGS[167.00]PEASISGSKGDLK	1.3387	LC/MS-MS	2-Dimensional
GNL1	EEQTDT[181.01]SDGESVTHHIR	1.3309	LC/MS-MS	2-Dimensional
TCOF1	SLGNILQAKPTS[167.00]SPAKGPPQK	1.3266	LC/MS-MS	2-Dimensional
AKAP2	YLDEVLEANCCDSAVDGTYNGTSS[167.00]PEPGAVVLVGGLSPPVHEATQPEPTER	1.3255	LC/MS-MS	2-Dimensional
DCDC2	KS[167.00]T[181.01]VGSSDNSSPQPLK.R	1.3254	LC/MS-MS	2-Dimensional
TCEAL3	REDEGEPGDEGQLEDEGS[167.00]QEKQGR	1.3198	LC/MS-MS	2-Dimensional
ZFR	QY[243.03]Y[243.03]QQPAATEAGSSSSCCCCCNSCLDR	1.3194	LC/MS-MS	2-Dimensional
TCEAL3	REDEGEPGDEGQLEDEGS[167.00]QEK	1.3190	LC/MS-MS	2-Dimensional
ITPR3	KQS[167.00]VFSAPSLSAGASAAEPLDR	1.3101	LC/MS-MS	2-Dimensional

WDR44	TKEYVSNDAAQS[167.00]DDEEKLQSQPTDTDGGR	1.3071	LC/MS-MS	2-Dimensional
ZC3H18	ELDEHELDYDEEVPEEPAPAVQEDEAEKAGAEDDEEKGEGT[181.01]PR	1.3060	LC/MS-MS	2-Dimensional
none	FCCGCCPY[243.03]T[181.01]S[167.00]GCGV	1.3040	LC/MS-MS	2-Dimensional
BAZ2B	SVVS[167.00]EIDK	0.7996	LC/MS-MS	2-Dimensional
CHD4	EDNS[167.00]EGEEILEEVGGDLEEEDDHHMEFCR	0.7992	LC/MS-MS	2-Dimensional
FILIP1L	RIS[167.00]DPQVFSK	0.7961	LC/MS-MS	2-Dimensional
PPP1R13L	APS[167.00]PRPGPGPLR	0.7909	LC/MS-MS	2-Dimensional
PRKAR2B	RAS[167.00]VCAEAYNPDEEEDDAESR	0.7905	LC/MS-MS	2-Dimensional
ADAMTS10	RGTGATAES[167.00]R	0.7899	LC/MS-MS	2-Dimensional
SLC4A1AP	SLQEEQSRPPT[181.01]AVSSPGGPAR	0.7838	LC/MS-MS	2-Dimensional
RASAL2	LEVPAERS[167.00]PR	0.7814	LC/MS-MS	2-Dimensional
ZYX	FS[167.00]PGAPGGSGSQPNQK	0.7803	LC/MS-MS	2-Dimensional
FLCN	AHS[167.00]PAEGASVESSSPGPK	0.7797	LC/MS-MS	2-Dimensional
DYNC1LI2	DFQDYMEPEEGCQGS[167.00]PQRR	0.7779	LC/MS-MS	2-Dimensional
MLLT4	NHFAY[243.03]Y[243.03]NYHTYEDGSDS[167.00]R	0.7717	LC/MS-MS	2-Dimensional
THRAP3	ASAVSELS[167.00]PR	0.7716	LC/MS-MS	2-Dimensional
FANCM	QQDHCLNS[167.00]VPS[167.00]GSS[167.00]AQSK	0.7681	LC/MS-MS	2-Dimensional
FOXK1	EGS[167.00]PIPHDPEFGSK	0.7665	LC/MS-MS	2-Dimensional
POLQ	MRT[181.01]MLLVYVMR	0.7626	LC/MS-MS	2-Dimensional
SNRK	ASPSENNAGGGS[167.00]PSSGSGGNPTNTSGTTR	0.7582	LC/MS-MS	2-Dimensional
DNAI1	VTEEELMT[181.01]PK	0.7579	LC/MS-MS	2-Dimensional
TNS1	RSYSPY[243.03]DYQPCLAGPNQDFHSK.S	0.7564	LC/MS-MS	2-Dimensional
RAB18	MDEDVLT[181.01]T[181.01]LK	0.7553	LC/MS-MS	2-Dimensional
MCM2	RTDALTS[167.00]SPGR	0.7499	LC/MS-MS	2-Dimensional

EEF1D	ATAPQTQHVS[167.00]PMR	0.7498	LC/MS-MS	2-Dimensional
MARCKS	LSGFS[167.00]FK	0.7489	LC/MS-MS	2-Dimensional
SNX19	EINRT[181.01]IQMIIR	0.7426	LC/MS-MS	2-Dimensional
PRKAR2B	RASVCAEAY[243.03]NPDEEEDDAESR	0.7425	LC/MS-MS	2-Dimensional
CRKL	RNSNSYGIPEPAHAYAQPQTTTPLPAVSGSPGAAITPLPS[167.00]TQNGPVFAK.A	0.7371	LC/MS-MS	2-Dimensional
DCLK1	S[167.00]PS[167.00]PSPTSPGSLR	0.7350	LC/MS-MS	2-Dimensional
PALLD	S[167.00]PSGHPHVR	0.7329	LC/MS-MS	2-Dimensional
FSIP2	S[167.00]LIQIHRVIQS[167.00]DTICFGR	0.7227	LC/MS-MS	2-Dimensional
WRNIP1	RPAAAAAAGSAS[167.00]PR	0.7220	LC/MS-MS	2-Dimensional
SRRM2	SATRPSPS[167.00]PER	0.7219	LC/MS-MS	2-Dimensional
WAC	QQGHEPVS[167.00]PR	0.7152	LC/MS-MS	2-Dimensional
MAP7D1	RKPNAGGS[167.00]PAPVR	0.7120	LC/MS-MS	2-Dimensional
TCP11L1	VQRPHS[167.00]SPPR	0.7059	LC/MS-MS	2-Dimensional
UHRF2	RPIS[167.00]DDDCPSASK	0.7001	LC/MS-MS	2-Dimensional
MID1	ASVSGPNS[167.00]PSETRR	0.6941	LC/MS-MS	2-Dimensional
RBM26	RLNHS[167.00]PPQSSSR	0.6929	LC/MS-MS	2-Dimensional
MERTK	AAIS[167.00]VVT[181.01]AEVHDSKPHEGR	0.6705	LC/MS-MS	2-Dimensional
SIPA1	ARAHS[167.00]HEEASRPAATSTR	0.6435	LC/MS-MS	2-Dimensional
CABYR	T[181.01]LLEGISR	0.6350	LC/MS-MS	2-Dimensional
IRF2BP1	AGGAS[167.00]PAASSTAQPPTQHR	0.6261	LC/MS-MS	2-Dimensional
SRRM2	SRT[181.01]PPSAPSQSR	0.6230	LC/MS-MS	2-Dimensional
PTRF	ESEALPEKEGEELGEGERPEEDAAALELS[167.00]S[167.00]DEAVEVEEVIEESR	0.6094	LC/MS-MS	2-Dimensional
DST	S[167.00]PVQFENLEEIFDTSVSK	0.5943	LC/MS-MS	2-Dimensional
CNN3	GASQAGMLAPGT[181.01]RR	0.5872	LC/MS-MS	2-Dimensional

8 Phosphoproteome Data Set Technical Replicate 1. KSHV infection alters global host cellular phosphoproteome analysis. Heat map of fold change levels of peptide profiled in this study at 48 hpi. For comparisons, shaded cells, yellow-bolded values indicate $p < 0.01$ (red indicates that the mean values are significantly higher for that comparison and green indicates that the values are significantly lower). Shaded cells wih blue-bolded values indicate $p < 0.5$ (light orange indicates that the mean values trend higher for that comparison and light green indicates that the mean values trend lower). All data are normalized to BCA assays prior to protein trypsinization and then peptide quantification was normalized with Pierce Quantitative Fluorometric Peptide assay. Modifications: phosphotyrosine [243.03], phosphoserine [167.00], phosphothreonine [181.01].

Table 3. Technical replicate 2 of the phosphoproteome analysis in KSHV infected cells compared to mock infected cells at 48 hpi.

Protein Name	Peptide with Modified Amino Acid Residue	Fold Change	Platform	HPLC
STAT3	KYCRPESQEHPEADPGAAPY[243.03]LK.T	4.1325	LC/MS-MS	1-Dimensional
STAT3	KYCRPESQEHPEADPGSAAPY[243.03]LK.T	3.9182	LC/MS-MS	1-Dimensional
TCAP	S[167.00]MSQEAQR	2.5988	LC/MS-MS	1-Dimensional
ITGA1	NS[167.00]MT[181.01]FS[167.00]GPVEDMFGYTVQQYENEEGK	2.0212	LC/MS-MS	1-Dimensional
DIP2C	SACLMT[181.01]TQLICK	1.9767	LC/MS-MS	1-Dimensional
SNX1	WES[167.00]RVTQYERDFER	1.9328	LC/MS-MS	1-Dimensional
PECAM1	KKDTETVY[243.03]SEVRK.A	1.8576	LC/MS-MS	1-Dimensional
ZFYVE19	RAS[167.00]GFPALGRGGTVPVGVWGGAGQGR	1.7331	LC/MS-MS	1-Dimensional
CAV1	KYVDSEGHLY[243.03]TVPIREQGNIYKPNNK.A	1.6132	LC/MS-MS	1-Dimensional
RSRC2	GMGLGFT[181.01]S[167.00]S[167.00]MRGMDAV	1.5938	LC/MS-MS	2-Dimensional
C1orf173	ECTLETEAMQDRNS[167.00]EGDGDMEGEGNT[181.01]QKNEGMGGGR	1.5929	LC/MS-MS	2-Dimensional
MTMR8	T[181.01]PTMSEFLS[167.00]GLESSGWLR	1.5905	LC/MS-MS	2-Dimensional
PGM2	LLTFLIRKY[243.03]ILEL	1.5687	LC/MS-MS	2-Dimensional
SP100	LNECIS[167.00]PVANEMNHLPAHSHDLQR	1.5478	LC/MS-MS	2-Dimensional
AKAP12	SEDSIAGSGVEHSTPDTEPGKEESWVS[167.00]IKK	1.5378	LC/MS-MS	2-Dimensional
PECAM1	KDTETVY[243.03]SEVRK.A	1.5214	LC/MS-MS	2-Dimensional
DNM1L	SKPIPIMPAS[167.00]PQKGHAVNLLDVPVPVAR	1.5192	LC/MS-MS	2-Dimensional
CASKIN2	EQEGT[181.01]PSASTK	1.5146	LC/MS-MS	2-Dimensional
TCEAL3	EDEGEPGDEGQLEDEGS[167.00]QEKQGR	1.4772	LC/MS-MS	2-Dimensional
AKAP12	SAESPTS[167.00]PVTSETGSTFKK	1.4768	LC/MS-MS	2-Dimensional
CTRC	TMVCAGGDGVIS[167.00]ACNGDSGGPLNCQLENGSWEVFGIVS[167.00]FGS[167.00]R	1.4635	LC/MS-MS	2-Dimensional
MXD4	VAWS[167.00]WERGPPAS[167.00]LS[167.00]SR	1.4570	LC/MS-MS	2-Dimensional
AKAP12	EGVTPWAS[167.00]FK	1.4476	LC/MS-MS	2-Dimensional
RBM10	RESATADAGY[243.03]AILEK	1.4302	LC/MS-MS	2-Dimensional
GNAS	RARHNY[243.03]NDLCPPIGR	1.4258	LC/MS-MS	2-Dimensional
SAFB	SEPVKEESSELEQPFAQDT[181.01]SSVGPDRK	1.4187	LC/MS-MS	2-Dimensional
SP100	GFENVIHDKLPLQES[167.00]EEEER	1.4137	LC/MS-MS	2-Dimensional
WDR44	EYVSNDAAQS[167.00]DDEEKLQSQPTDTDGGRLK	1.4096	LC/MS-MS	2-Dimensional
ARID1A	SNS[167.00]VGIQDAFNDGSDSTFQKR	1.4066	LC/MS-MS	2-Dimensional
FLJ20896	TPPDTTFPEPTCLSASPPNVPPRQS[167.00]KR	1.4059	LC/MS-MS	2-Dimensional
EEF1B2	YGPADVEDTTGS[167.00]GATDSKDDDDIDLFGSDDEEESEEAKR	1.4049	LC/MS-MS	2-Dimensional
MBD1	RRPGAQPLPPPPPSQS[167.00]PEPTEPHPR	1.3967	LC/MS-MS	2-Dimensional
MAP4K4	RDS[167.00]PLQGSGQQNSQAGQR	1.3962	LC/MS-MS	2-Dimensional

PEA15	YKDIIRQPS[167.00]EEEIIK	1.3957	LC/MS-MS	2-Dimensional
MAP2	SGTSTPTTPGSTAITPGT[181.01]PPSYSSR	1.3954	LC/MS-MS	2-Dimensional
DKFZp779J2370	MDST[181.01]HPQHCACNSQIRPRWDCVAHCFLWAPGLPS[167.00]R	1.3944	LC/MS-MS	2-Dimensional
SSFA2	SVHIS[167.00]TPEKEPCAPLTIPSIR	1.3900	LC/MS-MS	2-Dimensional
BNIP1	RT[181.01]ILDANEEFK.S	1.3841	LC/MS-MS	2-Dimensional
NUFIP2	DYEIESQNPLAS[167.00]PTNTLLGSAK	1.3672	LC/MS-MS	2-Dimensional
VIM	ETNLDS[167.00]LPLVDTHSKR	1.3540	LC/MS-MS	2-Dimensional
FAM195B	S[167.00]PPSSSEIFTPAHEENVR	1.3502	LC/MS-MS	2-Dimensional
IRF2BP2	RPAS[167.00]VSSSAAVEHEQR	1.3482	LC/MS-MS	2-Dimensional
HABP4	SLPAPVAQRPDS[167.00]PGGGLQAPGQK	1.3467	LC/MS-MS	2-Dimensional
HTT	EKEPGEQASVPLS[167.00]PK	1.3445	LC/MS-MS	2-Dimensional
ANXA2	KLSLEGDHSTPPSAY[243.03]GSVK.A	1.3435	LC/MS-MS	2-Dimensional
PECAM1	KDTETVY[243.03]SEVR.K	1.3395	LC/MS-MS	2-Dimensional
DSN1	AS[167.00]DFSLEAS[167.00]VAEMK	1.3385	LC/MS-MS	2-Dimensional
SP100	GFENVIHDKLPLQES[167.00]EEEEREER	1.3356	LC/MS-MS	2-Dimensional
BAZ2A	QPSS[167.00]PSHNTNLR	0.7664	LC/MS-MS	2-Dimensional
LPP	RNDSDPTY[243.03]GQQGHPNTWKR.E	0.7662	LC/MS-MS	2-Dimensional
NRAP	Y[243.03]EGVGMDRR	0.7629	LC/MS-MS	2-Dimensional
SRRM2	RRPS[167.00]PQPSPR	0.7563	LC/MS-MS	2-Dimensional
HDAC2	MLPHAPGVQMQAIPEDAVHEDS[167.00]GDEDGEDPDKR	0.7561	LC/MS-MS	2-Dimensional
AZI1	RSNS[167.00]TTQVSQPR	0.7553	LC/MS-MS	2-Dimensional
SRRM1	APQTSSS[167.00]PPPVRR	0.7539	LC/MS-MS	2-Dimensional
UBAP2L	STSAPQMSPGSSDNQSSS[167.00]PQPAQQK	0.7500	LC/MS-MS	2-Dimensional
HIG-1	QTAELGY[243.03]PK	0.7493	LC/MS-MS	2-Dimensional
CDK1	KIGEGTY[243.03]GVVYK.G	0.7484	LC/MS-MS	2-Dimensional
TAF1L	RMLLVAGS[167.00]AAS[167.00]GNNHR.D	0.7338	LC/MS-MS	2-Dimensional
MDC1	ESEDSETQPFDT[181.01]HLEAYGPCLSPPR	0.7324	LC/MS-MS	2-Dimensional
TRA2A	RAHTPT[181.01]PGIYMGRPTHSGGGGGGGGGGGGGGGR	0.7275	LC/MS-MS	2-Dimensional
BLM	S[167.00]AQNLASR	0.7268	LC/MS-MS	2-Dimensional
WAC	QQGHEPVS[167.00]PR	0.7235	LC/MS-MS	2-Dimensional
HNRNPK	RDYDDMS[167.00]PR	0.7193	LC/MS-MS	2-Dimensional
ARHGAP29	LLLAS[167.00]PPNER	0.7093	LC/MS-MS	2-Dimensional
WRNIP1	RPAAAAAAGSAS[167.00]PR	0.7064	LC/MS-MS	2-Dimensional
ARHGAP29	IRPVS[167.00]LPVDR	0.7045	LC/MS-MS	2-Dimensional
PLTP	MHAAFGGT[181.01]FK	0.7027	LC/MS-MS	2-Dimensional
ZNF318	RSS[167.00]PPPPPSGSSSR	0.7021	LC/MS-MS	2-Dimensional

FUBP1	QQAAYYAQT[181.01]SPQGMPQHPPAPQGQ	**0.6975**	LC/MS-MS	2-Dimensional
MCM4	SGVRGT[181.01]PVR	**0.6971**	LC/MS-MS	2-Dimensional
PPFIA1	RIPHS[167.00]PAR	**0.6936**	LC/MS-MS	2-Dimensional
none	CGCS[167.00]IRAGTASR	**0.6912**	LC/MS-MS	2-Dimensional
ILK	S[167.00]RDFNEECPR	**0.6819**	LC/MS-MS	2-Dimensional
NUFIP2	TIQNSSVSPTSS[167.00]SSSSSSTGETQTQSSSR	**0.6784**	LC/MS-MS	2-Dimensional
PALMD	SEHQNSS[167.00]PTCQEDEEDVR	**0.6757**	LC/MS-MS	2-Dimensional
DDX21	EEPSQNDIS[167.00]PK	**0.6733**	LC/MS-MS	2-Dimensional
CDC42BPA	GCQT[181.01]VTSGK	**0.6716**	LC/MS-MS	2-Dimensional
AHNAK2	DAHDVS[167.00]PTSTDTEAQLTVER	**0.6653**	LC/MS-MS	2-Dimensional
GPR111	RVS[167.00]PISFFLS[167.00]K	**0.6636**	LC/MS-MS	2-Dimensional
CCDC25	VENMS[167.00]S[167.00]NQDGNDS[167.00]DEFM	**0.6585**	LC/MS-MS	2-Dimensional
CNN3	GASQAGMLAPGT[181.01]RR	**0.6406**	LC/MS-MS	2-Dimensional
PTPRF	AYIATQGPLAEST[181.01]EDFWR	**0.6318**	LC/MS-MS	2-Dimensional
WEE2	S[167.00]ARSSSFTS[167.00]GEREPLH	**0.6175**	LC/MS-MS	2-Dimensional
SIPA1	ARAHS[167.00]HEEASRPAATSTR	**0.6160**	LC/MS-MS	2-Dimensional
MCRS1	SREVPALTCPIS[167.00]PDHPGQSNQG	**0.5390**	LC/MS-MS	2-Dimensional
LIG1	TIQEVLEEQS[167.00]EDEDREAK	**0.5190**	LC/MS-MS	2-Dimensional
NDNL2	GPGGSQGSQGPS[167.00]PQGARR	**0.4491**	LC/MS-MS	2-Dimensional
KIRREL3	QRVPTGMSFT[181.01]NIY[243.03]STLSGQGR	**0.3273**	LC/MS-MS	2-Dimensional
NETO2	VLLIT[181.01]VLVVEGIAVAQK	**0.3147**	LC/MS-MS	2-Dimensional
PCIA2	RRVLS[167.00]LENQR	**0.2623**	LC/MS-MS	2-Dimensional
KIF3A	QAVSVDEMRGTIT[181.01]VHK	**0.2502**	LC/MS-MS	2-Dimensional
PLCD3	DGASLS[167.00]PATLFIQIRIQRS	**0.2291**	LC/MS-MS	2-Dimensional

Table 3 Phosphoproteome Data Set Technical Replicate 2. KSHV infection alters global host cellular phosphoproteome analysis. Heat map of fold change levels of peptide profiled in this study at 48 hpi. For comparisons, shaded cells, yellow-bolded values indicate $p < 0.01$ (red indicates that the mean values are significantly higher for that comparison and green indicates that the values are significantly lower). Shaded cells wih blue-bolded values indicate $p < 0.5$ (light orange indicates that the mean values trend higher for that comparison and light green indicates that the mean values trend lower). All data are normalized to BCA assays prior to protein trypsinization and then peptide quantification was normalized with Pierce Quantitative Fluorometric Peptide assay. Modifications: phosphotyrosine [243.03], phosphoserine [167.00], phosphothreonine [181.01].

Table 4. Technical replicate 1 of the proteome analysis in KSHV infected cells compared to mock infected cells at 48 hpi.

Protein Name	Fold Change	Platform	HPLC
GSDMD	4.470	LC/MS-MS	2-Dimensional
IGFN1	3.418	LC/MS-MS	2-Dimensional
RNF213	3.133	LC/MS-MS	2-Dimensional
DDX58	3.006	LC/MS-MS	2-Dimensional
ANKRD17	3.003	LC/MS-MS	2-Dimensional
TRIP11	2.989	LC/MS-MS	2-Dimensional
MED11	2.726	LC/MS-MS	2-Dimensional
MT1E	2.705	LC/MS-MS	2-Dimensional
MAP3K12	2.659	LC/MS-MS	2-Dimensional
JPH4	2.638	LC/MS-MS	2-Dimensional
HLA-B	2.614	LC/MS-MS	2-Dimensional
TCHH	2.569	LC/MS-MS	2-Dimensional
TFPT	2.502	LC/MS-MS	2-Dimensional
CAPN1	2.476	LC/MS-MS	2-Dimensional
ADAMTS13	2.447	LC/MS-MS	2-Dimensional
SPR	2.431	LC/MS-MS	2-Dimensional
CDK5	2.430	LC/MS-MS	2-Dimensional
NUP98	2.408	LC/MS-MS	2-Dimensional
PRKAR1A	2.360	LC/MS-MS	2-Dimensional
PPP4R4	2.354	LC/MS-MS	2-Dimensional
ACAP2	2.321	LC/MS-MS	2-Dimensional
40435	2.317	LC/MS-MS	2-Dimensional
ZBED2	2.273	LC/MS-MS	2-Dimensional
AKNA	2.221	LC/MS-MS	2-Dimensional
OLA1	2.217	LC/MS-MS	2-Dimensional
TTYH3	2.214	LC/MS-MS	2-Dimensional
PLAUR	2.214	LC/MS-MS	2-Dimensional
IL1A	2.202	LC/MS-MS	2-Dimensional
CORO1C	2.194	LC/MS-MS	2-Dimensional
PACSIN3	2.189	LC/MS-MS	2-Dimensional
BCR	2.185	LC/MS-MS	2-Dimensional
MGAT1	2.181	LC/MS-MS	2-Dimensional
IGF2R	2.175	LC/MS-MS	2-Dimensional

HTATSF1	2.172	LC/MS-MS	2-Dimensional
FOSL2	2.170	LC/MS-MS	2-Dimensional
EXOC4	2.166	LC/MS-MS	2-Dimensional
SUCLA2	2.166	LC/MS-MS	2-Dimensional
PI4K2B	2.147	LC/MS-MS	2-Dimensional
MMS22L	2.147	LC/MS-MS	2-Dimensional
SMARCAL1	2.131	LC/MS-MS	2-Dimensional
PLCG2	2.128	LC/MS-MS	2-Dimensional
TRADD	2.128	LC/MS-MS	2-Dimensional
SF3A1	2.107	LC/MS-MS	2-Dimensional
FGG	2.099	LC/MS-MS	2-Dimensional
MPHOSPH10	2.091	LC/MS-MS	2-Dimensional
DKFZp686M0430	2.081	LC/MS-MS	2-Dimensional
EPB41L2	2.080	LC/MS-MS	2-Dimensional
AKAP2	2.076	LC/MS-MS	2-Dimensional
SSBP1	2.074	LC/MS-MS	2-Dimensional
TPX2	2.071	LC/MS-MS	2-Dimensional
NQO1	2.070	LC/MS-MS	2-Dimensional
VAMP1	2.062	LC/MS-MS	2-Dimensional
PLBD2	2.061	LC/MS-MS	2-Dimensional
PLXND1	2.053	LC/MS-MS	2-Dimensional
HLA-A	2.038	LC/MS-MS	2-Dimensional
NKRF	2.036	LC/MS-MS	2-Dimensional
PSMB2	2.034	LC/MS-MS	2-Dimensional
PRRC1	2.031	LC/MS-MS	2-Dimensional
TYRP1	2.030	LC/MS-MS	2-Dimensional
RAI1	2.027	LC/MS-MS	2-Dimensional
IFIT3	2.026	LC/MS-MS	2-Dimensional
TRIP12	2.025	LC/MS-MS	2-Dimensional
PARG	2.021	LC/MS-MS	2-Dimensional
HSD17B12	2.020	LC/MS-MS	2-Dimensional
SERPINB9	2.013	LC/MS-MS	2-Dimensional
RAB3D	2.012	LC/MS-MS	2-Dimensional
SH3TC1	2.011	LC/MS-MS	2-Dimensional
ITPRIP	2.005	LC/MS-MS	2-Dimensional
PRPF38A	2.002	LC/MS-MS	2-Dimensional
MLKL	2.002	LC/MS-MS	2-Dimensional
NFKB1	2.001	LC/MS-MS	2-Dimensional

LEPREL4	2.000	LC/MS-MS	2-Dimensional
WDR3	2.000	LC/MS-MS	2-Dimensional
PNKD	1.989	LC/MS-MS	2-Dimensional
CCDC158	1.980	LC/MS-MS	2-Dimensional
PLEKHG5	1.977	LC/MS-MS	2-Dimensional
HMOX1	1.976	LC/MS-MS	2-Dimensional
LOXL2	1.975	LC/MS-MS	2-Dimensional
TOR1AIP1	1.968	LC/MS-MS	2-Dimensional
DOCK7	1.967	LC/MS-MS	2-Dimensional
SERINC1	1.961	LC/MS-MS	2-Dimensional
SYNE3	1.961	LC/MS-MS	2-Dimensional
ALKBH4	1.956	LC/MS-MS	2-Dimensional
OAS3	1.952	LC/MS-MS	2-Dimensional
PRCP	1.946	LC/MS-MS	2-Dimensional
TXN	1.946	LC/MS-MS	2-Dimensional
CYB5R3	1.945	LC/MS-MS	2-Dimensional
SERF2	1.943	LC/MS-MS	2-Dimensional
SDE2	1.940	LC/MS-MS	2-Dimensional
TIMM50	1.104	LC/MS-MS	2-Dimensional
NDUFS6	1.103	LC/MS-MS	2-Dimensional
FN3KRP	1.102	LC/MS-MS	2-Dimensional
TAGLN	1.101	LC/MS-MS	2-Dimensional
FNBP1L	1.100	LC/MS-MS	2-Dimensional
TPM1	1.097	LC/MS-MS	2-Dimensional
GPHN	1.097	LC/MS-MS	2-Dimensional
C15orf38	1.096	LC/MS-MS	2-Dimensional
GATAD2B	1.094	LC/MS-MS	2-Dimensional
YIPF3	1.092	LC/MS-MS	2-Dimensional
CALML3	1.090	LC/MS-MS	2-Dimensional
SPTSSA	1.088	LC/MS-MS	2-Dimensional
CHD4	1.088	LC/MS-MS	2-Dimensional
FAM192A	1.085	LC/MS-MS	2-Dimensional
GTF2A1	1.083	LC/MS-MS	2-Dimensional
CROCC	1.082	LC/MS-MS	2-Dimensional
RPLP1	1.079	LC/MS-MS	2-Dimensional
KCTD12	1.078	LC/MS-MS	2-Dimensional
CDV3	1.075	LC/MS-MS	2-Dimensional
WDSUB1	1.074	LC/MS-MS	2-Dimensional

SMARCA4	1.073	LC/MS-MS	2-Dimensional
FAM107B	1.068	LC/MS-MS	2-Dimensional
DNAH5	1.068	LC/MS-MS	2-Dimensional
FRMD6-AS1	1.068	LC/MS-MS	2-Dimensional
SNRPD3	1.065	LC/MS-MS	2-Dimensional
ACAT2	1.064	LC/MS-MS	2-Dimensional
ACAD9	1.060	LC/MS-MS	2-Dimensional
ALB	1.060	LC/MS-MS	2-Dimensional
DNAJC9	1.057	LC/MS-MS	2-Dimensional
PSMA6	1.056	LC/MS-MS	2-Dimensional
CCNDBP1	1.053	LC/MS-MS	2-Dimensional
LTF	1.051	LC/MS-MS	2-Dimensional
TJP2	1.049	LC/MS-MS	2-Dimensional
SNRPA1	1.047	LC/MS-MS	2-Dimensional
POLD2	1.046	LC/MS-MS	2-Dimensional
CNTRL	1.044	LC/MS-MS	2-Dimensional
DDAH1	1.041	LC/MS-MS	2-Dimensional
TCEAL3	1.039	LC/MS-MS	2-Dimensional
RPL10	1.035	LC/MS-MS	2-Dimensional
COMP	1.035	LC/MS-MS	2-Dimensional
HBA1	1.034	LC/MS-MS	2-Dimensional
RBM3	1.030	LC/MS-MS	2-Dimensional
CSDE1	1.023	LC/MS-MS	2-Dimensional
TBC1D5	1.019	LC/MS-MS	2-Dimensional
HHIP	1.015	LC/MS-MS	2-Dimensional
TCP11L1	1.011	LC/MS-MS	2-Dimensional
FILIP1L	1.010	LC/MS-MS	2-Dimensional
NEXN	1.008	LC/MS-MS	2-Dimensional
PHF5A	1.006	LC/MS-MS	2-Dimensional
RASA1	1.005	LC/MS-MS	2-Dimensional
AMBP	1.002	LC/MS-MS	2-Dimensional
VPS26A	0.995	LC/MS-MS	2-Dimensional
TCEA1	0.995	LC/MS-MS	2-Dimensional
DNAJC1	0.994	LC/MS-MS	2-Dimensional
PLOD2	0.970	LC/MS-MS	2-Dimensional
STIM2	0.970	LC/MS-MS	2-Dimensional
RBMX2	0.966	LC/MS-MS	2-Dimensional
RUFY1	0.964	LC/MS-MS	2-Dimensional

BTF3L4	0.962	LC/MS-MS	2-Dimensional
LMF2	0.956	LC/MS-MS	2-Dimensional
FAM96B	0.955	LC/MS-MS	2-Dimensional
PDHB	0.949	LC/MS-MS	2-Dimensional
CCT6B	0.935	LC/MS-MS	2-Dimensional
GC	0.933	LC/MS-MS	2-Dimensional
ART4	0.914	LC/MS-MS	2-Dimensional
OGFR	0.913	LC/MS-MS	2-Dimensional
RAVER1	0.909	LC/MS-MS	2-Dimensional
MCM7	0.909	LC/MS-MS	2-Dimensional
SPC24	0.904	LC/MS-MS	2-Dimensional
RBBP7	0.903	LC/MS-MS	2-Dimensional
CTCF	0.893	LC/MS-MS	2-Dimensional
CDC42EP4	0.879	LC/MS-MS	2-Dimensional
PLEKHA8P1	0.876	LC/MS-MS	2-Dimensional
NUDT1	0.874	LC/MS-MS	2-Dimensional
NCLN	0.873	LC/MS-MS	2-Dimensional
ASPH	0.861	LC/MS-MS	2-Dimensional
GPR179	0.846	LC/MS-MS	2-Dimensional
ATRX	0.838	LC/MS-MS	2-Dimensional
A1BG	0.815	LC/MS-MS	2-Dimensional
HIRIP3	0.783	LC/MS-MS	2-Dimensional
RPS21	0.778	LC/MS-MS	2-Dimensional
PNKP	0.777	LC/MS-MS	2-Dimensional
TF	0.775	LC/MS-MS	2-Dimensional
TAGLN3	0.737	LC/MS-MS	2-Dimensional
SPCS2	0.675	LC/MS-MS	2-Dimensional
KIF15	0.603	LC/MS-MS	2-Dimensional
KCMF1	0.495	LC/MS-MS	2-Dimensional
MCM3	0.465	LC/MS-MS	2-Dimensional

Table 4. Proteome Data Set Technical Replicate 1. KSHV infection alters global host cellular phosphoproteome analysis. Heat map of fold change levels of peptide profiled in this study at 48 hpi. For comparisons, shaded cells, yellow-bolded values indicate $p < 0.01$ (red indicates that the mean values are significantly higher for that comparison and green indicates that the values are significantly lower). Shaded cells with blue-bolded values indicate $p < 0.5$ (light orange indicates that the mean values trend higher for that comparison and light green indicates that the mean values trend lower). All data are normalized to BCA assays prior to protein trypsinization and then peptide quantification was normalized with Pierce Quantitative Fluorometric Peptide assay.

Table 5. Technical replicate 2 of the proteome analysis in KSHV infected cells compared to mock infected cells at 48 hpi.

Protein	Fold Change	Platform	HPLC
CCNH	3.425	LC/MS-MS	2-Dimensional
HNRNPH2	2.980	LC/MS-MS	2-Dimensional
HLA-B	2.102	LC/MS-MS	2-Dimensional
PPFIA4	2.065	LC/MS-MS	2-Dimensional
DNMT3B	2.023	LC/MS-MS	2-Dimensional
SERPINB9	1.965	LC/MS-MS	2-Dimensional
PSMB3	1.948	LC/MS-MS	2-Dimensional
HLA-A	1.936	LC/MS-MS	2-Dimensional
EIF3D	1.899	LC/MS-MS	2-Dimensional
MED11	1.884	LC/MS-MS	2-Dimensional
MT1E	1.859	LC/MS-MS	2-Dimensional
MT1A	1.809	LC/MS-MS	2-Dimensional
PPP4R4	1.803	LC/MS-MS	2-Dimensional
TFPT	1.800	LC/MS-MS	2-Dimensional
MLYCD	1.756	LC/MS-MS	2-Dimensional
NPLOC4	1.752	LC/MS-MS	2-Dimensional
ANKRD17	1.730	LC/MS-MS	2-Dimensional
ATP6V1B2	1.710	LC/MS-MS	2-Dimensional
CENPJ	1.691	LC/MS-MS	2-Dimensional
DKFZp686M0430	1.686	LC/MS-MS	2-Dimensional
RIF1	1.676	LC/MS-MS	2-Dimensional
SSBP1	1.674	LC/MS-MS	2-Dimensional
HELZ2	1.667	LC/MS-MS	2-Dimensional
SAMM50	1.666	LC/MS-MS	2-Dimensional
FGG	1.661	LC/MS-MS	2-Dimensional
EHHADH	1.656	LC/MS-MS	2-Dimensional
DIAPH2	1.646	LC/MS-MS	2-Dimensional
CYB5R3	1.642	LC/MS-MS	2-Dimensional
DHX16	1.636	LC/MS-MS	2-Dimensional
AKAP12	1.635	LC/MS-MS	2-Dimensional
FAM73B	1.631	LC/MS-MS	2-Dimensional
PSME2	1.627	LC/MS-MS	2-Dimensional
HTATSF1	1.612	LC/MS-MS	2-Dimensional
ZNF536	1.607	LC/MS-MS	2-Dimensional

JPH4	1.606	LC/MS-MS	2-Dimensional
PSMD4	1.602	LC/MS-MS	2-Dimensional
FH	1.591	LC/MS-MS	2-Dimensional
LZTS2	1.578	LC/MS-MS	2-Dimensional
ITGA4	1.578	LC/MS-MS	2-Dimensional
MCM9	1.577	LC/MS-MS	2-Dimensional
CD47	1.572	LC/MS-MS	2-Dimensional
AMFR	1.567	LC/MS-MS	2-Dimensional
SSR1	1.566	LC/MS-MS	2-Dimensional
NUFIP2	1.561	LC/MS-MS	2-Dimensional
PROCR	1.555	LC/MS-MS	2-Dimensional
BCL2L1	1.538	LC/MS-MS	2-Dimensional
ZBED2	1.532	LC/MS-MS	2-Dimensional
PIP5K1B	1.530	LC/MS-MS	2-Dimensional
MLEC	1.528	LC/MS-MS	2-Dimensional
ARHGAP22	1.527	LC/MS-MS	2-Dimensional
HTRA1	1.511	LC/MS-MS	2-Dimensional
PNP	1.508	LC/MS-MS	2-Dimensional
ERC1	1.503	LC/MS-MS	2-Dimensional
AKAP8L	1.499	LC/MS-MS	2-Dimensional
UBA7	1.496	LC/MS-MS	2-Dimensional
TXNRD1	1.493	LC/MS-MS	2-Dimensional
PODXL	1.492	LC/MS-MS	2-Dimensional
ERP44	1.488	LC/MS-MS	2-Dimensional
HMGB1	1.488	LC/MS-MS	2-Dimensional
TSFM	1.486	LC/MS-MS	2-Dimensional
FKBP15	1.481	LC/MS-MS	2-Dimensional
AKAP2	1.479	LC/MS-MS	2-Dimensional
PML	1.478	LC/MS-MS	2-Dimensional
CCDC158	1.473	LC/MS-MS	2-Dimensional
UQCRFS1	1.471	LC/MS-MS	2-Dimensional
WNK4	1.469	LC/MS-MS	2-Dimensional
C19orf10	1.466	LC/MS-MS	2-Dimensional
HEATR5A	1.466	LC/MS-MS	2-Dimensional
GPX8	1.463	LC/MS-MS	2-Dimensional
CLCN7	1.462	LC/MS-MS	2-Dimensional
EIF4A2	1.460	LC/MS-MS	2-Dimensional
DNAJB11	1.460	LC/MS-MS	2-Dimensional

LOC202789	1.460	LC/MS-MS	2-Dimensional
RCN1	1.458	LC/MS-MS	2-Dimensional
XPO5	1.454	LC/MS-MS	2-Dimensional
TTC37	1.453	LC/MS-MS	2-Dimensional
PRDX5	1.451	LC/MS-MS	2-Dimensional
IL6ST	1.449	LC/MS-MS	2-Dimensional
SLC3A2	1.448	LC/MS-MS	2-Dimensional
GSDMD	1.443	LC/MS-MS	2-Dimensional
ISG15	1.442	LC/MS-MS	2-Dimensional
NOL12	1.439	LC/MS-MS	2-Dimensional
VAC14	1.435	LC/MS-MS	2-Dimensional
GATAD2B	1.432	LC/MS-MS	2-Dimensional
GLG1	1.429	LC/MS-MS	2-Dimensional
SQSTM1	1.425	LC/MS-MS	2-Dimensional
ANXA6	1.424	LC/MS-MS	2-Dimensional
TRPV3	1.424	LC/MS-MS	2-Dimensional
TNNT1	1.423	LC/MS-MS	2-Dimensional
SYT1	1.415	LC/MS-MS	2-Dimensional
CTSL1	1.413	LC/MS-MS	2-Dimensional
GRASP	1.412	LC/MS-MS	2-Dimensional
STRBP	1.411	LC/MS-MS	2-Dimensional
CCDC117	1.411	LC/MS-MS	2-Dimensional
SLC4A1AP	1.407	LC/MS-MS	2-Dimensional
TRIP13	0.800	LC/MS-MS	2-Dimensional
GLIPR2	0.799	LC/MS-MS	2-Dimensional
C1orf123	0.798	LC/MS-MS	2-Dimensional
BCAR3	0.798	LC/MS-MS	2-Dimensional
TMSB4X	0.796	LC/MS-MS	2-Dimensional
SDF2	0.796	LC/MS-MS	2-Dimensional
RAI1	0.794	LC/MS-MS	2-Dimensional
HN1	0.793	LC/MS-MS	2-Dimensional
BGN	0.793	LC/MS-MS	2-Dimensional
UQCRC1	0.790	LC/MS-MS	2-Dimensional
HIST1H2AD	0.789	LC/MS-MS	2-Dimensional
RSF1	0.789	LC/MS-MS	2-Dimensional
GPR37L1	0.789	LC/MS-MS	2-Dimensional
SUMO2	0.787	LC/MS-MS	2-Dimensional
ICAM2	0.787	LC/MS-MS	2-Dimensional

TNKS1BP1	0.787	LC/MS-MS	2-Dimensional
AMBP	0.783	LC/MS-MS	2-Dimensional
EIF4B	0.781	LC/MS-MS	2-Dimensional
LYRM7	0.780	LC/MS-MS	2-Dimensional
USP16	0.778	LC/MS-MS	2-Dimensional
DDX42	0.777	LC/MS-MS	2-Dimensional
QSOX2	0.774	LC/MS-MS	2-Dimensional
BECN1	0.774	LC/MS-MS	2-Dimensional
ITIH2	0.774	LC/MS-MS	2-Dimensional
CDV3	0.773	LC/MS-MS	2-Dimensional
ITPR2	0.773	LC/MS-MS	2-Dimensional
AHSG	0.772	LC/MS-MS	2-Dimensional
MTX1	0.770	LC/MS-MS	2-Dimensional
RPL6	0.770	LC/MS-MS	2-Dimensional
SYNGR3	0.766	LC/MS-MS	2-Dimensional
SMTNL2	0.766	LC/MS-MS	2-Dimensional
TBL3	0.764	LC/MS-MS	2-Dimensional
CTCF	0.764	LC/MS-MS	2-Dimensional
SNRPF	0.762	LC/MS-MS	2-Dimensional
DOCK6	0.762	LC/MS-MS	2-Dimensional
MCM7	0.760	LC/MS-MS	2-Dimensional
HMGB2	0.759	LC/MS-MS	2-Dimensional
MEF2B	0.756	LC/MS-MS	2-Dimensional
PARK7	0.750	LC/MS-MS	2-Dimensional
ALB	0.749	LC/MS-MS	2-Dimensional
GAS2L1	0.745	LC/MS-MS	2-Dimensional
ITSN1	0.745	LC/MS-MS	2-Dimensional
DIS3	0.744	LC/MS-MS	2-Dimensional
PID1	0.743	LC/MS-MS	2-Dimensional
TCERG1	0.742	LC/MS-MS	2-Dimensional
EPB41L3	0.740	LC/MS-MS	2-Dimensional
PRPF19	0.736	LC/MS-MS	2-Dimensional
TUBB8	0.734	LC/MS-MS	2-Dimensional
AKAP4	0.733	LC/MS-MS	2-Dimensional
HBZ	0.731	LC/MS-MS	2-Dimensional
MRPL46	0.730	LC/MS-MS	2-Dimensional
STX3	0.729	LC/MS-MS	2-Dimensional
MCM3AP	0.727	LC/MS-MS	2-Dimensional

HLA-DQB1	0.727	LC/MS-MS	2-Dimensional
C15orf38	0.723	LC/MS-MS	2-Dimensional
TIMM50	0.721	LC/MS-MS	2-Dimensional
CCKAR	0.720	LC/MS-MS	2-Dimensional
MARCKSL1	0.719	LC/MS-MS	2-Dimensional
ART4	0.719	LC/MS-MS	2-Dimensional
KIF15	0.713	LC/MS-MS	2-Dimensional
WDSUB1	0.706	LC/MS-MS	2-Dimensional
LTF	0.703	LC/MS-MS	2-Dimensional
KPG	0.700	LC/MS-MS	2-Dimensional
SPARC	0.698	LC/MS-MS	2-Dimensional
ENAH	0.698	LC/MS-MS	2-Dimensional
CDK1	0.698	LC/MS-MS	2-Dimensional
TNIK	0.697	LC/MS-MS	2-Dimensional
UTP3	0.692	LC/MS-MS	2-Dimensional
PZP	0.687	LC/MS-MS	2-Dimensional
GZF1	0.686	LC/MS-MS	2-Dimensional
TGFB1I1	0.676	LC/MS-MS	2-Dimensional
RASGRP3	0.671	LC/MS-MS	2-Dimensional
ZCCHC3	0.668	LC/MS-MS	2-Dimensional
PLEKHA8P1	0.652	LC/MS-MS	2-Dimensional
HMGN2	0.648	LC/MS-MS	2-Dimensional
CILP2	0.647	LC/MS-MS	2-Dimensional
SPICE1	0.643	LC/MS-MS	2-Dimensional
TAGLN	0.636	LC/MS-MS	2-Dimensional
PACS1	0.630	LC/MS-MS	2-Dimensional
RAB5C	0.625	LC/MS-MS	2-Dimensional
SLC25A12	0.618	LC/MS-MS	2-Dimensional
FIP1L1	0.597	LC/MS-MS	2-Dimensional
RBBP7	0.532	LC/MS-MS	2-Dimensional
CLEC4F	0.510	LC/MS-MS	2-Dimensional
DNAJC1	0.415	LC/MS-MS	2-Dimensional

Table 5. Proteome Data Set Technical Replicate 2. KSHV infection alters global host cellular phosphoproteome analysis. Heat map of fold change levels of peptide profiled in this study at 48 hpi. For comparisons, shaded cells, yellow-bolded values indicate $p < 0.01$ (red indicates that the mean values are significantly higher for that comparison and green indicates that the values are significantly lower). Shaded cells with blue-bolded values indicate $p < 0.5$ (light orange indicates that the mean values trend higher for that comparison and light green indicates that the mean values trend lower). All data are normalized to BCA assays prior to protein trypsinization and then peptide quantification was normalized with Pierce Quantitative Fluorometric Peptide assay.

Chapter 4. KSHV Modulates Oxidoreductase Proteins to Regulate Intracellular Redox Homeostasis During Latent Infection

Adapted from manuscript in preparation

Zoi E. Sychev[1], Yashmira Naidoo[2], Alejandro Wolf-Yadlin[3], Michael Lagunoff [2#]

[1]Molecular and Cellular Biology Program, University of Washington, Seattle, Washington, USA,
[2]Department of Microbiology, University of Washington, Seattle, Washington, USA,
[3]Department of Genome Science, University of Washington, Seattle, Washington, USA

4.1 Abstract:

Kaposi's Sarcoma Herpesvirus (KSHV), an oncogenic gamma herpesvirus, is the etiologic agent of Kaposi's Sarcoma (KS). The main tumor cell of KS, the spindle cell, is of endothelial origin and predominantly supports latent KSHV infection. To maintain a persistent infection KSHV must modulate numerous responses in the host cell including oxidative stress. Latent infection of endothelial cells leads to increases in reactive oxygen species indicative of oxidative stress. Following KSHV infection, we found a significant upregulation of thioredoxin (TXN), an oxidoreductase protein involved in regulating redox stress, as well as a TXN reduction partner peroxiredoxin1 (PRDX1). Viral gene expression is required for the induction of TXN and the KSHV major latent locus is sufficient to induce TXN. Knockdown of TXN gene expression led to a significant increase in reactive oxygen species in KSHV infected cells. Upon knockdown of TXN expression there was significant increases in cell death of latently infected endothelial cells but not in the mock controls. Jun N-terminal kinase (JNK) phosphorylation, involved in TXN death

signaling of death pathways, is induced in latently infected endothelial cells. These findings indicate that KSHV latently infected endothelial cells rely on the TXN antioxidant systems and controls reactive oxygen species ultimately for the survival of latently infected cells.

4.2 Importance:

Kaposi's Sarcoma (KS) is the most common tumor of AIDS patients world-wide and is one of the leading tumors overall in parts of sub-saharan Africa. Kaposi's Sarcoma Herpesvirus (KSHV), a gammaherpesvirus, is the etiologic agent of KS. Oxidative stress can be beneficial to viral infections or detrimental depending on the virus and the cell type infected. While excess reactive oxygen species can induce lytic replication, the mechanism of control of ROS during latent infection is unknown. Here we show that KSHV induces the oxidoreductase antioxidant protein, TXN, to control reactive oxygen species during latent infection and protect the infected cells from ROS induced cell death. Therefore, the TXN system provides an interesting therapeutic target for KSHV latency.

4.3 Introduction

Kaposi's Sarcoma-Associated Herpesvirus (KSHV), is a human gamma-herpesvirus associated with Primary Effusion Lymphomas (PEL), Multicentric Castleman Disease (MCD) and as its name indicates, Kaposi's Sarcoma (KS) (4-6). The predominant tumor cell of the KS tumor is the spindle cell, a cell with characteristics of endothelium. In late stage tumors, the spindle cells support KSHV infections (112, 113). As with all herpesviruses, KSHV has both lytic and latent phase infections. During lytic replication, temporal viral gene expression is activated to produce

infectious virions to maintain dissemination. However, during latency, limited viral genes are expressed predominantly from a single viral locus known as the major latent locus. This region encodes proteins from 4 main open reading frames as well as miRNAs from 12 miRNA loci. KSHV spindle cells predominantly support latent infection with only approximately 5% of the cells expressing markers of lytic replication.

To maintain a persistent infection, KSHV must control many cellular responses including oxidative stress. Redox homeostasis is a balance between reducing molecules and oxidizing reactive oxygen species (ROS) within cells, (68, 162-167). Cells regulate redox balance through modulating three major scavengers, the glutaredoxin (GXN) and thioredoxin (TXN) systems and the peroxisome specific catalase system (168). These systems allow for intracellular buffering of the oxidative capacity in response to oxidative stress (168). The Thioredoxin system involves three main key players: TXN, TXNR and NADPH. TXN through redox interactions with the peroxiredoxin1 (PRDX1) system can reduce hydrogen peroxide. TXN can also interact with signaling protein systems including ASK1 and JNK to prevent apoptosis in cells that have been exposed to multiple oxidative insults. The TXN protein has been shown to be expressed at high levels in most cancers cells, and is thought to protect the rapidly dividing cancer cells from high levels of oxidative stress (169).

KSHV infections induce oxidative stress in PEL and hDMVECs (80, 83). Reactive oxygen species (ROS) levels are altered upon primary infection of endothelial cells and play a role in viral entry (83). Interestingly, ROS also play a role in vascular permeability in KSHV infected human umbilical vein endothelial cells (HUVECs) (80, 81, 83) indicating potential importance for this system in KSHV pathogenesis and KS. PEL cell lines also have high levels of ROS again implicating KSHV infection in the induction of oxidative stress. While there are high levels of

ROS in KSHV infected cells, exogenous addition of H_2O_2, a reactive oxygen species, to KSHV infected B-cells or endothelial cells induces low levels of reactivation (80, 81). Therefore, it may be critical for KSHV to maintain an optimal balance of oxidative stress in the latently infected cells to maintain latency.

Little is known about how KSHV latently infected endothelial cells regulate intracellular ROS to maintain a long-term infection. Our previous proteomic analysis (170) of endothelial cells latently infected with KSHV identified that TXN is upregulated during latent infection. Here we investigate the role of TXN during latent KSHV infection of endothelial cells. TXN and one of its interacting partners, PRX1 are induced during latent infection and viral gene expression is required for increased TXN levels. The major latent locus is sufficient to upregulate TXN in endothelial cells. TXN expression is required for control of ROS in latently infected endothelial cells and TXN is important for the survival endothelial cells latently infected with KSHV likely through activation of JNK.

4.4 Results

4.4.1 KSHV infection upregulates TXN protein expression levels during latency

KSHV infection upregulates TXN protein expression levels during latency

Analysis of our previous proteomics data comparing mock and KSHV infected endothelial cells during latent KSHV infection at 48 hours post infection (hpi) indicated that TXN is significantly upregulated by KSHV (170). To validate this, we evaluated the protein expression levels of TXN in TIME cells at 48 and 96 hpi. Tert-immortalized microvascular endothelial cells (TIME cells) were infected with KSHV and levels of latent and lytic antigens were quantified by

immunofluorescence. Only infections where greater than 90% of the cells expressed LANA, a latent antigen, and less than 2% of the cells expressed a lytic marker of infection, ORF 59, at 48 hpi were used (data not shown). At 48 and 96 hpi cells were stained with an antibody to TXN and flow cytometry was used to quantify the protein levels on a single cell basis. There was an approximately two-fold increase in TXN levels at 48 hpi and over three-fold increase at 96 hpi (Figure 4.1 A-C). Western blot analysis and subsequent quantification on a Licor imager system showed that there was also a significant increase in TXN protein levels in primary human dermal microvascular endothelial cells (hDMVECs) at 96 hpi. (Figure 4.1 D-E).

4.4.2 KSHV latency locus is sufficient to induce TXN protein expression in endothelial cells

To determine if viral gene expression was necessary for TXN induction we compared TXN levels in mock, KSHV and UV-irradiated KSHV infections. UV irradiated virus can bind and enter cells but does not express viral genes. Flow cytometry analysis of cells stained with a TXN antibody at 96 hpi showed no increase in the expression of TXN following infection with UV irradiated virus (Figure 4.2 A-B) compared to mock infected cells while TXN was significantly increased as before. Therefore, the increase of TXN in latently infected cells requires KSHV gene expression and the upregulation of TXN protein expression is not mediated by a cellular response to virus binding or entry into the cell.

To determine if the gene expression from the major latent locus is sufficient to upregulate the expression of TXN, we used a helper dependent adenovirus containing the KSHV latency region comprised of LANA, vCyclin, vFLIP, Kaposins and the 12 microRNA loci. The helper dependent Adenovirus does not express any adenovirus genes as was described previously (170).

Cells were infected with a control gutted adenovirus (Ad) only expressing GFP (AdGFP) and the gutted adenovirus expressing the KSHV latency associated region (AdKLAR) and stained with TXN antibody. Infection rates for AdGFP and AdKLAR were greater than 90% as determined by expression of GFP or LANA measured by immunofluorescence respectively (not shown). In addition, to adjust for small differences in the infection rates, we gated on the GFP positive cells from the AdGFP infected cells and then compared to the AdKLAR cells. Cells infected with the AdKLAR expressing gutted adenovirus exhibited increased TXN protein expression compared to mock infected cells and AdGFP (Figure 4.2 C-D). Therefore, the latent locus is sufficient to induce TXN protein expression levels.

4.4.3 KSHV requires TXN during latency

Inhibition of TXN can lead to cell death in cancer cells (171). To determine the role of TXN during latent KSHV infection, we transiently knocked down TXN using siRNA complementary to the TXN mRNA in TIME cells. TXN was silenced by more than 85% at the gene expression level at 48 and 96 hours post transfection (Figure 4.3 A). Following silencing of TXN there was no overt effect on cell proliferation measured by quantifying the number of cells after transfection/ before seeding cells and compared with SCRB after 96 hours post seeding. Control (siRNA SCRB) and TXN knockdown cells (siTXN) were then mock and KSHV infected and cell death was quantified at 48 hpi by fluorescence for YOYO-1, a cell dye that only stains dead cells. There was a nearly 5-fold increase in relative YOYO-1 fluorescence in the KSHV infected cells transfected with the siRNA to TXN as compared to KSHV infected cells transfected with the control siRNA. (Figure 4.3 B-C). There was no significant difference in the staining for

YOYO-1 in the mock infected TXN knockdown cells compared to the control siRNA transfected cells. This data supports that KSHV requires TXN for the survival of latently infected endothelial cells. To determine if the increase in cell death in the KSHV infected cells in the absence of TXN was due to apoptosis, we used a pan-caspase inhibitor (QVD). There was no significant difference in the percentage of dead cells in KSHV infected cells with TXN silenced as compared the control siRNA transfected cells and to the mock infected cells, strongly suggesting that apoptosis is main cell death mechanism (Figure 4.3 B). These data indicate that KSHV infected endothelial cells require TXN to prevent apoptosis of latently infected cells.

TXN is part of the thioredoxin system that includes, TXN, thioredoxin reductase (TXNR) and NADPH. In the presence of oxidative stress, TXN, contains two cysteine residues in the catalytic center that when it interacts with an oxidize protein, donates its hydrogen becoming itself oxidized. TXNR is the enzyme that converts TXN from the oxidized state to the reduced form by scavenging hydrogen from NADPH. To evaluate if TXNR plays a role during latent KSHV infection, we utilized a pharmacologic inhibitor of TXNR, PMX464. TIME cells were mock and KSHV infected and overlaid with media containing PMX464 and at 48 hpi cell death was quantified by a trypan blue exclusion assay. PMX464 only slightly increased cell death in the mock infected cells. However, there was an approximately 5-fold increase in cell death in the KSHV infected cells treated with PMX464 cells compared to vehicle control treated KSHV infected TIME cells (Figure 4.3 D). Taken together, this data indicates that KSHV latently infected endothelial cells relies on the thioredoxin system for cell survival.

4.4.4 TXN is involved in regulating ROS during latency

To determine if TXN plays a role in KSHV regulation of intracellular ROS in endothelial cells, we transiently knocked down the gene expression levels of TXN using siRNA technology as mentioned above. TXN gene expression was knocked down by more than 85% using the siRNA described above. TIME cells transfected with the siRNA control (siSCRB) or the siRNA to TXN (siTXN) were mock or KSHV infected (iSLK derived) for 96 hours. Intracellular ROS levels were quantified by staining with a fluorescent probe (CELLROX) that binds to reactive oxygen species, followed by flow cytometry. KSHV infection of TIME cells transfected with the control siRNA induced a nearly two-fold increase in CELLROX fluorescent staining. Knockdown of TXN led to a nearly 2.5-fold increase in CELLROX fluorescence in the mock infected cells indicating that TXN controls the levels of ROS in uninfected cells. However, there was an even greater amount of CELLROX staining in the KSHV infected cells where TXN was knocked down (Figure 4.4 A). These results indicate that KSHV infection induces oxidative stress in latently infected cells but it controls the levels of ROS through induction of TXN.

4.4.5 PRDX1, a TXN binding partner, is upregulated and involved in regulating ROS in endothelial cells latently infected with KSHV

TXN has several binding partners that are involved in the of intracellular ROS levels, including PRDX1 (172, 173). We examined PRDX1 protein expression levels during latency in TIME cells and found that PRDX1 is also upregulated by more than 2-fold at 48 hpi of TIME cells (Figure 5. A-B). To determine if PRDX1 is also involved in regulating ROS, PRDX1 was knocked down by siRNA. PRDX1 mRNA was decreased by more than 75% in the TIME cells transfected

with siRNA directed to PRDX1 (Figure 4.5 C). Control endothelial cells (siSCRB) and PRDX1 knocked down cells were mock or KSHV infected reactive oxygen species were quantified at 96 hpi using CELLROX reactive oxygen species fluorescent probe and flow cytometry. There was a small but significant increase in reactive oxygen species levels in KSHV infected cells knocked down PRDX1 as compared to KSHV infection of the control siRNA transfected cells (Fig 4.5 D). This analysis demonstrates that there is an increase of reactive oxygen species levels in the absence of PRDX1 during KSHV latent infection indicating that PRDX1 is involved in regulating ROS in endothelial cells latently infected with KSHV.

4.4.6 The absence of TXN during KSHV infection activates phosphorylation of JNK

JNK and p38, are MAPK kinases involved in cellular signaling and stress responses including stress from reactive oxygen species (57, 174). Since TXN and PRDX1 are involved in regulating ROS, we evaluated the phosphorylation status of p38 and JNK in the absence of PRDX1 and TXN in mock and KSHV infected cells. TXN and PRDX1 gene expression was silenced using siRNA technology as above. Phospho-protein expression levels of p38 and JNK were determined by western blot of cells transfected with scrambled siRNA or siRNA to TXN or PRDX1 and mock or KSHV infected for 96 hours. We observed an increase in phosphorylation of JNK signaling in the KSHV infected TXN knocked down cells compared to the KSHV scrambled control (Figure 6. A). However, there was no significant induction of p38 phosphorylated (data not shown). Therefore, TXN controls reactive oxygen species and its downstream signaling.

4.4.7 The absence of TXN and PRDX1 during KSHV latent infection reduced lytic gene and protein expression levels of ORF59

TXN has been involved in regulating transcription factors mediated gene expression from PEBP2/CBF and NF-kB (175, 176). To evaluate if the absence of TXN and PRDX1 has an effect on lytic gene expression, we measured gene expression levels of ORF59 in the absence of TXN and PRDX1 genes. We mock and KSHV infected siSCRB, siTXN, siPRDX1 and evaluated gene expression levels using quantitative RT-PCR. We identified that in the absence of TXN and PRDX1 there is a decrease gene expression by approximately .50- and .40-fold, respectively and 2- and 4-fold decreased respectively, in protein expression levels of ORF59 measured by immunofluorescence (Figure 4.7 A-B) without altering LANA expression cells (Figure 4.7 C). These indicates that TXN and PRDX1 are involved in regulating gene expression of ORF59.

4.5 Discussion

Latent viruses must counteract cellular stress responses to allow survival of the persistently infected cell. ROS is often increased in infected cells and some viruses have evolved to utilize ROS for replication (83, 177). Interestingly, KSHV utilizes ROS during initial entry of the virus and there are elevated levels of ROS in KSHV infected PEL cells and increased ROS in de novo infected endothelial cells (80, 83). We also found that there is increased ROS in latently infected endothelial cells at later times during latency. Therefore, KSHV latent infections could also potentially benefit from increased ROS during latency in endothelial cells. In line with this, there is evidence for KSHV induced vascular permeability dependent on increases oxidative stress (81). Therefore, KSHV may utilize increased oxidative stress for initial infection as well as maintenance

of latency in endothelial cells. However, if unchecked, increased intracellular ROS levels can be deleterious to maintenance of a long-term infected cell. Additionally, the addition of H_2O_2 to cells induces reactivation. Therefore, KSHV has evolved mechanisms to control the balance of ROS levels during latent infection.

We found that TXN, the primary effector protein of the Thioredoxin system for scavenging ROS, is upregulated during KSHV latent infection of endothelial cells. Knockdown of TXN leads to larger increases of ROS in the latently infected cells supporting a role for viral induction of TXN to control of ROS during latent infection. Knockdown of TXN ultimately leads to increased cell death in latently infected endothelial cells indicating the likely importance of controlling ROS in latently infected cells. However, further work is necessary to determine if the increased cell death is due to the increase in ROS or if TXN is required for other essential activities in latently infected endothelial cells. Two map kinases, p38 and JNK, have been associated with oxidative stress. The phosphorylation of JNK but not p38 is altered in latently infected endothelial cells when TXN gene expression is silenced. Therefore, KSHV induction of TXN is likely to control the activation of phosphorylation of JNK cell signaling pathway to protect cells from ROS induced death (Figure 6. A).

TXN has been shown to physically interact with several binding partners such as TXNR, ASK-1, PRDX1, PRDX2, P53, NFK-B, TXNIP, Ape-1, etc. (58, 173, 178-180). PRDX1 is an oxidoreductase protein containing cysteine residues in the catalytic center and it interacts with H_2O_2 converting it to water and switching the redox states of its interacting proteins (172, 173). Western blot analysis showed that PRDX1 is upregulated at the protein level in latently infected endothelial cells. Additionally, in the absence of PRDX1 there is an increase ROS levels indicating

that PRDX1 also plays a role in regulating ROS during latent infection, likely in conjunction with the TXN system (Figure 4.5 A-D) as previously reviewed (172, 173, 178).

KSHV upregulation of TXN is not a simple cellular response to infection but rather driven by viral factors. UV irradiated virus does not induce TXN indicating binding and entry of the virus are not sufficient and that KSHV gene expression is required. The induction of TXN occurred during predominantly latent infection with KSHV, however, there is a very low percentage of cells that express markers of lytic replication during infection of endothelial cells in culture (117). To ensure that the low level of lytic genes was not responsible for the induction of TXN we expressed the major latent locus without any lytic genes from a gutted adenovirus and found that the latent locus was sufficient to induce TXN (Figure 4.2 A-D). Previous studies have shown that one latency associated protein, vFLIP, upregulates superoxide dismutase (MnSOD) which regulates the conversion of superoxide to H_2O_2 (36). vFLIP upregulation of MnSOD increased resistance of endothelial cells to superoxide mediated cell death (36). Here we found that KSHV also induces the TXN pathway to limit the accumulation of H_2O_2 in latently infected cells and maintain an orchestrated balance of oxidative stress during latent infection. Disruption of this balance leads to death of latently infected endothelium, thereby providing novel therapeutic avenues for treatment of KS.

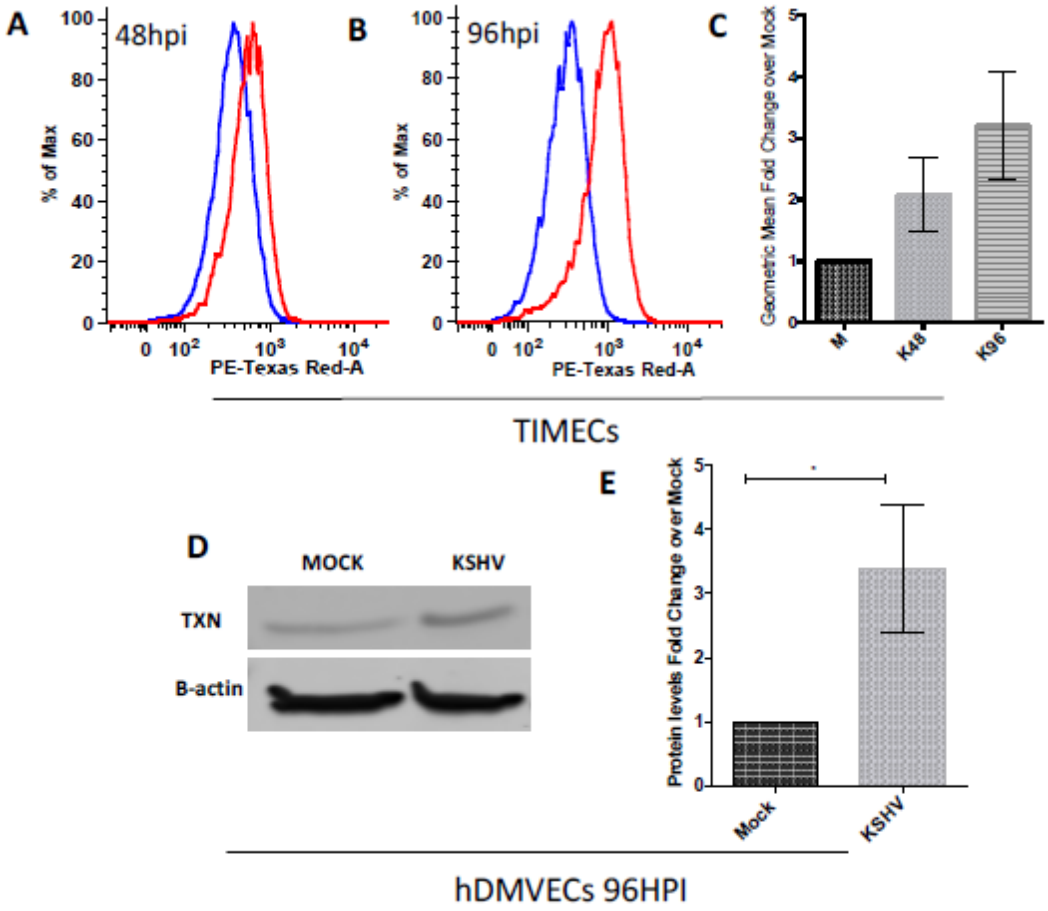

Figure 4.1 KSHV upregulates TXN protein expression levels (A-B.) TIME cells were mock and KSHV (iSLK derived) infected and at 48 and 96 hpi, cells were harvested, fixed and stained with antibody to TXN, for single cell analysis using flow cytometry. **(C.)** Geometric mean fold change analysis of KSHV (iSLK-derived) over mock at 48 and 96 hpi for three biological replicates from panel A and B, $p < 0.05$ student's t-test. **(D.)** Immunoblot analysis of TXN in mock and KSHV (BCBL1-derived) infected hDMVECs at 96 hpi**. (E.)** Geometric mean fold change of KSHV over mock at 96 hpi for three biological replicates from panel D, $p < 0.05$ student's t-test. The error bar reflects the standard error of the mean of three independent experiments.

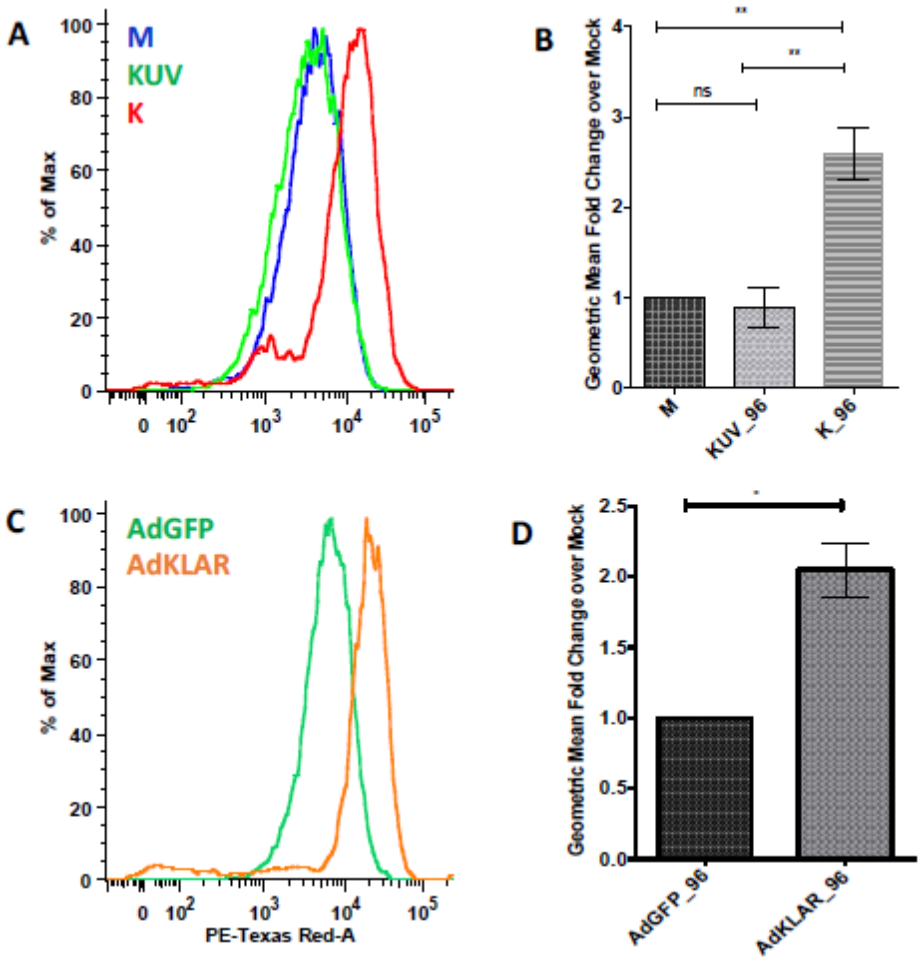

Figure 4.2 The KSHV latency region is sufficient to upregulate TXN. (A.) TIME cells were mock (M), KSHV UV irradiated (KUV, iSLK-derived) an KSHV (K) iSLK-derived, infected at 96 hpi, cells were harvested, fixed and stained with antibody to TXN, for single cell analysis using flow cytometry**. (B.)** Geometric mean fold change of KSHV UV irradiated (KUV) and KSHV (K) over mock (M) at 96 hpi for three biological replicates from panel A, $p < 0.05$ student's t-test. **(C.)** TIME cells were Adenovirus GFP (AdGFP, control) and Adenovirus KLAR (AdKLAR) infected and at 96 hpi cell were harvested, fixed and stained with antibody to TXN, for single cell analysis using flow cytometry. **(D.)** Geometric mean fold change of KSHV over mock at 96 hpi for three biological replicates from panel D, $p < 0.05$ student's t-test. The error bar reflects the standard error of the mean of three independent experiments.

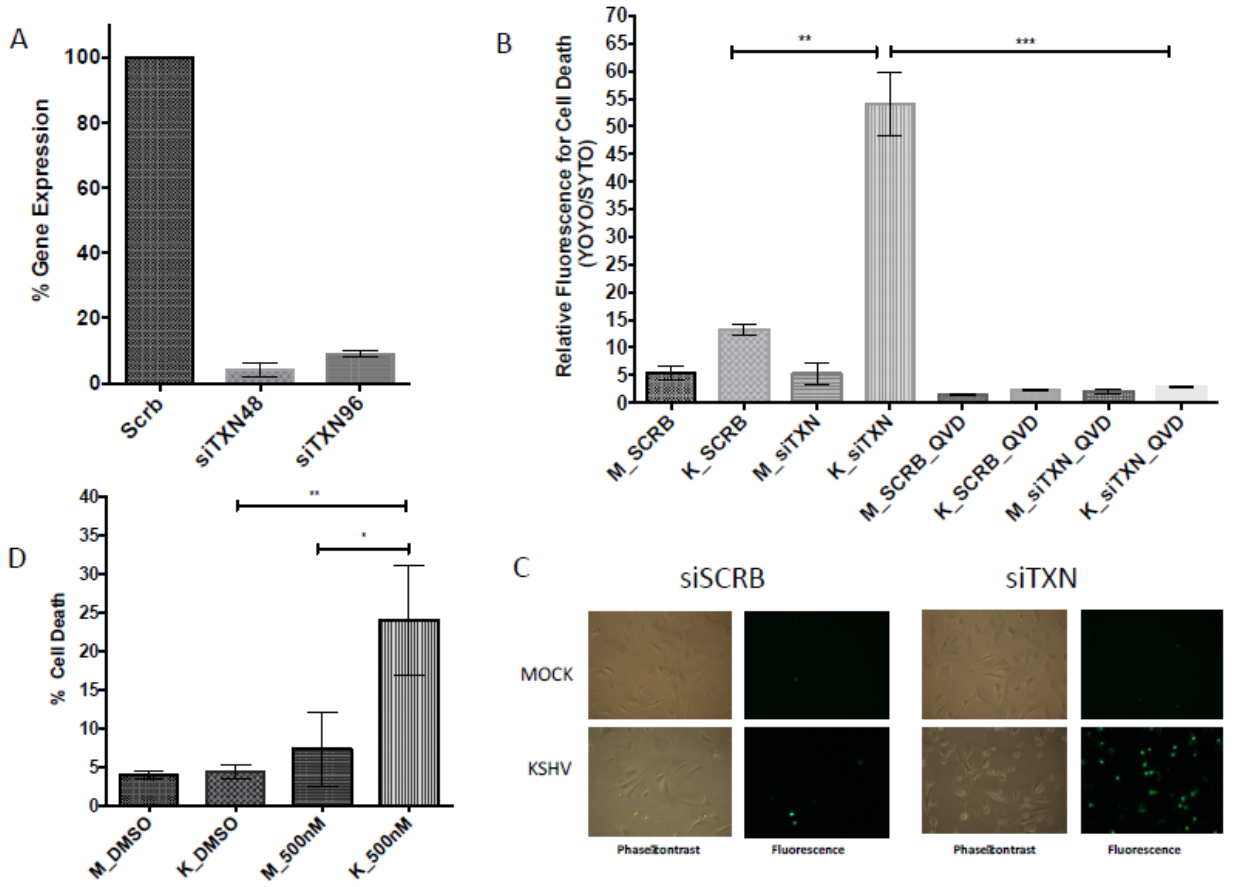

Figure 4.3 KSHV latently infected endothelial cells requires TXN and apoptosis is de main cell death mechanism. (A.) Quantitative real-time RT-PCR was used to analyze TXN mRNA expression levels of control siSCRB- or TXN siRNA-transfected TIME cells measured at 48 and 96 h post-transfection. The data are reported as percent gene expression in mRNA of TXN siRNA versus control siSCRB. **(B.)** TIME cells were transfected with siRNA control (siSCRB) and siRNA to TXN and at 24 hours post transfection cells were mock and KSHV (BCBL1-derived) infected for 48hpi. YOYO-1 or SytoGreen24 were added to wells to quantify dead cells and total cell numbers, respectively. Each condition was examined in triplicate, and scanned for relative fluorescence on the Typhoon scanner. Relative fluorescent percent cell death was calculated (YOYO-1 positive cells/SytoGreen24 positive cells). Data represents the average of three independent experiments. Relative fluorescence shown is normalized to SytoGreen24 levels (total cell count). **(C.)** Representative microscopy images of YOYO-1 samples at 48 hours post treatment. Live cell imaging was captured on the phase contrast microscope and picture were take using Qcapture software. **(D.)** TIME cells were infected with KSHV and treated with PMX464 for the duration of the infection (48 hpi) and cell death was evaluated by Trypan blue assay using a TC cell counter. The error bar reflects the standard error of the mean of three independent experiments $p < .05$

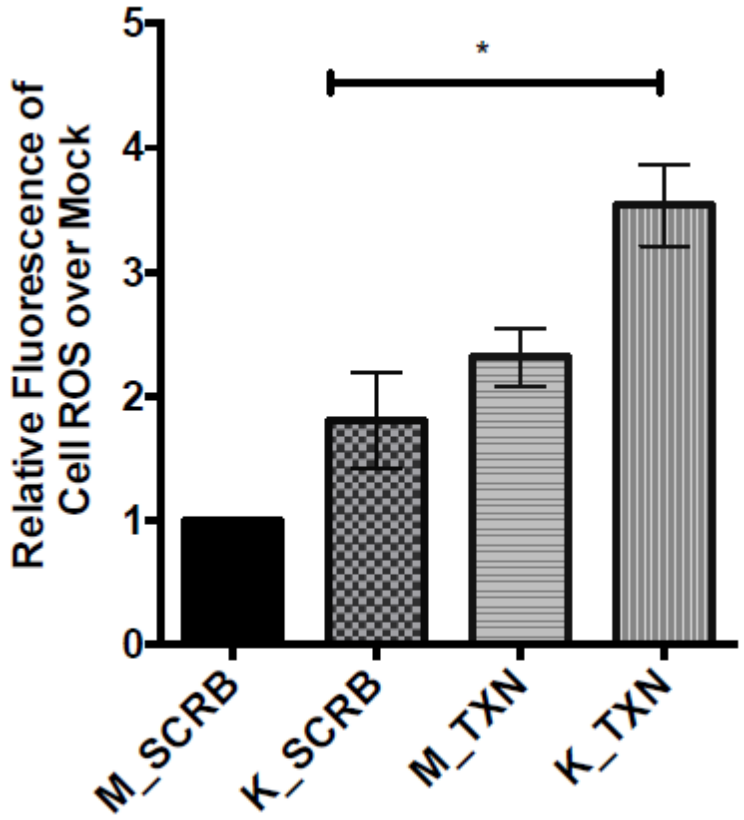

Figure 4.4 TXN is involved in regulating ROS in endothelial cells during KSHV latent infection. TIME cells were transfected with siRNA control (SCRB) and siRNA to TXN. At 24 hpt cells were re-seeded in a 6-well plate and then were mock and KSHV (iSLK-derived) infected for 96 hpi. 1uM of CELLROX was added for 30 minutes to each well and then cells were harvested and fixed for single cell analysis using flow cytometry. The error bar reflects the standard error of the mean of three independent experiments.

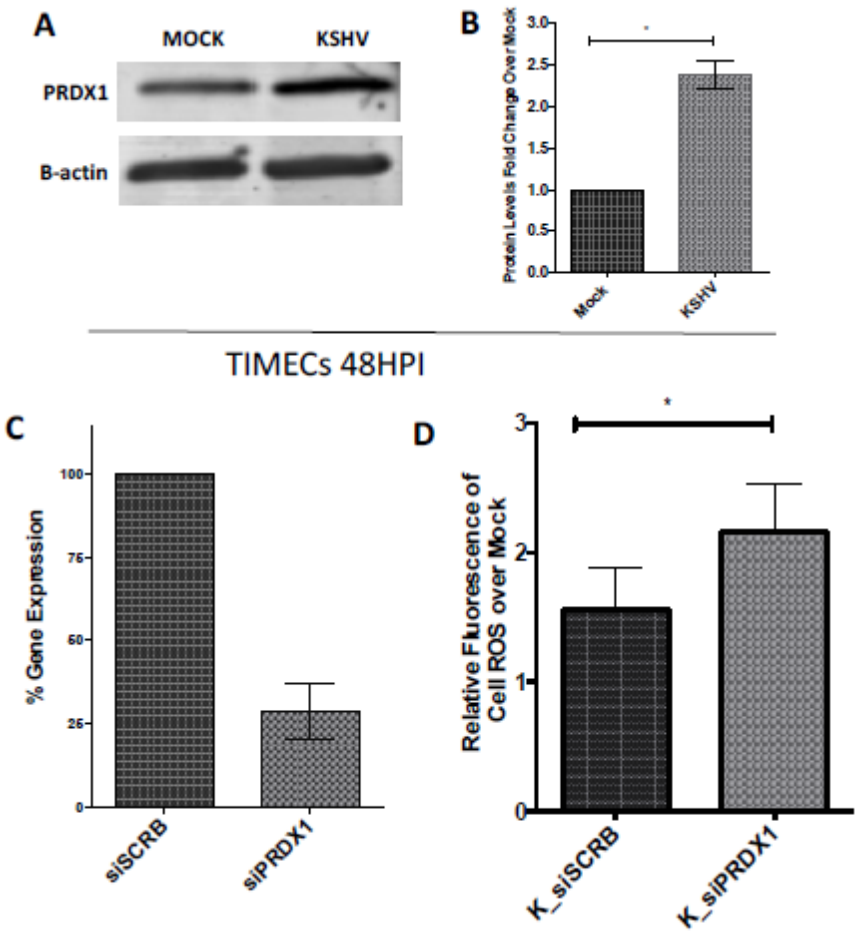

Figure 4.5 PRDX1, a TXN binding partner, is upregulated and its involved in ROS during latent KSHV infection. (A.) Immunoblot analysis of PRDX1 in mock and KSHV (BCBL1-derived) infected TIME cells at 96 hpi. **(B.)** Geometric mean fold change of KSHV over mock at 48 hpi for three biological replicates from panel A, $p < 0.05$ student's t-test. **(C.)** Quantitative real-time RT-PCR was used to analyze PRDX1 mRNA expression levels of control siSCRB- or PRDX1 siRNA-transfected TIME cells measured at 48 h post-transfection. The data are reported as fold change in mRNA of PRDX1 siRNA versus control siSCRB. **(D.)** TIME cells were transfected with siRNA control (SCRB) and siRNA to PRDX1. At 24 hpt cells were re-seeded in a 6-well plate and then were mock and KSHV (iSLK-derived) infected for 96 hpi. 1uM of CELLROX was added for 30 minutes to each well and then cells were harvested and fixed for single cell analysis using flow cytometry. The error bar reflects the standard error of the mean of three independent experiments.

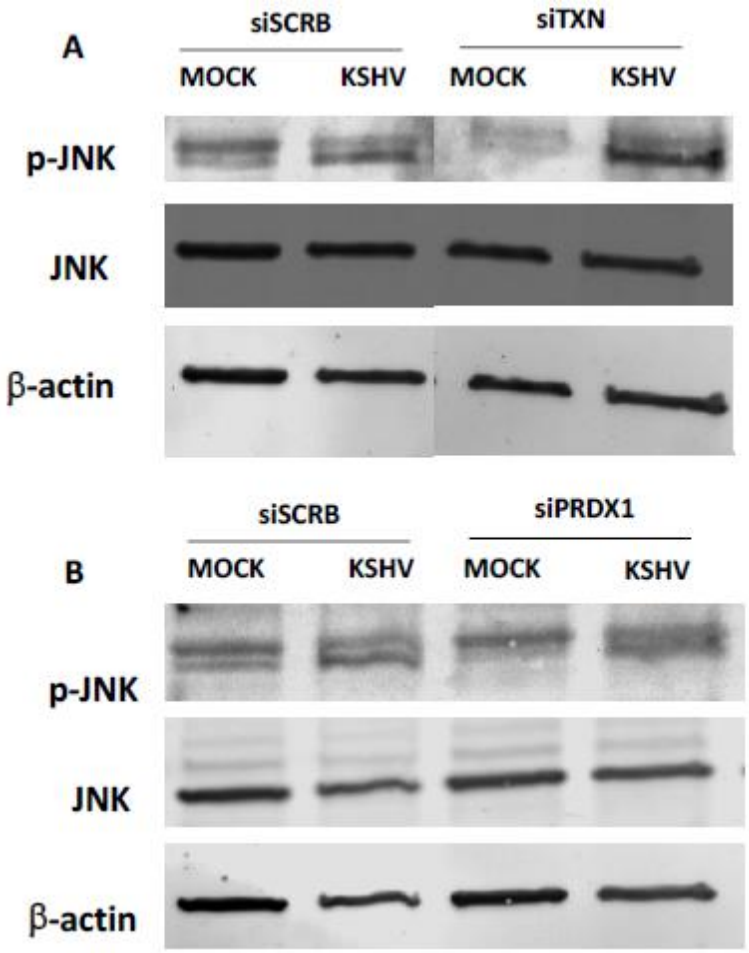

Figure 4.6 KSHV infection of endothelial cells increases phosphorylation levels of JNK. TIME cells were Mock- or KSHV-infected (BCBL1-derived) and whole-cell lysates were harvested at 96 hpi. Lysates were subjected to immunoblot analysis using the indicated antibodies. β-actin standard was included as loading controls. Representative immunoblots of **(A.)** phospho JNK was evaluated in siTXN samples **(B.)** phospho JNK was evaluated in siPRDX1 samples.

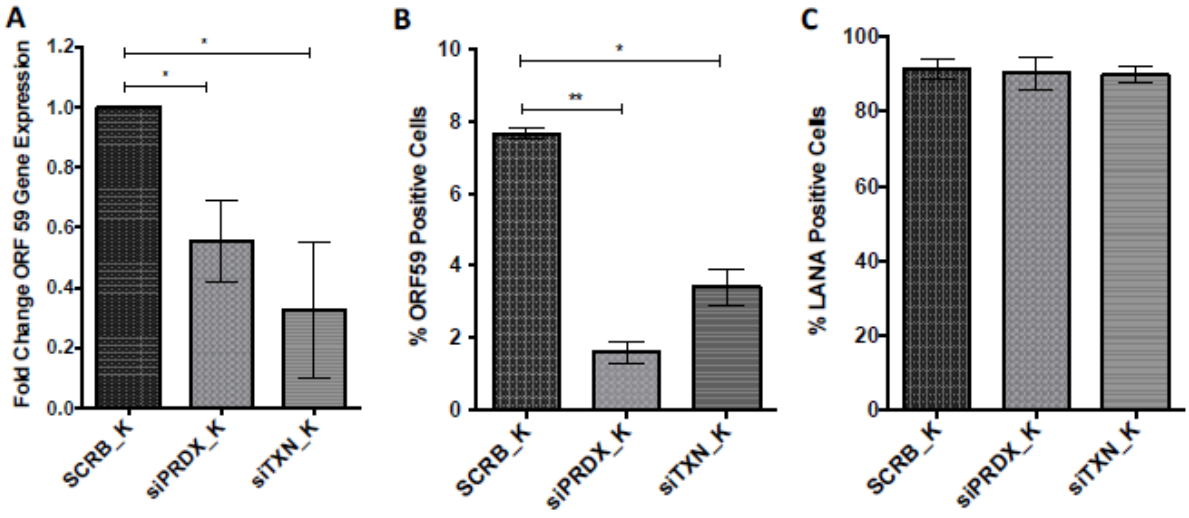

Figure 4.7 TXN and PRDX1 influences gene and protein expression of ORF59. TIME cells were transfected with siRNA control (SCRB) and siRNA to TXN. At 24 hpt cells were re-seeded in a 6-well plate and then were mock and KSHV (iSLK-derived) infected for 96 hpi and harvested for: **(A.)** ORF59 gene expression measured by RT-PCR **(B.)** % of ORF59 positive cells measured by immunofluorescence assay. **(C.)** % of LANA positive cells measured by immunofluorescence assay.

Chapter 5. Conclusions and Future Directions

5.1 Summary

KSHV alters host cellular signaling pathways to allow a long term latent infection (181). Modulating major signal transduction events can alter the cellular response allowing encampment of KSHV latent infection. Some of the major cellular alterations serve to establish an inflammatory and oxidative state conducive to the tumor microenvironment and induce angiogenesis leading to a positive feedback for tumor maintenance (81, 120). To allow this, KSHV reprograms carbon source utilization which provides biomolecules and metabolic precursor important to cancer biology while upregulating enzymes required to process increased oxidative burden generated in the course of increased lipid metabolism.(8, 120, 182-185).

Our lab has established that KSHV latent infections reprograms glucose and glutamine metabolism (70, 130). Other groups have shown through flux analysis that these carbon sources get metabolized to produce increased pools of fatty acids either to support membrane biogenesis or virion production in HSV and HCMV infections (70, 74, 75). Our lab has established that fatty acid synthesis is required during latency and lipid droplets formation is increased (40). This was confirmed by demonstrating that pharmacological inhibition of fatty acid synthesis resulted in more than 60% death of the infected cell population while addition of palmitate partially rescued cell death (40). However, how these lipids are utilized during KSHV latency has not been elucidated.

I used an integrated systems biology approach where two datasets, one from mass spectrometry based proteomics and the other from next generation sequencing for transcriptomics analysis, with similar conditions of mock and KSHV infected TIME cells were combined to

provide a more comprehensive view of the signaling events during latency. Proteomics and transcriptomics analysis data were collected for endothelial cells latently infected with KSHV under identical experimental conditions. Proteomics data provided signaling events from the upstream signal transduction mediated by proteins and phosphoproteins from mock- and KSHV-infected endothelial cells at 48 hpi. Transcriptomics analysis revealed downstream transcriptional responses following latent infection. To connect upstream protein signal transduction to downstream gene expression, we used transcriptomics data to predict putative transcription factors that might be in control of regulating gene expression. The identified transcription factors were then used to connect upstream signaling to downstream gene expression using a Steiner forest algorithm of protein-protein interactions. With this approach, we identified several pathways that were altered. Among these, peroxisome pathways were predicted and confirmed to be altered. More specifically, we identified that two peroxisomal proteins involved in transport of very long chain fatty acids (ABCD3) and an enzyme involved in partial breakdown of these lipids (ACOX1) are relied upon during latent KSHV infection. This finding is further corroborated by a previous metabolomics screen where DHA, the product of ACOX1 activity, is elevated. Biological significance of our findings is further substantiated by the observed increase of peroxisome organelles that is associated with the increase of lipid metabolism, providing insight into the cellular mechanisms of how these lipids are processed during the latent KSHV infection.

From the same proteomics screen, we determined that TXN protein levels are upregulated during KSHV latency and validated this finding experimentally. We also showed that TXN, an antioxidant protein, is required during the infection and that it is involved in regulating intracellular ROS during latency. Further we confirmed that the upregulation of TXN requires viral gene expression.

Findings from my work elucidate how KSHV processes intracellular ROS while metabolizing VLCF. KSHV infections induces inflammation and DHA has been involved in mitigating inflammation. Therefore, we can hypothesize that KSHV modulates peroxisomes to activate DHA synthesis that may be important stimulate anti-inflammatory responses preventing immune responses against inflammation.

5.2 Future Directions and Conclusions

5.2.1 Future Directions: KSHV upregulates and relies on peroxisome mediated lipid metabolism in latently infected endothelial cells.

Integration of mass spectrometry based proteomic techniques with other large-scale analyses is becoming more feasible. The advantages of combining high throughput approaches is to increase coverage, reliability and convergence in the findings that one dataset alone is not capable to provide with confidence. Prior to the presently discussed thesis project, there were no integrated analyses of multiple datasets applied to study herpesviruses, and more specifically, in KSHV infections. I have conducted the first global analysis of the proteome and phosphoproteome of endothelial cells in response to KSHV infection. We identify several proteins and phosphoproteins that were altered by KSHV. Out of these, several proteins were novel hits while others were previously known to be altered, which provided us with confidence that the methodological approach was valid. We were successful in enriching for low abundant phosphotyrosine residues that are normally very difficult to identify by mass spectrometry in highly complex samples. In particular, we identified phosphorylated STAT3, which is a protein that has been involved in several phenotypes during KSHV infection such as in angiogenesis,

inflammation, migration etc. (86, 186). We use a helper dependent gutted adenovirus empty (control) and expressing only the KSHV Latency Associated Region (KLAR). With this approach, we were able to narrow down that the upregulated peroxisome numbers observed are mediated by KLAR. This indicates that KLAR is sufficient. However, it does not indicate that the entire KLAR is required. Therefore, it will be interesting to evaluate individual latent viral genes and identify if these phenotypes are mediated by one viral gene or in combination. My preliminary data in cells over expressing LANA found that the number of peroxisome is increased as well as the peroxisome protein (ABCD3) (S_Figure 3.15 A, C-D). Therefore, I hypothesize that LANA alone is sufficient to increase peroxisome number or peroxisome count per cell. However, this experiment needs to be replicated. LANA is responsible for tethering the KSHV genome to the host genome, therefore deleting LANA will prevent the establishment of latency. Instead, I propose to perform single point mutations in LANA, vCyc, vFLIP, and Kaposins individually and test if these gene are required. Moreover, I evaluated if the microRNAs are required for the peroxisome phenotype. I used a deleted microRNAs KBAC virus and measured the peroxisome transporter, ABCD3. There was no decrease in expression of ABCD3 in the absence of the mircroRNA loci (S_Figure 3.15 B). This experiment indicated that the microRNAs were not required for the upregulation of ABCD3.

Another aspect that I am interested in evaluating from this work is identifying if DHA, the metabolite that is upregulated by our metabolomics screen, is involved in regulating anti-inflammatory responses. I would like to propose to rescue cell death of the KSHV latently infected cells in the absence of ACOX-1, the enzyme involved in synthesizing DHA and add back DHA to the cells. Also, I would like to evaluate if DHA is involved in anti-inflammation and if it is upregulated in KS tumors. I will examine this by silencing the gene expression of ACOX1 and

then measured the levels of PGE2, IL6 and COX2, which are cytokines involved in inflammation, before and after treatment with DHA. Previous evidence has shown that treatments with DHA in endothelial cells after LPS insults decrease the release of the cytokines mentioned above indicating that DHA is involved in anti-inflammatory responses (161).

In addition, ether lipids are metabolized in the peroxisome. We are also interested in evaluating the role of ether lipid metabolism during latency since it has been previously shown that Influenza virus requires ether lipid metabolism for virion production (45). Interestingly, from the metabolomics screen done in our lab, ether lipid metabolites were also upregulated. Future experiments will be needed to evaluate the role of these metabolites and others since these are synthesized in the peroxisome and play a vital role in other viral infections. My work opened new avenues to explore lipid metabolism and how these lipids are utilized during the latent KSHV infection.

5.2.2 Future Directions: KSHV modulates oxidoreductase proteins to regulate oxidative stress during latency and possibly in lytic reactivation.

From the proteomics analysis, I identified and validated that TXN as well as its binding partner PRDX1 are upregulated. We also found that TXN and PRDX1 are both involved in regulating oxidative stress and that KLAR was sufficient to upregulate TXN protein levels. Similarly, as mentioned above, it will be interesting to identify which single viral gene is mediating the induction of TXN protein expression. Previous studies have shown that in over expressing vFLIP cells, vFLIP upregulates MnSOD, a superoxide scavenger, in a NF-kB dependent manner (36). In addition, NF-kB inhibition leads to increase of ROS levels (36) and vFLIP is the master

regulator of inhibiting apoptosis during latency (2, 7). This leads me to hypothesize that vFLIP might be the viral gene involved in modulating host redox proteins (PRDX1 and TXN) to regulate oxidative stress thus preventing cells death.

I determined that KSHV viral gene expression is required for regulation of redox homeostasis during infection and that in the absence of TXN and PRDX1 there is decreased expression of ORF59, a lytic gene. This strongly suggests two alternative hypotheses that: 1.) TXN is involved in regulating the redox thiol states of cysteine residues of transcription factors (TF) regulating ORF59 gene expression directly, or the redox states of signaling molecules that in the absence of TXN fail to activate lytic gene expression leading to cell death; or 2.) cells are dying rapidly before reactivation has a chance to occur, therefore the decrease in lytic gene expression is an indirect effect of cell death. Further work needs to be done to evaluate redox states of the proteins involved in cell signaling in endothelial cells using redox native immunoblots. This will determine if, indeed, proteins driving cell signal transduction that leads to activation of gene transcription are sensitive to redox regulation. This work will identify targets in latent KSHV infection that are susceptible to pharmacological treatments.

5.2.3 Conclusions

In conclusion, using an integrating systems biology approach, we identified two novel pathways modulated by KSHV latent infection. I found that KSHV latent infection induces an increase in peroxisome organelle biogenesis and requires two peroxisome proteins (ABCD3 and ACOX1) involved in lipid metabolism of VLCFs. From the proteome analysis, I also identified that two oxidoreductase proteins (TXN and PRDX1) involved in regulating oxidative stress are required

during latent KSHV infection. These results indicate that the metabolism of VLCFs in the peroxisome and regulation of oxidative stress are vital biological processes required to support KSHV pathogenesis and influence KS development. Most notably, metabolism of VLCFs (24:6n3), to synthesize DHA, generates ROS. DHA may have anti-inflammatory properties important to KS biology while ROS produce oxidative stress that is managed by viral upregulation of host mechanisms produced as a by-product of increased lipid metabolism in the peroxisome that leads to activation of redox proteins (PRDX1 and TXN) to maintain homeostasis. Therefore, this works demonstrates two novel distinct metabolic pathways that play such an essential role in regulating KSHV latency as well as a putative connection between them. Further work needs to examine if VLCFs metabolism occurring in peroxisomes is the main source of ROS generated during latency. Therefore, identifying the main source of ROS production will be an interesting area for further examination. Additionally, the novel pathways identified in our work may serve to provide therapeutic targets that could handicap KSHV latent infection and treat KS tumors while avoiding reactivating cells to the lytic phase. This would prevent further viral dissemination and selectively affect KSHV latently infected cells allowing unimpeded proliferation to healthy cells.

Copyrights Permissions

Sychev ZE, Hu A, DiMaio TA, Gitter A, Camp ND, Noble WS, Wolf-Yadlin A, Lagunoff M.. Integrated systems biology analysis of KSHV latent infection reveals viral induction and reliance on peroxisome mediated lipid metabolism. PLoS Pathog. 2017;13(3):e1006256/ journal.ppat.1006256, Open access journal.

Zoi E. Sychev

Molecular and Cellular Biology Program,
Department of Microbiology and Genome Science
University of Washington
Box 357735
Seattle, WA 98195
Email: zvillasa@uw.edu

Education

2011-2017 University of Washington, Seattle WA
Ph.D., Molecular & Cellular Biology Program, predicted to Graduate in Winter, 2017

2004-2008 Florida International University, Miami FL
B.S. Biological Sciences concentration in Molecular Cell Biology and minor in Dietetics Nutrition

Research Experience

2011-Present **Graduate Student**
Michael Lagunoff PhD, Principal Investigator (Primary Mentor), UW Microbiology and MCB
Alejandro Wolf-Yadlin PhD, Principal Investigator (co-Mentor), UW Genome Science and MCB
Thesis: Unraveling the Proteome of Endothelial Cells Infected with KSHV during latency.

2008-2010 **Post-baccalaureate Research Technician**
Washington University in St Louis, School of Medicine
Department of Pathology and Immunology
Herbert Virgin MD, PhD and David Wang PhD, Principal Investigators
Project: Pathogen Discovery

2005-2008 **Undergraduate Independent Research**
Florida International University, Department of Biological Sciences
Alejandro M. Barbieri PhD, Principal Investigator
Project: Rabex-5 interactions with the Vps9 domain of insulin receptor tail during endosomal formation.

2007 **BioMedRAP Undergraduate Summer Research**
Washington University in St Louis, School of Medicine
Department Molecular Microbiology and Microbial Pathogenesis
Eduardo A. Groisman PhD, HHMI Principal Investigator (currently at Yale School of Medicine)
Project: Transcriptional Regulation of the PhoP/PhoQ system in *Salmonela E.*

Research Fellowships and Funding

2014-2017 National Science Foundation Graduate Fellow (NSF-GRFP), UW
2012-2014 Interdisciplinary Dual Mentor Fellowship in Cancer Research, UW
2006 -2008 MARC U*STAR Fellow, FIU
2005-2006 McNair Fellow, FIU

Awards

2016	41st Annual International Herpesvirus Workshop Travel Award
2016	SACNAS National Conference Travel Award
2007	McNair Undergraduate Symposium Oral Presentation Award

Publications

Sychev ZE, Wolf-Yadlin A, Lagunoff M. "KSHV Induces the Thioredoxin System to maintain redox regulation during latency" *(Manuscript in preparation)*. **2017**

Sychev ZE, Hu A, DiMaio TA, Gitter A, Camp ND, Noble WS, Wolf-Yadlin A, Lagunoff M. "Integrated Systems Biology Analysis of KSHV Latent Infection Reveals Viral Induction and Reliance on Peroxisome Mediated Lipid Metabolism". PLoS Pathog. 2017;13(3):e1006256

Loh J, Zhao G, Presti RM, Holtz LR, Finkbeiner SR, Droit L, ***Villasana Z**, Todd C, Pipas JM, Calgua B, Girones R, Wang D, Virgin HW. "Detection of novel sequences related to African Swine Fever virus in human serum and sewage". J Virol. 2009 Dec;83(24):13019-25.

Galvis A, Balmaceda V, Giambini H, Conde A, ***Villasana Z**, Fornes MW, Barbieri MA. "Inhibition of early endosome fusion by Rab5-binding defective Ras interference 1 mutants. Arch Biochem Biophys. 482(1-2):83-95 (2009).

Galvis A, Giambini H, ***Villasana Z** , Barbieri MA. "Functional determinants of ras interference 1 mutants required for their inhibitory activity on endocytosis. Exp Cell Res 10. 315 (5):820-35 (2009).

***(Maiden name: Villasana)**

Presentations at Scientific Conference in Graduate School

Oral Presentations

Sychev ZE, Hu A, DiMaio TA, Gitter A, Camp ND, Noble WS, Wolf-Yadlin A, Lagunoff M. Integrated Systems Biology Analysis of KSHV Latent Infection Reveals Viral Induction and Reliance on Peroxisome Mediated Lipid Metabolism. SACNAS Conference. October 2016. Long Beach, CA.

Sychev ZE, Hu A, DiMaio TA, Gitter A, Camp ND, Noble WS, Wolf-Yadlin A, Lagunoff M. Integrated Systems Biology Analysis of KSHV Latent Infection Reveals Viral Induction and Reliance on Peroxisome Mediated Lipid Metabolism. 41st Annual International Herpesvirus Workshop. July 2016. Madison, WI.

Sychev ZE, Hu A, DiMaio TA, Gitter A, Camp ND, Noble WS, Wolf-Yadlin A, Lagunoff M.

Integrated Systems Biology Analysis of KSHV Latent Infection Identifies that KSHV induces Peroxisome Biogenesis. SACNAS National Conference. October 2015. Washington, DC.

Sychev ZE, Hu A, DiMaio TA, Gitter A, Camp ND, Noble WS, Wolf-Yadlin A, Lagunoff M. Integrated Systems Biology Analysis of KSHV Latent Infection Identifies that KSHV induces Peroxisome Biogenesis. 18th Annual KSHV Workshop. July 2015. Miami, Fl.

Poster Presentations

Sychev ZE, Hu A, DiMaio TA, Gitter A, Camp ND, Noble WS, Wolf-Yadlin A, Lagunoff M. Integrated Systems Biology Analysis of KSHV Latent Infection Reveals Viral Induction and Reliance on Peroxisome Mediated Lipid Metabolism. 41st ANNUAL IHW. July 2016. Madison, WI.

Sychev ZE, Wolf-Yadlin A, Lagunoff M. Redox regulation proteins were identified in the proteome of KSHV infected endothelial cells. SACNAS National Conference. October 2014. Los Angeles, CA.

Sychev ZE, Wolf-Yadlin A, Lagunoff M. Redox regulation proteins were identified in the proteome of KSHV infected endothelial cells. HUPO Conference. April 2014. Seattle, WA.

Sychev ZE, Wolf-Yadlin A, Lagunoff M. Unraveling the proteome of endothelial cells infected with KSHV during latency. SACNAS National Conference. October 2013. San Antonio, TX.

Sychev ZE, Wolf-Yadlin A, Lagunoff M. Unraveling the proteome of endothelial cells infected with KSHV during latency. SACNAS National Conference. October 2012. Seattle, WA.

Laboratory Teaching/ Mentoring Experience

- Summer 2015-present: Undergraduate Research, Yashmira Naidoo
- Autumn 2015: Microbiology Rotation Graduate Student, Justin T. Ulrich-Lewis
- Winter 2014- Summer 2015: Post-baccalaureate Student, Victoria Ortega

Formal Teaching Experience

- Winter 2013: Biology 302: Molecular Techniques Laboratory
- Summer 2012: BioQuest Academy at Center for Infectious Disease Center

Society for the Advancement of Chicanos & Native Americans in Science (2011-present)

SACNAS is a STEM student-led chapter that connects students with opportunities to mentor and network with students and faculty in their field, and present their independent research. The organization was founded to increase the number of Native and Hispanic students in the research sciences and today hosts one of the largest annual research conferences for Underrepresented Minority (URM) students in STEM. I have helped organize and lead professional/academic workshops and I have held leadership roles in our UW Chapter. I have attended and presented at the National SACNAS Conference annually throughout graduate school.

SACNAS Leadership Positions

- 2015-2016: Chapter National Liaison
- 2014-2015: Chapter Treasurer
- 2013-2014: Chapter Secretary
- UW Molecular and Cell Biology Program STEM graduate student recruiter
- 2016 Academic development session: Chair and Speaker
- 2015 Academic development session: Chair and Speaker

UW SACNAS Chapter of the Year Awards: SACNAS National Conference

2015: Chapter Pillar Award
2014: Graduate School Chapter of the Year
2013: Distinguished Chapter Award
2012: Graduate School Chapter of the Year

Bibliography

1. Davison AJ, Eberle R, Ehlers B, Hayward GS, McGeoch DJ, Minson AC, et al. The order Herpesvirales. Arch Virol. 2009;154(1):171-7.
2. Fields BN KD, Howley PM. Fields Virology [Internet]. Fields Virology2007.
3. McGeoch DJ, Cook S, Dolan A, Jamieson FE, Telford EA. Molecular phylogeny and evolutionary timescale for the family of mammalian herpesviruses. J Mol Biol. 1995;247(3):443-58.
4. Chang Y, Cesarman E, Pessin MS, Lee F, Culpepper J, Knowles DM, et al. Identification of herpesvirus-like DNA sequences in AIDS-associated Kaposi's sarcoma. Science. 1994;266(5192):1865-9.
5. Cesarman E, Chang Y, Moore PS, Said JW, Knowles DM. Kaposi's sarcoma-associated herpesvirus-like DNA sequences in AIDS-related body-cavity-based lymphomas. N Engl J Med. 1995;332(18):1186-91.
6. Soulier J, Grollet L, Oksenhendler E, Cacoub P, Cazals-Hatem D, Babinet P, et al. Kaposi's sarcoma-associated herpesvirus-like DNA sequences in multicentric Castleman's disease. Blood. 1995;86(4):1276-80.
7. Ganem D. KSHV infection and the pathogenesis of Kaposi's sarcoma. Annu Rev Pathol. 2006;1:273-96.
8. Purushothaman P, Uppal T, Sarkar R, Verma SC. KSHV-Mediated Angiogenesis in Tumor Progression. Viruses. 2016;8(7).
9. Shepherd FA, Maher E, Cardella C, Cole E, Greig P, Wade JA, et al. Treatment of Kaposi's sarcoma after solid organ transplantation. J Clin Oncol. 1997;15(6):2371-7.
10. Montagnino G, Bencini PL, Tarantino A, Caputo R, Ponticelli C. Clinical features and course of Kaposi's sarcoma in kidney transplant patients: report of 13 cases. Am J Nephrol. 1994;14(2):121-6.
11. Lesnoni La Parola I, Masini C, Nanni G, Diociaiuti A, Panocchia N, Cerimele D. Kaposi's sarcoma in renal-transplant recipients: experience at the Catholic University in Rome, 1988-1996. Dermatology. 1997;194(3):229-33.
12. Lagunoff M, Ganem D. The structure and coding organization of the genomic termini of Kaposi's sarcoma-associated herpesvirus. Virology. 1997;236(1):147-54.
13. Dourmishev LA, Dourmishev AL, Palmeri D, Schwartz RA, Lukac DM. Molecular genetics of Kaposi's sarcoma-associated herpesvirus (human herpesvirus-8) epidemiology and pathogenesis. Microbiol Mol Biol Rev. 2003;67(2):175-212, table of contents.
14. Ohsaki E, Ueda K. Kaposi's Sarcoma-Associated Herpesvirus Genome Replication, Partitioning, and Maintenance in Latency. Front Microbiol. 2012;3:7.
15. Uppal T, Banerjee S, Sun Z, Verma SC, Robertson ES. KSHV LANA--the master regulator of KSHV latency. Viruses. 2014;6(12):4961-98.
16. Carroll PA, Kenerson HL, Yeung RS, Lagunoff M. Latent Kaposi's sarcoma-associated herpesvirus infection of endothelial cells activates hypoxia-induced factors. J Virol. 2006;80(21):10802-12.
17. Cai Q, Xiao B, Si H, Cervini A, Gao J, Lu J, et al. Kaposi's sarcoma herpesvirus upregulates Aurora A expression to promote p53 phosphorylation and ubiquitylation. PLoS Pathog. 2012;8(3):e1002566.
18. Borah S, Verma SC, Robertson ES. ORF73 of herpesvirus saimiri, a viral homolog of Kaposi's sarcoma-associated herpesvirus, modulates the two cellular tumor suppressor proteins p53 and pRb. J Virol. 2004;78(19):10336-47.

19. Liu J, Martin HJ, Liao G, Hayward SD. The Kaposi's sarcoma-associated herpesvirus LANA protein stabilizes and activates c-Myc. J Virol. 2007;81(19):10451-9.
20. Lu F, Tsai K, Chen HS, Wikramasinghe P, Davuluri RV, Showe L, et al. Identification of host-chromosome binding sites and candidate gene targets for Kaposi's sarcoma-associated herpesvirus LANA. J Virol. 2012;86(10):5752-62.
21. Fujimuro M, Hayward SD. Manipulation of glycogen-synthase kinase-3 activity in KSHV-associated cancers. J Mol Med (Berl). 2004;82(4):223-31.
22. Ojala PM, Yamamoto K, Castanos-Velez E, Biberfeld P, Korsmeyer SJ, Makela TP. The apoptotic v-cyclin-CDK6 complex phosphorylates and inactivates Bcl-2. Nat Cell Biol. 2000;2(11):819-25.
23. Ojala PM, Tiainen M, Salven P, Veikkola T, Castanos-Velez E, Sarid R, et al. Kaposi's sarcoma-associated herpesvirus-encoded v-cyclin triggers apoptosis in cells with high levels of cyclin-dependent kinase 6. Cancer Res. 1999;59(19):4984-9.
24. Matta H, Chaudhary PM. Activation of alternative NF-kappa B pathway by human herpes virus 8-encoded Fas-associated death domain-like IL-1 beta-converting enzyme inhibitory protein (vFLIP). Proc Natl Acad Sci U S A. 2004;101(25):9399-404.
25. Lee JS, Li Q, Lee JY, Lee SH, Jeong JH, Lee HR, et al. FLIP-mediated autophagy regulation in cell death control. Nat Cell Biol. 2009;11(11):1355-62.
26. Kliche S, Nagel W, Kremmer E, Atzler C, Ege A, Knorr T, et al. Signaling by human herpesvirus 8 kaposin A through direct membrane recruitment of cytohesin-1. Mol Cell. 2001;7(4):833-43.
27. McCormick C, Ganem D. The kaposin B protein of KSHV activates the p38/MK2 pathway and stabilizes cytokine mRNAs. Science. 2005;307(5710):739-41.
28. Pfeffer S, Sewer A, Lagos-Quintana M, Sheridan R, Sander C, Grasser FA, et al. Identification of microRNAs of the herpesvirus family. Nat Methods. 2005;2(4):269-76.
29. Yogev O, Lagos D, Enver T, Boshoff C. Kaposi's sarcoma herpesvirus microRNAs induce metabolic transformation of infected cells. PLoS Pathog. 2014;10(9):e1004400.
30. Samols MA, Skalsky RL, Maldonado AM, Riva A, Lopez MC, Baker HV, et al. Identification of cellular genes targeted by KSHV-encoded microRNAs. PLoS Pathog. 2007;3(5):e65.
31. Lukac DM, Renne R, Kirshner JR, Ganem D. Reactivation of Kaposi's sarcoma-associated herpesvirus infection from latency by expression of the ORF 50 transactivator, a homolog of the EBV R protein. Virology. 1998;252(2):304-12.
32. Chen J, Ye F, Xie J, Kuhne K, Gao SJ. Genome-wide identification of binding sites for Kaposi's sarcoma-associated herpesvirus lytic switch protein, RTA. Virology. 2009;386(2):290-302.
33. Moses AV, Fish KN, Ruhl R, Smith PP, Strussenberg JG, Zhu L, et al. Long-term infection and transformation of dermal microvascular endothelial cells by human herpesvirus 8. J Virol. 1999;73(8):6892-902.
34. Owen CB, Hughes DJ, Baquero-Perez B, Berndt A, Schumann S, Jackson BR, et al. Utilising proteomic approaches to understand oncogenic human herpesviruses (Review). Mol Clin Oncol. 2014;2(6):891-903.
35. Michalski A, Cox J, Mann M. More than 100,000 detectable peptide species elute in single shotgun proteomics runs but the majority is inaccessible to data-dependent LC-MS/MS. J Proteome Res. 2011;10(4):1785-93.
36. Thurau M, Marquardt G, Gonin-Laurent N, Weinlander K, Naschberger E, Jochmann R, et al. Viral inhibitor of apoptosis vFLIP/K13 protects endothelial cells against superoxide-induced cell death. J Virol. 2009;83(2):598-611.

37. Feng X, Zhang J, Chen WN, Ching CB. Proteome profiling of Epstein-Barr virus infected nasopharyngeal carcinoma cell line: identification of potential biomarkers by comparative iTRAQ-coupled 2D LC/MS-MS analysis. J Proteomics. 2011;74(4):567-76.
38. Bartee E, McCormack A, Fruh K. Quantitative membrane proteomics reveals new cellular targets of viral immune modulators. PLoS Pathog. 2006;2(10):e107.
39. Davis ZH, Verschueren E, Jang GM, Kleffman K, Johnson JR, Park J, et al. Global mapping of herpesvirus-host protein complexes reveals a transcription strategy for late genes. Mol Cell. 2015;57(2):349-60.
40. Delgado T, Sanchez EL, Camarda R, Lagunoff M. Global metabolic profiling of infection by an oncogenic virus: KSHV induces and requires lipogenesis for survival of latent infection. PLoS Pathog. 2012;8(8):e1002866.
41. Lodhi IJ, Semenkovich CF. Peroxisomes: a nexus for lipid metabolism and cellular signaling. Cell Metab. 2014;19(3):380-92.
42. Morita M, Imanaka T. Peroxisomal ABC transporters: structure, function and role in disease. Biochim Biophys Acta. 2012;1822(9):1387-96.
43. Lazarow PB. Viruses exploiting peroxisomes. Curr Opin Microbiol. 2011;14(4):458-69.
44. Odendall C, Kagan JC. Peroxisomes and the antiviral responses of mammalian cells. Subcell Biochem. 2013;69:67-75.
45. Tanner LB, Chng C, Guan XL, Lei Z, Rozen SG, Wenk MR. Lipidomics identifies a requirement for peroxisomal function during influenza virus replication. J Lipid Res. 2014;55(7):1357-65.
46. Bender S, Reuter A, Eberle F, Einhorn E, Binder M, Bartenschlager R. Activation of Type I and III Interferon Response by Mitochondrial and Peroxisomal MAVS and Inhibition by Hepatitis C Virus. PLoS Pathog. 2015;11(11):e1005264.
47. You J, Hou S, Malik-Soni N, Xu Z, Kumar A, Rachubinski RA, et al. Flavivirus Infection Impairs Peroxisome Biogenesis and Early Antiviral Signaling. J Virol. 2015;89(24):12349-61.
48. Zhou MT, Qin Y, Li M, Chen C, Chen X, Shu HB, et al. Quantitative Proteomics Reveals the Roles of Peroxisome-associated Proteins in Antiviral Innate Immune Responses. Mol Cell Proteomics. 2015;14(9):2535-49.
49. Wanders RJ. Metabolic and molecular basis of peroxisomal disorders: a review. Am J Med Genet A. 2004;126A(4):355-75.
50. Ferdinandusse S, Denis S, Mooijer PA, Zhang Z, Reddy JK, Spector AA, et al. Identification of the peroxisomal beta-oxidation enzymes involved in the biosynthesis of docosahexaenoic acid. J Lipid Res. 2001;42(12):1987-95.
51. Burdge GC. Metabolism of alpha-linolenic acid in humans. Prostaglandins Leukot Essent Fatty Acids. 2006;75(3):161-8.
52. Abe Y, Honsho M, Nakanishi H, Taguchi R, Fujiki Y. Very-long-chain polyunsaturated fatty acids accumulate in phosphatidylcholine of fibroblasts from patients with Zellweger syndrome and acyl-CoA oxidase1 deficiency. Biochim Biophys Acta. 2014;1841(4):610-9.
53. Valenca I, Pertega-Gomes N, Vizcaino JR, Henrique RM, Lopes C, Baltazar F, et al. Localization of MCT2 at peroxisomes is associated with malignant transformation in prostate cancer. J Cell Mol Med. 2015;19(4):723-33.
54. Gerschman R, Gilbert DL, Nye SW, Dwyer P, Fenn WO. Oxygen poisoning and x-irradiation: a mechanism in common. Science. 1954;119(3097):623-6.
55. McCord JM, Fridovich I. Superoxide dismutase. An enzymic function for erythrocuprein (hemocuprein). J Biol Chem. 1969;244(22):6049-55.
56. Mittal CK, Murad F. Activation of guanylate cyclase by superoxide dismutase and hydroxyl radical: a physiological regulator of guanosine 3',5'-monophosphate formation. Proc Natl Acad Sci U S A. 1977;74(10):4360-4.

57. Valko M, Leibfritz D, Moncol J, Cronin MT, Mazur M, Telser J. Free radicals and antioxidants in normal physiological functions and human disease. Int J Biochem Cell Biol. 2007;39(1):44-84.
58. Halliwell B, Gutteridge JM. Oxygen free radicals and iron in relation to biology and medicine: some problems and concepts. Arch Biochem Biophys. 1986;246(2):501-14.
59. Meyer M, Pahl HL, Baeuerle PA. Regulation of the transcription factors NF-kappa B and AP-1 by redox changes. Chem Biol Interact. 1994;91(2-3):91-100.
60. Sablina AA, Budanov AV, Ilyinskaya GV, Agapova LS, Kravchenko JE, Chumakov PM. The antioxidant function of the p53 tumor suppressor. Nat Med. 2005;11(12):1306-13.
61. Rao A, Luo C, Hogan PG. Transcription factors of the NFAT family: regulation and function. Annu Rev Immunol. 1997;15:707-47.
62. Pugh CW. Modulation of the Hypoxic Response. Adv Exp Med Biol. 2016;903:259-71.
63. Glineur C, Davioud-Charvet E, Vandenbunder B. The conserved redox-sensitive cysteine residue of the DNA-binding region in the c-Rel protein is involved in the regulation of the phosphorylation of the protein. Biochem J. 2000;352 Pt 2:583-91.
64. Galter D, Mihm S, Droge W. Distinct effects of glutathione disulphide on the nuclear transcription factor kappa B and the activator protein-1. Eur J Biochem. 1994;221(2):639-48.
65. Jagannathan L, Jose CC, Arita A, Kluz T, Sun H, Zhang X, et al. Nuclear Factor kappaB1/RelA Mediates Inflammation in Human Lung Epithelial Cells at Atmospheric Oxygen Levels. J Cell Physiol. 2016;231(7):1611-20.
66. Cairns RA, Harris IS, Mak TW. Regulation of cancer cell metabolism. Nat Rev Cancer. 2011;11(2):85-95.
67. DeBerardinis RJ, Lum JJ, Hatzivassiliou G, Thompson CB. The biology of cancer: metabolic reprogramming fuels cell growth and proliferation. Cell Metab. 2008;7(1):11-20.
68. Gorrini C, Harris IS, Mak TW. Modulation of oxidative stress as an anticancer strategy. Nat Rev Drug Discov. 2013;12(12):931-47.
69. Hanahan D, Weinberg RA. The hallmarks of cancer. Cell. 2000;100(1):57-70.
70. Sanchez EL, Carroll PA, Thalhofer AB, Lagunoff M. Latent KSHV Infected Endothelial Cells Are Glutamine Addicted and Require Glutaminolysis for Survival. PLoS Pathog. 2015;11(7):e1005052.
71. Birungi G, Chen SM, Loy BP, Ng ML, Li SF. Metabolomics approach for investigation of effects of dengue virus infection using the EA.hy926 cell line. J Proteome Res. 2010;9(12):6523-34.
72. Vastag L, Koyuncu E, Grady SL, Shenk TE, Rabinowitz JD. Divergent effects of human cytomegalovirus and herpes simplex virus-1 on cellular metabolism. PLoS Pathog. 2011;7(7):e1002124.
73. DeVito SR, Ortiz-Riano E, Martinez-Sobrido L, Munger J. Cytomegalovirus-mediated activation of pyrimidine biosynthesis drives UDP-sugar synthesis to support viral protein glycosylation. Proc Natl Acad Sci U S A. 2014;111(50):18019-24.
74. Koyuncu E, Purdy JG, Rabinowitz JD, Shenk T. Saturated very long chain fatty acids are required for the production of infectious human cytomegalovirus progeny. PLoS Pathog. 2013;9(5):e1003333.
75. Munger J, Bennett BD, Parikh A, Feng XJ, McArdle J, Rabitz HA, et al. Systems-level metabolic flux profiling identifies fatty acid synthesis as a target for antiviral therapy. Nat Biotechnol. 2008;26(10):1179-86.
76. Tilton C, Clippinger AJ, Maguire T, Alwine JC. Human cytomegalovirus induces multiple means to combat reactive oxygen species. J Virol. 2011;85(23):12585-93.

77. Lee J, Koh K, Kim YE, Ahn JH, Kim S. Upregulation of Nrf2 expression by human cytomegalovirus infection protects host cells from oxidative stress. J Gen Virol. 2013;94(Pt 7):1658-68.
78. Gargouri B, Nasr R, ben Mansour R, Lassoued S, Mseddi M, Attia H, et al. Reactive oxygen species production and antioxidant enzyme expression after Epstein-Barr virus lytic cycle induction in Raji cell line. Biol Trace Elem Res. 2011;144(1-3):1449-57.
79. Mesri EA, Feitelson MA, Munger K. Human viral oncogenesis: a cancer hallmarks analysis. Cell Host Microbe. 2014;15(3):266-82.
80. Li X, Feng J, Sun R. Oxidative stress induces reactivation of Kaposi's sarcoma-associated herpesvirus and death of primary effusion lymphoma cells. J Virol. 2011;85(2):715-24.
81. Ye F, Zhou F, Bedolla RG, Jones T, Lei X, Kang T, et al. Reactive oxygen species hydrogen peroxide mediates Kaposi's sarcoma-associated herpesvirus reactivation from latency. PLoS Pathog. 2011;7(5):e1002054.
82. Guilluy C, Zhang Z, Bhende PM, Sharek L, Wang L, Burridge K, et al. Latent KSHV infection increases the vascular permeability of human endothelial cells. Blood. 2011;118(19):5344-54.
83. Bottero V, Chakraborty S, Chandran B. Reactive oxygen species are induced by Kaposi's sarcoma-associated herpesvirus early during primary infection of endothelial cells to promote virus entry. J Virol. 2013;87(3):1733-49.
84. Venetsanakos E, Mirza A, Fanton C, Romanov SR, Tlsty T, McMahon M. Induction of tubulogenesis in telomerase-immortalized human microvascular endothelial cells by glioblastoma cells. Exp Cell Res. 2002;273(1):21-33.
85. Morris VA, Punjabi AS, Wells RC, Wittkopp CJ, Vart R, Lagunoff M. The KSHV viral IL-6 homolog is sufficient to induce blood to lymphatic endothelial cell differentiation. Virology. 2012;428(2):112-20.
86. Punjabi AS, Carroll PA, Chen L, Lagunoff M. Persistent activation of STAT3 by latent Kaposi's sarcoma-associated herpesvirus infection of endothelial cells. J Virol. 2007;81(5):2449-58.
87. Myoung J, Ganem D. Generation of a doxycycline-inducible KSHV producer cell line of endothelial origin: maintenance of tight latency with efficient reactivation upon induction. J Virol Methods. 2011;174(1-2):12-21.
88. Jain V, Plaisance-Bonstaff K, Sangani R, Lanier C, Dolce A, Hu J, et al. A Toolbox for Herpesvirus miRNA Research: Construction of a Complete Set of KSHV miRNA Deletion Mutants. Viruses. 2016;8(2).
89. Ong SE, Mann M. Mass spectrometry-based proteomics turns quantitative. Nat Chem Biol. 2005;1(5):252-62.
90. Eng JK, Jahan TA, Hoopmann MR. Comet: an open-source MS/MS sequence database search tool. Proteomics. 2013;13(1):22-4.
91. Deutsch EW, Mendoza L, Shteynberg D, Farrah T, Lam H, Tasman N, et al. A guided tour of the Trans-Proteomic Pipeline. Proteomics. 2010;10(6):1150-9.
92. Hoopmann MR, Finney GL, MacCoss MJ. High-speed data reduction, feature detection, and MS/MS spectrum quality assessment of shotgun proteomics data sets using high-resolution mass spectrometry. Anal Chem. 2007;79(15):5620-32.
93. Hoopmann MR, MacCoss MJ, Moritz RL. Identification of peptide features in precursor spectra using Hardklor and Kronik. Curr Protoc Bioinformatics. 2012;Chapter 13:Unit13 8.
94. Trapnell C, Pachter L, Salzberg SL. TopHat: discovering splice junctions with RNA-Seq. Bioinformatics. 2009;25(9):1105-11.
95. Langmead B, Trapnell C, Pop M, Salzberg SL. Ultrafast and memory-efficient alignment of short DNA sequences to the human genome. Genome Biol. 2009;10(3):R25.

96. Edgar R, Domrachev M, Lash AE. Gene Expression Omnibus: NCBI gene expression and hybridization array data repository. Nucleic Acids Res. 2002;30(1):207-10.
97. Bailly-Bechet M, Borgs C, Braunstein A, Chayes J, Dagkessamanskaia A, Francois JM, et al. Finding undetected protein associations in cell signaling by belief propagation. Proc Natl Acad Sci U S A. 2011;108(2):882-7.
98. Razick S, Magklaras G, Donaldson IM. iRefIndex: a consolidated protein interaction database with provenance. BMC Bioinformatics. 2008;9:405.
99. Stark C, Breitkreutz BJ, Reguly T, Boucher L, Breitkreutz A, Tyers M. BioGRID: a general repository for interaction datasets. Nucleic Acids Res. 2006;34(Database issue):D535-9.
100. Salwinski L, Miller CS, Smith AJ, Pettit FK, Bowie JU, Eisenberg D. The Database of Interacting Proteins: 2004 update. Nucleic Acids Res. 2004;32(Database issue):D449-51.
101. Keshava Prasad TS, Goel R, Kandasamy K, Keerthikumar S, Kumar S, Mathivanan S, et al. Human Protein Reference Database--2009 update. Nucleic Acids Res. 2009;37(Database issue):D767-72.
102. Orchard S, Ammari M, Aranda B, Breuza L, Briganti L, Broackes-Carter F, et al. The MIntAct project--IntAct as a common curation platform for 11 molecular interaction databases. Nucleic Acids Res. 2014;42(Database issue):D358-63.
103. Ceol A, Chatr Aryamontri A, Licata L, Peluso D, Briganti L, Perfetto L, et al. MINT, the molecular interaction database: 2009 update. Nucleic Acids Res. 2010;38(Database issue):D532-9.
104. Guirimand T, Delmotte S, Navratil V. VirHostNet 2.0: surfing on the web of virus/host molecular interactions data. Nucleic Acids Res. 2015;43(Database issue):D583-7.
105. Wang J, Duncan D, Shi Z, Zhang B. WEB-based GEne SeT AnaLysis Toolkit (WebGestalt): update 2013. Nucleic Acids Res. 2013;41(Web Server issue):W77-83.
106. Kanehisa M, Sato Y, Kawashima M, Furumichi M, Tanabe M. KEGG as a reference resource for gene and protein annotation. Nucleic Acids Res. 2016;44(D1):D457-62.
107. Shannon P, Markiel A, Ozier O, Baliga NS, Wang JT, Ramage D, et al. Cytoscape: a software environment for integrated models of biomolecular interaction networks. Genome Res. 2003;13(11):2498-504.
108. Sanchez EL, Lagunoff M. Viral activation of cellular metabolism. Virology. 2015;479-480:609-18.
109. Jarviluoma A, Ojala PM. Cell signaling pathways engaged by KSHV. Biochim Biophys Acta. 2006;1766(1):140-58.
110. Hanahan D, Weinberg RA. Hallmarks of cancer: the next generation. Cell. 2011;144(5):646-74.
111. Chokunonga E, Levy LM, Bassett MT, Mauchaza BG, Thomas DB, Parkin DM. Cancer incidence in the African population of Harare, Zimbabwe: second results from the cancer registry 1993-1995. Int J Cancer. 2000;85(1):54-9.
112. Boshoff C, Schulz TF, Kennedy MM, Graham AK, Fisher C, Thomas A, et al. Kaposi's sarcoma-associated herpesvirus infects endothelial and spindle cells. Nat Med. 1995;1(12):1274-8.
113. Staskus KA, Zhong W, Gebhard K, Herndier B, Wang H, Renne R, et al. Kaposi's sarcoma-associated herpesvirus gene expression in endothelial (spindle) tumor cells. J Virol. 1997;71(1):715-9.
114. Samols MA, Hu J, Skalsky RL, Renne R. Cloning and identification of a microRNA cluster within the latency-associated region of Kaposi's sarcoma-associated herpesvirus. J Virol. 2005;79(14):9301-5.

115. Zhong W, Wang H, Herndier B, Ganem D. Restricted expression of Kaposi sarcoma-associated herpesvirus (human herpesvirus 8) genes in Kaposi sarcoma. Proc Natl Acad Sci U S A. 1996;93(13):6641-6.
116. Ciufo DM, Cannon JS, Poole LJ, Wu FY, Murray P, Ambinder RF, et al. Spindle cell conversion by Kaposi's sarcoma-associated herpesvirus: formation of colonies and plaques with mixed lytic and latent gene expression in infected primary dermal microvascular endothelial cell cultures. J Virol. 2001;75(12):5614-26.
117. Lagunoff M, Bechtel J, Venetsanakos E, Roy AM, Abbey N, Herndier B, et al. De novo infection and serial transmission of Kaposi's sarcoma-associated herpesvirus in cultured endothelial cells. J Virol. 2002;76(5):2440-8.
118. Chang HH, Ganem D. A unique herpesviral transcriptional program in KSHV-infected lymphatic endothelial cells leads to mTORC1 activation and rapamycin sensitivity. Cell Host Microbe. 2013;13(4):429-40.
119. DiMaio TA, Gutierrez KD, Lagunoff M. Latent KSHV infection of endothelial cells induces integrin beta3 to activate angiogenic phenotypes. PLoS Pathog. 2011;7(12):e1002424.
120. Sharma-Walia N, Raghu H, Sadagopan S, Sivakumar R, Veettil MV, Naranatt PP, et al. Cyclooxygenase 2 induced by Kaposi's sarcoma-associated herpesvirus early during in vitro infection of target cells plays a role in the maintenance of latent viral gene expression. J Virol. 2006;80(13):6534-52.
121. Aebersold R, Mann M. Mass spectrometry-based proteomics. Nature. 2003;422(6928):198-207.
122. Nesvizhskii AI, Vitek O, Aebersold R. Analysis and validation of proteomic data generated by tandem mass spectrometry. Nat Methods. 2007;4(10):787-97.
123. Kulakovskiy IV, Medvedeva YA, Schaefer U, Kasianov AS, Vorontsov IE, Bajic VB, et al. HOCOMOCO: a comprehensive collection of human transcription factor binding sites models. Nucleic Acids Res. 2013;41(Database issue):D195-202.
124. Huang SS, Clarke DC, Gosline SJ, Labadorf A, Chouinard CR, Gordon W, et al. Linking proteomic and transcriptional data through the interactome and epigenome reveals a map of oncogene-induced signaling. PLoS Comput Biol. 2013;9(2):e1002887.
125. Osmanbeyoglu HU, Pelossof R, Bromberg JF, Leslie CS. Linking signaling pathways to transcriptional programs in breast cancer. Genome Res. 2014;24(11):1869-80.
126. Gosline SJ, Spencer SJ, Ursu O, Fraenkel E. SAMNet: a network-based approach to integrate multi-dimensional high throughput datasets. Integr Biol (Camb). 2012;4(11):1415-27.
127. Chasman D, Ho YH, Berry DB, Nemec CM, MacGilvray ME, Hose J, et al. Pathway connectivity and signaling coordination in the yeast stress-activated signaling network. Mol Syst Biol. 2014;10:759.
128. Chasman D, Walters KB, Lopes TJ, Eisfeld AJ, Kawaoka Y, Roy S. Integrating Transcriptomic and Proteomic Data Using Predictive Regulatory Network Models of Host Response to Pathogens. PLoS Comput Biol. 2016;12(7):e1005013.
129. Ross PL, Huang YN, Marchese JN, Williamson B, Parker K, Hattan S, et al. Multiplexed protein quantitation in Saccharomyces cerevisiae using amine-reactive isobaric tagging reagents. Mol Cell Proteomics. 2004;3(12):1154-69.
130. Delgado T, Carroll PA, Punjabi AS, Margineantu D, Hockenbery DM, Lagunoff M. Induction of the Warburg effect by Kaposi's sarcoma herpesvirus is required for the maintenance of latently infected endothelial cells. Proc Natl Acad Sci U S A. 2010;107(23):10696-701.
131. Grant CE, Bailey TL, Noble WS. FIMO: scanning for occurrences of a given motif. Bioinformatics. 2011;27(7):1017-8.
132. Shiraishi Y, Okada-Hatakeyama M, Miyano S. A rank-based statistical test for measuring synergistic effects between two gene sets. Bioinformatics. 2011;27(17):2399-405.

133. Radkov SA, Kellam P, Boshoff C. The latent nuclear antigen of Kaposi sarcoma-associated herpesvirus targets the retinoblastoma-E2F pathway and with the oncogene Hras transforms primary rat cells. Nat Med. 2000;6(10):1121-7.
134. Tuncbag N, Gosline SJ, Kedaigle A, Soltis AR, Gitter A, Fraenkel E. Network-Based Interpretation of Diverse High-Throughput Datasets through the Omics Integrator Software Package. PLoS Comput Biol. 2016;12(4):e1004879.
135. Lefebvre C, Rajbhandari P, Alvarez MJ, Bandaru P, Lim WK, Sato M, et al. A human B-cell interactome identifies MYB and FOXM1 as master regulators of proliferation in germinal centers. Mol Syst Biol. 2010;6:377.
136. Gitter A, Carmi M, Barkai N, Bar-Joseph Z. Linking the signaling cascades and dynamic regulatory networks controlling stress responses. Genome Res. 2013;23(2):365-76.
137. Wang J, Huo K, Ma L, Tang L, Li D, Huang X, et al. Toward an understanding of the protein interaction network of the human liver. Mol Syst Biol. 2011;7:536.
138. van der Zand A, Braakman I, Geuze HJ, Tabak HF. The return of the peroxisome. J Cell Sci. 2006;119(Pt 6):989-94.
139. Nakamura MT, Nara TY. Essential fatty acid synthesis and its regulation in mammals. Prostaglandins Leukot Essent Fatty Acids. 2003;68(2):145-50.
140. Avey D, Tepper S, Li W, Turpin Z, Zhu F. Phosphoproteomic Analysis of KSHV-Infected Cells Reveals Roles of ORF45-Activated RSK during Lytic Replication. PLoS Pathog. 2015;11(7):e1004993.
141. Baquero-Perez B, Whitehouse A. Hsp70 Isoforms Are Essential for the Formation of Kaposi's Sarcoma-Associated Herpesvirus Replication and Transcription Compartments. PLoS Pathog. 2015;11(11):e1005274.
142. Gan J, Wang C, Jin Y, Guo Y, Xu F, Zhu Q, et al. Proteomic profiling identifies the SIM-associated complex of KSHV-encoded LANA. Proteomics. 2015;15(12):2023-37.
143. Marcos-Villar L, Gallego P, Munoz-Fontela C, de la Cruz-Herrera CF, Campagna M, Gonzalez D, et al. Kaposi's sarcoma-associated herpesvirus lana2 protein interacts with the pocket proteins and inhibits their sumoylation. Oncogene. 2014;33(4):495-503.
144. Nayar U, Lu P, Goldstein RL, Vider J, Ballon G, Rodina A, et al. Targeting the Hsp90-associated viral oncoproteome in gammaherpesvirus-associated malignancies. Blood. 2013;122(16):2837-47.
145. Purushothaman P, McDowell ME, McGuinness J, Salas R, Rumjahn SM, Verma SC. Kaposi's sarcoma-associated herpesvirus-encoded LANA recruits topoisomerase IIbeta for latent DNA replication of the terminal repeats. J Virol. 2012;86(18):9983-94.
146. Salinas E, Byrum SD, Moreland LE, Mackintosh SG, Tackett AJ, Forrest JC. Identification of Viral and Host Proteins That Interact with Murine Gammaherpesvirus 68 Latency-Associated Nuclear Antigen during Lytic Replication: a Role for Hsc70 in Viral Replication. J Virol. 2015;90(3):1397-413.
147. Si H, Verma SC, Robertson ES. Proteomic analysis of the Kaposi's sarcoma-associated herpesvirus terminal repeat element binding proteins. J Virol. 2006;80(18):9017-30.
148. Sun Q, Tsurimoto T, Juillard F, Li L, Li S, De Leon Vazquez E, et al. Kaposi's sarcoma-associated herpesvirus LANA recruits the DNA polymerase clamp loader to mediate efficient replication and virus persistence. Proc Natl Acad Sci U S A. 2014;111(32):11816-21.
149. Wood JJ, Boyne JR, Paulus C, Jackson BR, Nevels MM, Whitehouse A, et al. ARID3B: a Novel Regulator of the Kaposi's Sarcoma-Associated Herpesvirus Lytic Cycle. J Virol. 2016;90(20):9543-55.
150. Clyde K, Glaunsinger BA. Deep sequencing reveals direct targets of gammaherpesvirus-induced mRNA decay and suggests that multiple mechanisms govern cellular transcript escape. PLoS One. 2011;6(5):e19655.

151. Rossetto CC, Tarrant-Elorza M, Verma S, Purushothaman P, Pari GS. Regulation of viral and cellular gene expression by Kaposi's sarcoma-associated herpesvirus polyadenylated nuclear RNA. J Virol. 2013;87(10):5540-53.
152. Mercier A, Arias C, Madrid AS, Holdorf MM, Ganem D. Site-specific association with host and viral chromatin by Kaposi's sarcoma-associated herpesvirus LANA and its reversal during lytic reactivation. J Virol. 2014;88(12):6762-77.
153. Abate F, Ambrosio MR, Mundo L, Laginestra MA, Fuligni F, Rossi M, et al. Distinct Viral and Mutational Spectrum of Endemic Burkitt Lymphoma. PLoS Pathog. 2015;11(10):e1005158.
154. Strahan R, Uppal T, Verma SC. Next-Generation Sequencing in the Understanding of Kaposi's Sarcoma-Associated Herpesvirus (KSHV) Biology. Viruses. 2016;8(4):92.
155. Moses AV, Jarvis MA, Raggo C, Bell YC, Ruhl R, Luukkonen BG, et al. Kaposi's sarcoma-associated herpesvirus-induced upregulation of the c-kit proto-oncogene, as identified by gene expression profiling, is essential for the transformation of endothelial cells. J Virol. 2002;76(16):8383-99.
156. Poole LJ, Yu Y, Kim PS, Zheng QZ, Pevsner J, Hayward GS. Altered patterns of cellular gene expression in dermal microvascular endothelial cells infected with Kaposi's sarcoma-associated herpesvirus. J Virol. 2002;76(7):3395-420.
157. Punj V, Matta H, Schamus S, Chaudhary PM. Integrated microarray and multiplex cytokine analyses of Kaposi's Sarcoma Associated Herpesvirus viral FLICE Inhibitory Protein K13 affected genes and cytokines in human blood vascular endothelial cells. BMC Med Genomics. 2009;2:50.
158. Wang HW, Trotter MW, Lagos D, Bourboulia D, Henderson S, Makinen T, et al. Kaposi sarcoma herpesvirus-induced cellular reprogramming contributes to the lymphatic endothelial gene expression in Kaposi sarcoma. Nat Genet. 2004;36(7):687-93.
159. Calder PC. Mechanisms of action of (n-3) fatty acids. J Nutr. 2012;142(3):592S-9S.
160. Mullen A, Loscher CE, Roche HM. Anti-inflammatory effects of EPA and DHA are dependent upon time and dose-response elements associated with LPS stimulation in THP-1-derived macrophages. J Nutr Biochem. 2010;21(5):444-50.
161. Lee SA, Kim HJ, Chang KC, Baek JC, Park JK, Shin JK, et al. DHA and EPA Down-regulate COX-2 Expression through Suppression of NF-kappaB Activity in LPS-treated Human Umbilical Vein Endothelial Cells. Korean J Physiol Pharmacol. 2009;13(4):301-7.
162. Schafer FQ, Buettner GR. Redox environment of the cell as viewed through the redox state of the glutathione disulfide/glutathione couple. Free Radic Biol Med. 2001;30(11):1191-212.
163. Sen CK. Cellular thiols and redox-regulated signal transduction. Curr Top Cell Regul. 2000;36:1-30.
164. Thannickal VJ, Fanburg BL. Reactive oxygen species in cell signaling. Am J Physiol Lung Cell Mol Physiol. 2000;279(6):L1005-28.
165. Kitazawa M, Nakano T, Chuujou H, Shiojiri E, Iwasaki K, Sakamoto K. Intracellular redox regulation by a cystine derivative suppresses UV-induced NF-kappa B activation. FEBS Lett. 2002;526(1-3):106-10.
166. Staal FJ, Anderson MT, Herzenberg LA. Redox regulation of activation of NF-kappa B transcription factor complex: effects of N-acetylcysteine. Methods Enzymol. 1995;252:168-74.
167. Flohe L, Brigelius-Flohe R, Saliou C, Traber MG, Packer L. Redox regulation of NF-kappa B activation. Free Radic Biol Med. 1997;22(6):1115-26.
168. Nordberg J, Arner ES. Reactive oxygen species, antioxidants, and the mammalian thioredoxin system. Free Radic Biol Med. 2001;31(11):1287-312.
169. Baker A, Payne CM, Briehl MM, Powis G. Thioredoxin, a gene found overexpressed in human cancer, inhibits apoptosis in vitro and in vivo. Cancer Res. 1997;57(22):5162-7.

170. Sychev ZE, Hu A, DiMaio TA, Gitter A, Camp ND, Noble WS, et al. Integrated systems biology analysis of KSHV latent infection reveals viral induction and reliance on peroxisome mediated lipid metabolism. PLoS Pathog. 2017;13(3):e1006256.
171. Raninga PV, Di Trapani G, Vuckovic S, Bhatia M, Tonissen KF. Inhibition of thioredoxin 1 leads to apoptosis in drug-resistant multiple myeloma. Oncotarget. 2015;6(17):15410-24.
172. Kim SY, Kim TJ, Lee KY. A novel function of peroxiredoxin 1 (Prx-1) in apoptosis signal-regulating kinase 1 (ASK1)-mediated signaling pathway. FEBS Lett. 2008;582(13):1913-8.
173. Jarvis RM, Hughes SM, Ledgerwood EC. Peroxiredoxin 1 functions as a signal peroxidase to receive, transduce, and transmit peroxide signals in mammalian cells. Free Radic Biol Med. 2012;53(7):1522-30.
174. Matsuzawa A, Ichijo H. Redox control of cell fate by MAP kinase: physiological roles of ASK1-MAP kinase pathway in stress signaling. Biochim Biophys Acta. 2008;1780(11):1325-36.
175. Akamatsu Y, Ohno T, Hirota K, Kagoshima H, Yodoi J, Shigesada K. Redox regulation of the DNA binding activity in transcription factor PEBP2. The roles of two conserved cysteine residues. J Biol Chem. 1997;272(23):14497-500.
176. Xie J, Wu H, Dai C, Pan Q, Ding Z, Hu D, et al. Beyond Warburg effect--dual metabolic nature of cancer cells. Sci Rep. 2014;4:4927.
177. Cai J, Chen Y, Seth S, Furukawa S, Compans RW, Jones DP. Inhibition of influenza infection by glutathione. Free Radic Biol Med. 2003;34(7):928-36.
178. Kalinina EV, Chernov NN, Saprin AN. Involvement of thio-, peroxi-, and glutaredoxins in cellular redox-dependent processes. Biochemistry (Moscow). 2009;73(13):1493-510.
179. Kang SW, Rhee SG, Chang TS, Jeong W, Choi MH. 2-Cys peroxiredoxin function in intracellular signal transduction: therapeutic implications. Trends Mol Med. 2005;11(12):571-8.
180. Mukherjee A, Martin SG. The thioredoxin system: a key target in tumour and endothelial cells. Br J Radiol. 2008;81 Spec No 1:S57-68.
181. Saha A, Kaul R, Murakami M, Robertson ES. Tumor viruses and cancer biology: Modulating signaling pathways for therapeutic intervention. Cancer Biol Ther. 2010;10(10):961-78.
182. Chandrasekharan JA, Huang XM, Hwang AC, Sharma-Walia N. Altering the Anti-inflammatory Lipoxin Microenvironment: a New Insight into Kaposi's Sarcoma-Associated Herpesvirus Pathogenesis. J Virol. 2016;90(24):11020-31.
183. Baresova P, Pitha PM, Lubyova B. Distinct roles of Kaposi's sarcoma-associated herpesvirus-encoded viral interferon regulatory factors in inflammatory response and cancer. J Virol. 2013;87(17):9398-410.
184. Ballon G, Akar G, Cesarman E. Systemic expression of Kaposi sarcoma herpesvirus (KSHV) Vflip in endothelial cells leads to a profound proinflammatory phenotype and myeloid lineage remodeling in vivo. PLoS Pathog. 2015;11(1):e1004581.
185. Sharma-Walia N, Paul AG, Bottero V, Sadagopan S, Veettil MV, Kerur N, et al. Kaposi's sarcoma associated herpes virus (KSHV) induced COX-2: a key factor in latency, inflammation, angiogenesis, cell survival and invasion. PLoS Pathog. 2010;6(2):e1000777.
186. Morris VA, Punjabi AS, Lagunoff M. Activation of Akt through gp130 receptor signaling is required for Kaposi's sarcoma-associated herpesvirus-induced lymphatic reprogramming of endothelial cells. J Virol. 2008;82(17):8771-9.